Analysis of 2-D Scattering and Radiation Problems Using the Generalized Multipole Technique

by

Mohamed Khalil Ouda

A thesis

presented to the University of Manitoba

in fulfilment of the

thesis requirement for the degree of

Master of Science

in

Electrical and Computer Engineering

Winnipeg, Manitoba, Canada 1992

ISBN 0-315-77736-2

ANALYSIS OF 2-D SCATTERING AND RADIATION PROBLEMS USING THE GENERALIZED MULTIPOLE TECHNIQUE

BY

MOHAMED KHALIL OUDA

A Thesis submitted to the Faculty of Graduate Studies of the University of Manitoba in partial fulfillment of the requirements for the degree of

MASTER OF SCIENCE

I hereby declare that I am the sole author of this thesis.

I authorize the University of Manitoba to lend this thesis to other institutions or individuals for the purpose of scholarly research.

I further authorize the University of Manitoba to reproduce this thesis by photocopying or by other means, in total or in part, at the request of other institutions or individuals for the purpose of scholarly research.

ABSTRACT

A numerical method is presented for the problems of transverse electric (TE) and transverse magnetic (TM) scattered fields from homogeneous dielectric, imperfectly and perfectly conducting cylinders of arbitrary cross section. Furthermore, the solutions are presented for single and multiple scatterers and for radiation by slotted cylinders. The numerical solution uses fictitious sources to simulate the field scattered or radiated by the cylinders. The amplitudes of the fictitious sources are determined for subject to the regular boundary conditions or impedance boundary conditions according to the type of material composing the cylinders. Numerical results are given and compared with available analytical and numerical solutions.

ACKNOWLEDGEMENTS

I would like to express my sincere gratitude to Professor A. Sebak for his advice, continuous encouragement and helpful discussion throughout the course of this research. I would also like to thank my examining committee members, Professor L. Shafai and Professor W.D. Trim , for their valuable comments and advice.

Finally, I would like to acknowledge the financial assistance of the Natural Science and Engineering Research Council of Canada and the Department of National Defense through Professor Y. Antar. possible.

TABLE OF CONTENTS

LIST OF FIGURES

FIGURE PAGE

CHAPTER 1

Introduction

Various numerical methods have been developed to solve scattering and radiation of electromagnetic waves by two-dimensional objects. Recently the generalized multiple multipole technique and its special case the multifilament current model have became the subject of extensive studies due to their simplicity and capability of handling various types of geometries with very high accuracy.

Canonical geometries are usually considered for purely analytic solutions, allowing the use of an orthogonal coordinate system. In such a system, the field equation is solved by the separation of variables and the boundaries coincide coordinate surfaces in order to allow a simple enforcement of the boundary conditions. Unfortunately, the separation of variable is successful only for a few coordinate systems. Thus the geometries of analytically solvable problems are quite restricted. In 1900, the German physicist G. Mie [1] calculated guided electromagnetic waves on a transmission line with two circular wires. Since the Laplacian operator is not separable in the bipolar coordinate system which is well suited to formulate the boundary conditions, he applied, in addition to the bipolar coordinate, two polar coordinate systems with origins at the center of each circular wire. From the separation of variables in the polar coordinates, he obtained a multipole expansion for each wire and by applying the coordinate transformation he solved the equation resulted from applying the boundary conditions. A strong mathematical basis for Mie's multipole expansion had been worked out in 1948 by the Russian mathematician I. N. Vekua [2] and some years later by the Japanese scholar K. Yasuura [3]. Several authors success-

fully used multipole expansion together with the simple point matching technique to solve for electromagnetic problems [4],[5], [6] and [7]. However, some others encountered problems and considered this method to be analytically insufficient [8], [9]. A recent study of the problem using the multipole expansion combined with the point matching technique (PMT) by Hafner [3] showed that these were only numerical problems. To overcome these problems, he introduced additional, analytically unnecessary, multipoles. The name multiple multipole was proposed as well, and may be considered as a combination of method of moments (MoM) and point matching technique [10].

The unknowns for the conventional MoM approach are currents flowing on the surface where the boundary conditions are enforced [11]. The currents are presumed to be continuous so that the solution is represented by an integral equation, which has a kernel with singularity when it is evaluated on the same surface where the currents flow. The integral equation is transformed into a matrix equation by the MoM, which is described by Harrington [11] as the unifying principle for all techniques for reducing functional equations to matrix equations. On the other hand, the generalized multiple multipole technique uses the expansion coefficients of the analytical solution of the field equations as unknowns. The specific choice is similar to the choice of the basis function in MoM [10]. Spherical wave multipole functions, or the equivalent two-dimensional cylindrical waves are one choice [12], [13] and [14]. Another choice is infinitesimal electric dipoles, or the equivalent two-dimensional current filaments [15] and [16], which is a special case of the multipoles. In principle, any set of analytic solutions of Maxwell's equations could be used [17]. By choosing a discrete set of solutions, and matching the boundary conditions at a discrete set of points, the resulting equation is automatically a matrix equation. By choosing solutions corresponding to sources some distance away from the bound-

ary, the fields form a set of smooth functions on the boundary and in particular singularities are totally avoided. The matrix equation may be over-determined and solved to provide a least-squares fit to the boundary condition. Since each solution in the set is known analytically, it is not necessary to integrate currents to determine fields during any stage of the solution-filling the matrix, checking the results, or computing near and far fields or other quantities of interest.

1.1 Literature Review

1.1.1 Single Scatterer

The problem of scattering from a single cylinder of arbitrary cross section has been treated by several numerical methods. Richmond [18], [19] has treated the problem of homogeneous and inhomogeneous dielectric cylinders in terms of a polarization current induced in the dielectric. For a homogeneous dielectric cylinder the surface integral equation formulation can also be applied [20] in which the problem is formulated in terms of equivalent electric and magnetic surface currents. Mullin *et al* [4] used the two-dimensional multipole with a single origin for all sources to solve for geometries where the cross section is ellipse-like with no more than a 2:1 ratio of major and minor axes. Leviatan *et al.* [21],[22] have dealt with problems for homogeneous dielectric cylinders of arbitrary smooth cross section using multifilament current model. In their analysis, the fields of two sets of filamentary sources are used to simulate equivalent situations, inside and outside the cylinder. Application of the boundary conditions results in a matrix equation for the unknown filamentary sources, which can be solved using standard numerical techniques.

1.1.2 Imperfectly Conducting Objects

For imperfectly conducting objects, when a plane electromagnetic wave impinges on a scattering body, the simple relation between the electric and magnetic fields of the plane wave in free space is modified due to currents induced in the surface both interior to and exterior to the body, such that the well known boundary condition for the tangential electric fields at the surface of the scattered body are satisfied. In many practical cases, such as absorbed and coated bodies, the field does not penetrate deeply into the scattering body. In such cases, the scattering problem simplifies considerably because it is then sufficient to solve for the fields exterior to the body only subject to the impedance boundary condition [23]. The impedance boundary condition states that the ratio between the tangential electric and magnetic fields at the surface of the scattered body equals to an impedance at the surface of the body which depends on the electrical properties of the body. The usefulness of the IBCs in determining the scattered fields was studied by Mitzner [24] using an integral equation formulation. Generalization of IBCs integral equations ; i.e., the electric and magnetic field integral equations(EFIE and MFIE), was presented by Jones [25] who has also demonstrated the uniqueness of the solution for its combined form (CFIE). Numerical results, based on the integral-equation approach, are presented in [23] and [26] for two- dimensional scattering by impedance cylinders of arbitrary cross section. In [27] and [28] the integral equation approach is applied to solve the EFIE, MFIE and CFIE of three-dimensional objects with IBCs.

1.1.3 Multiple Scatterers

The scattering by parallel conducting cylinders of arbitrary cross section was investigated numerically by Andreason [29]. The problem was formulated in terms of an integral equation for the induced surface current. The method of moments

was then used to reduce the integral equation into a matrix form which was solved numerically for the unknown surface currents. A formulation based on the single multipole expansion of the scattered field due to two or three parallel conducting cylinders is presented by Howarth and Pavlasek [30], [31]. They also evaluated the diffracted field and the induced current on the surface of the cylinders and verified their numerical results experimentally. Olaofe [32] has investigated the problem of scattering by two circular cylinders using a boundary value method. His solution reduces the problem to the solution of a system of algebraic simultaneous linear equations for the multiple scattering amplitude coefficients in terms of the known single particle scattering amplitude coefficients. Ragheb and Hamid [33] used Twersky's iterative technique to solve for the scattering by N parallel cylinders. Elsherbeni and Hamid [34] used the modified method of moments to solve for the problem of scattering by two circular cylinders. Zitron and Karp [35] have investigated the problem of diffraction of plane electromagnetic or acoustic waves by two arbitrary shaped parallel cylinder.

1.1.4 Slotted Cylinders

The radiation of electromagnetic wave from an infinite axially slotted cylinder has received great attention in the literature. Hurd [36] has studied the directional properties and the radiation patterns of dielectric coated slotted cylinders. A uniform field distribution in the slot was assumed and results for the special case of a narrow slot were given. Olte [37] studied the radiation by an elementary cylindrical antenna through slotted enclosure. He reduced the problem to a Fredholm integral equation of the first kind, and then solved for a narrow slot as a special case. Richmond and Gilreath [38] studied a flush-mounted dielectric-loaded axial slot on circular cylinder antenna. Their analysis was carried out using the boundary value method

and then Galerkin's method was introduced to complete the solution. Leviatan and Haller [39] studied the electromagnetic scattering from slotted conducting circular cylindrical shell using the multifilament current model.

1.2 Overview

In chapter 2, the multifilament current model (MFCM) and the generalized multiple multipole technique (GMMP) are used for solving transverse electric (TE) and transverse magnetic (TM) scattering from lossy homogeneous dielectric and perfectly conducting cylinders of arbitrary cross section. For both techniques, the problem is formulated using only one set of fictitious sources placed inside the cylinder surface to simulate its scattered field. The fictitious sources are placed at some distances from the boundary surface, the field they generate actually constitute a basis of smooth field functions capable of representing a smooth field at the boundary surface. Applying the IBCs at selected points on the cylinder surface results in a matrix equation which is solved for the unknown filamentary currents in the case of MFCM and the expansion coefficients in the case of the GMMP. These unknowns are then used to determine the scattered field and other parameters of interest. Results for various geometries are given and compared with available analytical and numerical solutions. Also a discussion on the location of sources and the treatment of the singularities of the fields at sharp edges is included.

In chapter 3, the multifilament current model [21] and [22] is used to solve for the problem of multiple scattering by parallel cylinders of arbitrary cross sections. The problem is classified into two parts; transverse magnetic (TM) and transverse electric (TE) according to the type of excitation. For each excitation type, the formulation is carried out for the problems of homogeneous dielectric and imperfectly conducting cylinders. For the case of homogeneous dielectric cylinders, the problem

is formulated using two sets of fictitious filamentary sources to simulate the fields of each cylinder. For each cylinder, one set of sources is placed inside it to simulate its scattered field. The other set of sources is placed outside each cylinder to simulate the fields inside the respective cylinder. Application of the boundary conditions yields a system of linear equations which can be solved for the unknown filamentary currents.

For imperfectly conducting cylinders with impedance boundary conditions, only one set of filamentary sources is needed to simulate the fields of each cylinder. This set of sources is placed inside each cylinder to simulate its scattered field. The case of perfectly conducting cylinders can be handled as a special case of the imperfectly conducting cylinders by setting the surface impedance to zero. Again application of the IBCs results in a system of linear equations which can be solved for the unknown filamentary currents. Once the strengths of the filamentary currents are computed, the scattered field and other parameters of interest can be obtained. Results for the normalized echo width for selected geometries of arbitrary cross section and of different parameters are obtained and compared with the MoM solutions.

In chapter 4, the multifilament current model (MFCM) and the generalized multiple multipole technique (GMMP) are used for solving transverse electric (TE) radiating from slotted perfectly conducting cylinder of arbitrary cross section. For both techniques, the problem is formulated using one set of fictitious sources placed inside the cylinder surface to simulate the radiated field. The fictitious sources are placed at some distances from the boundary surface, the field they generate actually constitutes a basis of smooth field functions capable of representing a smooth field at the boundary surface. Applying the boundary conditions at selected points on the cylinder surface and on the slot results in a matrix equation which is solved for the unknown filamentary currents in the case of MFCM and the expansion coefficient

in the case of the GMMP. These unknowns are then used to determine the radiated field and other parameters of interest. Results for slotted circular cylinders are given and compared with analytical solutions.

Conclusion with discussion of the results are included in chapter 5.

CHAPTER 2

Scattering by Imperfectly Conducting Cylinders

2.1 Introduction

In this chapter, the multifilament current model (MFCM) and the generalized multiple multipole technique (GMMP) are used to solve for the problem of scattering by imperfectly conducting cylinders of arbitrary cross section. The problem is classified into two parts; transverse electric (TE) and transverse magnetic (TM) according to the type of excitation. For each excitation type, the formulation is carried out for the scattering problem using MFCM and GMMP.

The solution for the problem of homogeneous dielectric cylinders using the MFCM simulation [21], [22] will be presented for the sake of completeness and comparison. In this case, the problem is formulated using two sets of fictitious filamentary sources to simulate the fields of the cylinder. One set of sources is placed inside the cylinder at some distance from its surface to simulate its scattered field. The other set of sources is placed outside the cylinder at some distance from its surface to simulate the field transmitted inside the cylinder. The filamentary sources in both sets carry of yet to be determined constant complex currents. They generate smooth field functions capable of representing smooth fields on the boundary surface. Applications of the boundary conditions yield a system of linear equations which can be solved for the unknown filamentary currents.

For imperfectly conducting cylinders, the multifilament current model simulation uses only one set of filamentary sources to simulate the field scattered by the

cylinder. This set of sources is placed inside the cylinder at some distance from its surface to simulate its scattered field. The sources carry constant complex currents, yet to be determined. They generate smooth field functions capable of representing smooth fields on the boundary surface. Applications of the Impedance Boundary Conditions result in a system of linear equations which can be solved for the unknown filamentary currents. The GMMP simulation is similar to the MFCM simulation; however, the GMMP simulation uses a set of multipole line sources to simulate the field scattered by the cylinder. Again, this set of multipoles is situated inside the cylinder to simulate its scattered filed. The unknowns of the multipoles expansion coefficients can be obtained by solving the system of linear equations resulting from applying the IBCs at selected points on the surface of the cylinder. The case of perfectly conducting cylinders can be handled as a special case of the imperfectly conducting cylinders by setting the surface impedance to zero.

In the following sections, the formulation will be carried out in details for TE case. The solution for the TM case will be discussed briefly in a later section. Results for selected geometries of arbitrary cross section and of various parameters are given and compared with available analytical solutions.

2.2 Problem Specification for TE case.

The scattering geometry considered is shown in Fig. 2.1. An infinitely long lossy dielectric cylinder of arbitrary cross section whose axis is taken to be parallel with the $z-$axis of a rectangular coordinate system. The cylinder composed of homogeneous dielectric material of permittivity ε, permeability μ and conductivity σ_c and the region surrounding the cylinder is free space of permittivity ε_o and permeability μ_o.

Let the cylinders be immersed in an incident transverse electric plane wave (TE) characterized by

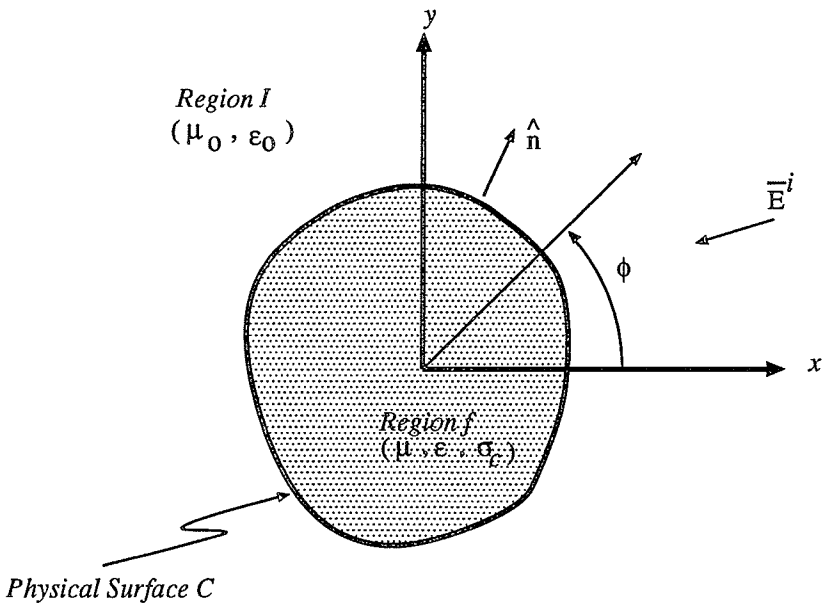

Figure 2.1: Geometry of the problem

$$\bar{H}^i = \hat{u}_z H_z^i \tag{2.1}$$

$$\bar{E}^i = \hat{u}_x E_x^i + \hat{u}_y E_y^i \tag{2.2}$$

where the time dependent $e^{j\omega t}$ is understood. Here, $\hat{u}_x$, $\hat{u}_y$, and $\hat{u}_z$ denote the unit vectors in the x, y, and z directions, respectively, and

$$H_z^i = e^{jk_o(xcos\phi^i + ysin\phi^i)} \tag{2.3}$$

$$E_x^i = \eta_o sin\phi^i e^{jk_o(xcos\phi^i + ysin\phi^i)} \tag{2.4}$$

$$E_y^i = -\eta_o cos\phi^i e^{jk_o(xcos\phi^i + ysin\phi^i)} \tag{2.5}$$

where η_o and k_o are, respectively, the intrinsic impedance and the wave number in free space, and ϕ^i is the angle of incidence. The problem is a two-dimensional one and can be worked out in some z =constant plane because $\bar{H}^i$ is $z-$directed and independent of z and the cylinder cross section is uniform along the z direction.

2.3 Multifilament Current Model

For homogeneous dielectric cylinders, the objective is to calculate the fields scattered by the cylinder, and the fields transmitted inside the cylinder. Therefore, we set two simulated equivalent situations to the original ones in regions I and f shown in Fig. 2.1. In the simulated equivalence for region I, shown in Fig. 2.2, the fields scattered by the cylinder are simulated by the fields of a set of fictitious magnetic current filaments placed on a closed surface enclosed by C. These filaments are z directed, infinite in extent and carry, yet undetermined, constant magnetic currents $K_i^I, i = 1, 2, 3..N^I$, where N^I is the number of sources inside the cylinder. They are treated as magnetic current sources radiating in free space. In Fig. 2.2, (E^s, H^s) are the electromagnetic scattered fields due to all fictitious current filaments inside the cylinder and (E^i, H^i) are the fields of the incident wave as given by (2.1) and (2.2). The total fields $(E^s + E^i, H^s + H^i)$ in the region I are approximations of the fields in region I in the original situation. Similarly, in the simulated equivalence for the interior regions f, shown in Fig. 2.3, the transmitted fields inside the cylinder are simulated by the fields of a set of fictitious magnetic current filaments. These filaments are placed on a closed surface enclosing C. Again, these filaments are z directed, infinite in extent and carry, yet undetermined, constant currents $K_i^f, i = 1, 2, 3..N^f$, where N^f is the number of filaments surrounding the cylinder. The set is treated as magnetic current sources radiating in a space filled with homogeneous material identical to the material composing the cylinder. The fields (E^f, H^f) due to the fictitious current filaments K_i^f are approximations of the field in region f in the original situation. The relationship between the electromagnetic fields $(E^s + E^i, H^s + H^i)$ and (E^f, H^f) in the simulated equivalent situation shown in Figs. 2.2 and 2.3, respectively, is dictated by the boundary conditions at the sur-

face of the cylinder shown in Fig. 2.1. Specifically, the continuity of the tangential electric and magnetic field components across C.

2.3.1 Expression for E^s and H^s

The scattered fields (E^s, H^s) at an observation point (x, y) in some z =constant plane due to the current filaments $K_i^I, i = 1, 2, 3, ...N^I$ radiating in an unbounded free space are given by

$$\bar{H}^s = \hat{u}_z \sum_{i=1}^{N^I} H_{zi}^s \tag{2.6}$$

$$\bar{E}^s = \hat{u}_x \sum_{i=1}^{N^I} E_{xi}^s + \hat{u}_y \sum_{i=1}^{N^I} E_{yi}^s \tag{2.7}$$

where H_{zi}^s, E_{xi}^s and E_{yi}^s are, respectively, the scattered magnetic and electric field components at an observation point (x, y) in the exterior region due to a magnetic current filament K_i^I situated at (x_i^I, y_i^I) inside C and they are given by

$$H_{zi}^s = -\frac{k_o K_i^I}{4\eta_o} H_o^{(2)}(k_o \rho_i^I) \tag{2.8}$$

$$E_{xi}^s = \frac{k_o K_i^I (y - y_i^I)}{4j\rho_i^I} H_1^{(2)}(k_o \rho_i^I) \tag{2.9}$$

$$E_{yi}^s = \frac{k_o K_i^I (x_i^I - x)}{4j\rho_i^I} H_1^{(2)}(k_o \rho_i^I) \tag{2.10}$$

$$\rho_i^I = \sqrt{(x - x_i^I)^2 + (y - y_i^I)^2} \tag{2.11}$$

where $H_0^{(2)}$ and $H_1^{(2)}$ are the second kind Hankel functions of zero order and first order , respectively and ρ_i^I is the radial distance between the source point and the observation point under consideration.

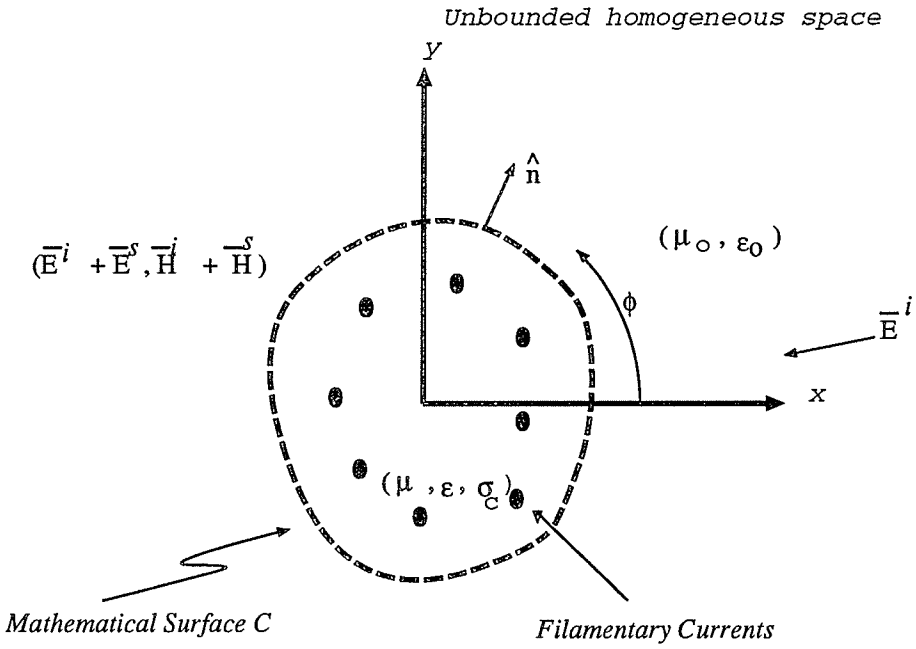

Figure 2.2: Simulated equivalence situation for region I

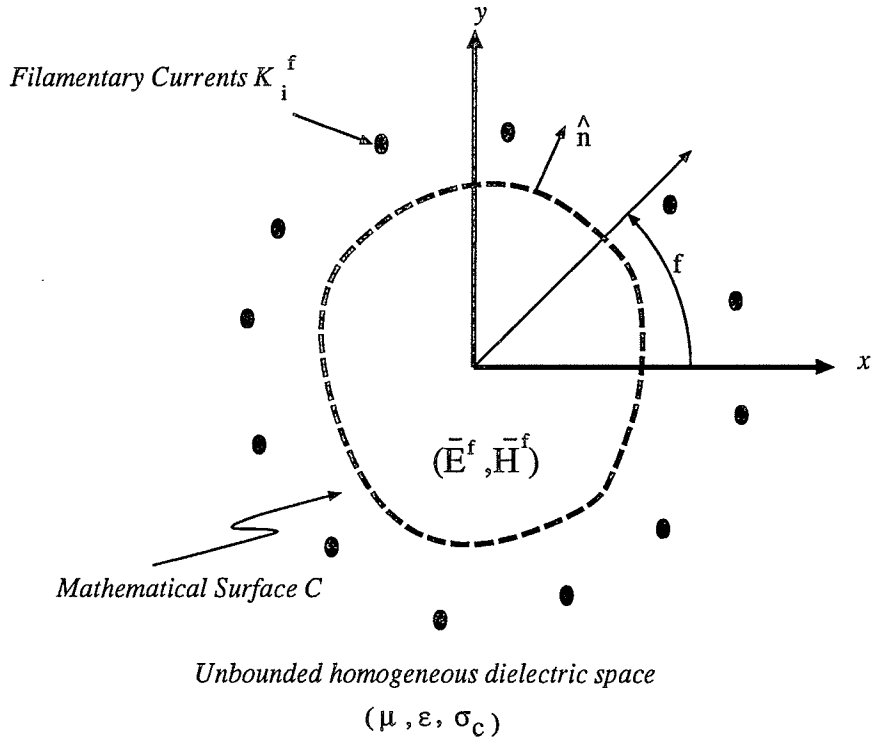

Figure 2.3: Simulated equivalence situation for region f

2.3.2 Expression for E^f and H^f

The transmitted fields (E^f, H^f) at an observation point (x, y) in some z =constant plane due to the current filaments $K_i^f, i = 1, 2, 3, ...N^f$ radiating in an unbounded homogeneous dielectric space are given by

$$\bar{H}^f = \hat{u}_z \sum_{i=1}^{N^f} H_{iz}^f \tag{2.12}$$

$$\bar{E}^f = \hat{u}_x \sum_{i=1}^{N^f} E_{ix}^f + \hat{u}_y \sum_{i=1}^{N^f} E_{iy}^f \tag{2.13}$$

where H_{zi}^f, E_{xi}^f and E_{yi}^f are, respectively, the transmitted magnetic and electric field components at an observation point (x, y) outside the cylinder due to a magnetic current filament K_i^f situated at (x_i^f, y_i^f) outside C and are given by

$$H_{iz}^f = -\frac{kK_i^f}{4\eta} H_0^{(2)}(k\rho_i^f) \tag{2.14}$$

$$E_{ix}^f = \frac{kK_i^f(y - y_i^f)}{4j\rho_i^f} H_1^{(2)}(k\rho_i^f) \tag{2.15}$$

$$E_{iy}^f = -\frac{kK_i^f(x - x_i^f)}{4j\rho_i^f} H_1^{(2)}(k\rho_i^f) \tag{2.16}$$

$$\rho_i^f = \sqrt{(x - x_i^f)^2 + (y - y_i^f)^2} \tag{2.17}$$

Here η and k are, respectively, the intrinsic impedance and the wave number inside the dielectric, and ρ_i^f is the radial distance between the source point and the observation point under consideration.

2.3.3 Evaluation of the Unknown Magnetic Currents K_i^I and K_i^f

For a dielectric object, the tangential components of the electric and magnetic fields must be continuous across the boundary. This leads to the operator equations on C.

$$\hat{n}\mathrm{x}(\bar{E}^s - \bar{E}^f) = -\hat{n}\mathrm{x}\bar{E}^i \tag{2.18}$$

$$\hat{n}\mathrm{x}(\bar{H}^s - \bar{H}^f) = -\hat{n}\mathrm{x}\bar{H}^i \tag{2.19}$$

where $\hat{n}$ is a unit vector normal to the cylinder surface and pointing toward region I as shown in Fig.2.1. Selecting N^C matching points on the surface of the cylinder and enforcing the boundary conditions (2.18) and (2.19) at the matching points result in a system of linear equations. These equations can be written in a matrix form

$$\mathbf{A}\,\mathbf{K} = \mathbf{V} \tag{2.20}$$

where

$$\mathbf{A} = \begin{bmatrix} \mathbf{A}^{I_e} & -\mathbf{A}^{f_e} \\ \mathbf{A}^{I_h} & -\mathbf{A}^{f_h} \end{bmatrix} \tag{2.21}$$

$$\mathbf{K} = \begin{bmatrix} \mathbf{K}_1^I \\ \mathbf{K}_2^I \end{bmatrix} \tag{2.22}$$

$$\mathbf{V} = \begin{bmatrix} -\mathbf{V}^{i_e} \\ -\mathbf{V}^{i_h} \end{bmatrix} \tag{2.23}$$

Here, $\mathbf{A}_{(2N_C, N^I+N^f)}$ is the generalized impedance matrix. The elements of $\mathbf{A}^{I_e}{}_{(N^C,N^I)}$ are the tangential electric field intensities due to the sources inside the cylinder. Similarly, the elements of $\mathbf{A}^{f_e}{}_{(N^C,N^f)}$ are the tangential electric field intensities due to the filaments outside the cylinder. The elements of $\mathbf{A}^{I_h}{}_{(N^C,N^I)}$ are the magnetic

field intensities due to the filaments inside the cylinder. The elements of $\mathbf{A}^{f_h}{}_{(N^C,N^f)}$ are the magnetic field intensities due to the filaments outside the cylinder. $\mathbf{K}_{(N^I,N^f)}$ is the generalized unknown current vector. $\mathbf{V}_{(2N^C)}$ is the generalized voltage source vector. The elements of $\mathbf{V}^{i_e}$ and $\mathbf{V}^{i_h}$ are, respectively, the incident tangential electric and magnetic field intensities evaluated at the matching points under consideration.

Having formulated the matrix equation (2.20), the unknown current vector $\mathbf{K}$ can be solved for by inversion or elimination if the boundary conditions are enforced at $N^C = N_l^I = N_l^f$ selected points on C. On the other hand, if the BCs are enforced at $N^C > N_l^I$ or $N^C > N^f$ selected points on C the least-square error solution to (2.20) may be used [21]. This solution minimizes the standard norm of the vector $\mathbf{AK} - \mathbf{V}$ and is given by

$$\mathbf{K} = (\tilde{\mathbf{A}} * \mathbf{A})^{-1} \tilde{\mathbf{A}}^* \mathbf{V} \tag{2.24}$$

where $\tilde{\mathbf{A}}$ is the transpose of $\mathbf{A}$ and the asterisk denotes complex conjugate.

2.4 Multifilament Current Model with IBCs

For imperfectly conducting cylinders, the surface impedance boundary conditions (IBCs) simplify the formulation by eliminating the need for the inclusion of the interior field [40]. Therefore, the multifilament current model simulation uses only one set of filamentary sources to simulate the fields scattered by the cylinder. This set of sources is placed inside the cylinder at some distance from its surface to simulate its scattered fields. The sources carry of yet to be determined constant complex currents. They generate smooth field functions capable of representing smooth field on the boundary surface. Applications of the IBCs result in a system of linear equations which can be solved for the unknown filamentary currents.

Fig. 2.2 shows the simulation of the field scattered by the cylinder, where the scattered field is simulated by the field of a set of fictitious magnetic current filaments placed on a closed surface enclosed by C. These filaments are z directed, infinite in extent and carry, yet to be determined, constant currents $K_i^I, i = 1, 2, 3, ...N^I$. They are treated as magnetic current sources radiated in free space. In Fig. 2.2, (E^s, H^s) are the electromagnetic scattered fields due to the fictitious current filaments and (E^i, H^i) are the fields of the incident wave as given by (2.1) and (2.2). The total field $(E^s + E^i, H^s + H^i)$ in the surrounding region in Fig. 2.2 is an approximation of the field in the surrounding region in the original situation. Note that the location of the filaments inside C has not been specified. As far as the formulation is concerned, their locations can be arbitrary. The question of selecting filament locations suitable for a numerical solution will be dealt with later on. The expression for the incident and scattered fields are given by (2.1)–(2.11).

2.4.1 Expression for the IBCs

For objects with IBCs the total electric and magnetic fields are related by [24]

$$\bar{E} - (\hat{n} \cdot \bar{E})\hat{n} = Z_c(\rho)(\hat{n} \times \bar{H}) \tag{2.25}$$

$$Z_c(\rho) = Z_w(1 - q(\rho)) \tag{2.26}$$

with

$$Z_w = \sqrt{\frac{j\omega\mu}{j\omega\varepsilon + \sigma_c}} \tag{2.27}$$

$$q(\rho) = \frac{1}{4}(1 - j)\delta[k_u(\rho) - k_v(\rho)] \tag{2.28}$$

where $\hat{n}$ is a unit vector normal to the cylinder surface and pointing toward region I as shown in Fig.2.1, σ_c is the conductivity of the material, δ is the skin depth,

Z_w is the wave impedance within the object and $k_u(\rho)$ and $k_v(\rho)$ are the principle curvatures of C at ρ. For small signal penetration, or for objects with large radii of curvature, $Z_c(\rho)$ can be assumed constant and equals to Z_w. The impedance boundary condition in (2.25) can be reduced to

$$E_t = -Z_c(\rho)H_z \tag{2.29}$$

where E_t is the total tangential electric field in the exterior region and H_z is the total magnetic field in that region. In the case of a circular cylinder $E_t = E_\phi$.

2.4.2 Evaluation of the Unknown Magnetic Currents K_i^I

.

The unknown magnetic currents may be determined by imposing the impedance boundary conditions on the surface of the cylinder. Therefore, by enforcing the IBCs at selected number of matching points on C, one can evaluate the unknowns K_i^I. Selecting N^C matching points on the surface of the cylinder and enforcing the boundary condition (2.29) at the j^{th}, $j = 1, 2, ...N^C$, matching point we get

$$(E_{tj}^s + E_{tj}^i) = -Z_c(\rho_j)(H_{zj}^s + H_{zj}^i) \tag{2.30}$$

where E_{tj}^s, E_{tj}^i, H_{zj}^s and H_{zj}^i are E_t^s, E_t^i, H_z^s and H_z^i evaluated at the j^{th} matching point. Enforcing equation (2.30) at all the matching points results in a set of linear equations which can be written in a matrix form in which the various matrices are interpreted in terms of generalized network parameters. The result is

$$\mathbf{A}\,\mathbf{K} = \mathbf{V} \tag{2.31}$$

where, for $i = 1, 2, 3...N^I$ and $j = 1, 2, 3...N^C$,

$$\mathbf{A} = \begin{bmatrix} A^{s_e}_{11} + Z_c(\rho_1)A^{s_h}_{11} & A^{s_e}_{12} + Z_c(\rho_1)A^{s_h}_{12} & \cdots & A^{s_e}_{1N^I} + Z_c(\rho_1)A^{s_h}_{1N^I} \\ A^{s_e}_{21} + Z_c(\rho_2)A^{s_h}_{21} & A^{s_e}_{22} + Z_c(\rho_2)A^{s_h}_{22} & \cdots & A^{s_e}_{2N^I} + Z_c(\rho_2)A^{s_h}_{2N^I} \\ ..... & ..... & ... & ..... \\ A^{s_e}_{N^C1} + Z_c(\rho_{N^C})A^{s_h}_{N^C1} & A^{s_e}_{N^C2} + Z_c(\rho_{N^C})A^{s_h}_{N^C2} & \cdots & A^{s_e}_{N^CN^I} + Z_c(\rho_{N^C})A^{s_h}_{N^CN^I} \end{bmatrix} \quad (2.32)$$

$$\mathbb{K} = \begin{bmatrix} K_1 \\ K_2 \\ \vdots \\ K_{N^I} \end{bmatrix} \quad (2.33)$$

$$\mathbf{V} = \begin{bmatrix} (-E^i_{t_1} + Z_c(\rho_1)H^i_{z1}) \\ -(E^i_{t_2} + Z_c(\rho_2)H^i_{z_2}) \\ \vdots \\ (-E^i_{t_{N^C}} + Z_c(\rho_{N^C})H^i_{z_{N^C}}) \end{bmatrix} \quad (2.34)$$

with

$$A^{s_e}_{ji} = \frac{k_o(y_j - y^I_i)t_{xj} - (x_j - x^I_i)t_{yj}}{4j\rho^I_{ji}} H^{(2)}_1(k_o\rho^I_{ji}) \quad (2.35)$$

$$A^{s_h}_{ji} = -\frac{k_o}{4\eta_o} H^{(2)}_o(k_o\rho^I_{ji}) \quad (2.36)$$

$$\rho^I_{ji} = \sqrt{(x_j - x^I_i)^2 + (y_j - y^I_i)^2} \quad (2.37)$$

Here, $\mathbf{A}_{(N^C,N^I)}$ is the generalized impedance matrix. $\mathbf{K}_{(N^I)}$ is the generalized unknown current vector, and $\mathbf{V}_{(N^C)}$ is the generalized voltage source vector. In (2.32), $A^{s_e}_{ji}$ and $A^{s_h}_{ji}$ are, respectively, the tangential electric field and magnetic field intensities due to a filament K^I_i of unit magnetic current evaluated at ρ^I_{ji} on C.

In (2.34), $E^i_{t_j}$, $H^i_{z_j}$ are, respectively, the incident tangential electric field intensity and the incident magnetic field intensity at observation point at ρ_j on C and ρ^I_{ji} is the radial distance between the i^{th} source and the j^{th} matching point. t_{xj} and t_{yj} are, respectively, the x and y components of the tangential unit vector evaluated at the j^{th} matching point.

Having formulated the matrix equation (2.31), the unknown current vector $\mathbf{K}$ can be solved for by inversion or elimination if the IBCs are enforced at $N^C = N^I$ selected points on C. On the other hand, if the IBCs are enforced at $N^C > N^I$ selected points on C the least-square error solution to (2.31) may be used [22]. This solution minimizes the standard norm of the vector $\mathbf{AK} - \mathbf{V}$ as given in (2.24)

2.5 Generalized Multiple Multipole with IBCs

The generalized multiple multipole technique (GMMP) represents the scattered fields by multiple expansions with different origins of out-ward cylindrical waves. The multiplicity of the origins for the out-ward waves can be interpreted as equivalent source locations within the boundary of the cylinder. Then, the total scattered field is represented as a sum over the contribution from each origin. Furthermore, the source distribution at each origin generates a field represented as a sum over cylindrical waves, each of which is generated by a specific source component at that origin. The sources are multipoles which includes monopoles, dipoles and higher order multipole line sources. As a result, we have a distribution of equivalent sources within the boundary which create a field on the boundary that leads to the satisfaction of the boundary conditions. Applying the impedance boundary conditions in the least square sense results in a system of linear equations which can be solved for the unknown expansion coefficients. The GMMP simulation for the field scattered

by the cylinder is similar to the multifilament current model simulation. However, the MFCM uses a set of filamentary sources, which is a monopole line sources, to simulate the scattered field. The procedure of the solution for the unknown expansion coefficients is exactly the same as the MFCM procedure. The simulation of the scattered filed is shown in Fig. 2.2 where the filamentary sources are replaced by multipoles line sources. The GMMP formulation is given in the following section.

2.5.1 Expression for E^s and H^s

The scattered fields (E^s, H^s) at an observation point (x, y) in some z =constant plane due to the multipoles source $K_i^I, i = 1, 2, 3, ...N^I$ radiating in an unbounded free space are given by [3]

$$\bar{H}^s = \hat{u}_z \sum_{i=1}^{N^I} H_{zi}^s \tag{2.38}$$

$$\bar{E}^s = \hat{u}_x \sum_{i=1}^{N^I} E_{xi}^s + \hat{u}_y \sum_{i=1}^{N^I} E_{yi}^s \tag{2.39}$$

where H_{zi}^s, E_{xi}^s and E_{yi}^s are, respectively, the scattered magnetic and electric field components at an observation point (x, y) in the exterior region due to a multipole line source K_i^I situated at (x_i^I, y_i^I) inside C and are given by

$$H_{zij}^s(\rho_{ji}^I) = \sum_{n=0}^{N_i^I} P_{in} H_n^{(2)}(k_o \rho_{ji}^I) \cos(n\phi_{ji}) + \sum_{n=1}^{N_i^I} Q_{in} H_n^{(2)}(k_o \rho_{ji}^I) \sin(n\phi_{ji}) \tag{2.40}$$

$$E_{xij}^s(\rho_{ji}^I) = \frac{j(y_j - y_i^I)}{\eta_o \rho_{ji}^I} \left[\sum_{n=0}^{N_i^I} P_{in} H_n'^{(2)}(k_o \rho_{ji}^I) \cos(n\phi_{ji}) + \sum_{n=1}^{N_i^I} Q_{in} H_n'^{(2)}(k_o \rho_i^I) \sin(n\phi_i) \right] \tag{2.41}$$

$$E^s_{yij}(\rho^I_{ji}) = -\frac{j(x_j - x^I_i)}{\eta_o \rho^I_{ji}} \left[\sum_{n=0}^{N^I_i} P_{in} H^{\prime(2)}_n(k_o \rho^I_{ji}) \cos(n\phi_{ji}) \right.$$
$$\left. + Q_{in} H^{\prime(2)}_n(k_o \rho^I_{ji}) \sin(n\phi_i) \right] \qquad (2.42)$$

where H^s_{zij}, E^s_{xij} *and* E^s_{yij} are, respectively, the scattered magnetic and electric field components at an observation point (x_j, y_j) in the exterior region due to the i^th source K^I_i situated at (x^I_i, y^I_i) inside C, N^I_i is the truncation number of the i^th source, P_{in} and Q_{in} are unknown expansion coefficients and

$$\rho^I_{ji} = \sqrt{(x_j - x^I_i)^2 + (y_j - y^I_i)^2} \qquad (2.43)$$

$$\phi_{ji} = \arctan\left((y_j - y^I_i)/(x_j - x^I_i)\right) \qquad (2.44)$$

2.5.2 Evaluation of the Unknowns P_{in} and Q_{in}

In order to compute the unknown parameters, P_{in} and Q_{in} in the GMMP expansions, only the boundary conditions have to be fulfilled because the field equations are completely satisfied by the GMMP expansions. Selecting N^C matching points and enforcing the boundary conditions in (2.29) at all the matching points result in a set of linear equations which can be written in a matrix form as

$$\mathbf{A}\,\mathbf{K} = \mathbf{V} \qquad (2.45)$$

where

$$\mathbf{A} = \begin{bmatrix} \mathbf{A}_{11} & \mathbf{A}_{12} & \ldots & \mathbf{A}_{1N^I} & \mathbf{B}_{11} & \mathbf{B}_{12} & \ldots & \mathbf{B}_{1N^I} \\ \mathbf{A}_{21} & \mathbf{A}_{22} & \ldots & \mathbf{A}_{2N^I} & \mathbf{B}_{21} & \mathbf{B}_{22} & \ldots & \mathbf{B}_{2N^I} \\ \ldots & \ldots & \ldots & \ldots & \ldots & \ldots & \ldots & \ldots \\ \mathbf{A}_{N^C1} & \mathbf{A}_{N^C2} & \ldots & \mathbf{A}_{N^CN^I} & \mathbf{B}_{N^C1} & \mathbf{B}_{N^C2} & \ldots & \mathbf{B}_{N^CN^I} \end{bmatrix} \qquad (2.46)$$

$$\mathbb{K} = \begin{bmatrix} \mathbb{P}_1 \\ \mathbb{P}_2 \\ \vdots \\ \mathbb{P}_{N^I} \\ \mathbb{Q}_1 \\ \mathbb{Q}_2 \\ \vdots \\ \mathbb{Q}_{N^I} \end{bmatrix} \tag{2.47}$$

$$\mathbf{V} = \begin{bmatrix} -(E^i_{t1} + Z_c(\rho_1)H^i_{z1}) \\ -(E^i_{t2} + Z_c(\rho_2)H^i_{z2}) \\ \vdots \\ -(E^i_{tN^C} + Z_c(\rho_{N^C})H^i_{zN^C}) \end{bmatrix} \tag{2.48}$$

with

$$\mathbf{A}^T_{ji} = \begin{bmatrix} (A^{s_t}_{ji0} + Z_c(\rho_j)A^{s_z}_{ji0}) \\ (A^{s_t}_{ji1} + Z_c(\rho_j)A^{s_z}_{ji1}) \\ \vdots \\ (A^{s_t}_{jiN_i} + Z_c(\rho_j)A^{s_z}_{jiN_i}) \end{bmatrix} \tag{2.49}$$

$$\mathbf{B}^T_{ji} = \begin{bmatrix} (B^{s_t}_{ji1} + Z_c(\rho_j)B^{s_z}_{ji1}) \\ (B^{s_t}_{ji2} + Z_c(\rho_j)B^{s_z}_{ji2}) \\ \vdots \\ (B^{s_t}_{jiN_i} + Z_c(\rho_j)B^{s_z}_{jiN_i}) \end{bmatrix} \tag{2.50}$$

$$A_{jin}^{st} = \frac{(x_j - x_i^I)t_{yj} - (y_j - y_i^I)t_{xj}}{j\eta_o \rho_{ji}^I} H_n'^{(2)}(k_o \rho_{ji}^I) cos(n\phi_{ji}) \tag{2.51}$$

$$A_{jin}^{sz} = H_n^{(2)}(k_o \rho_{ji}^I) cos(n\phi_{ji}) \tag{2.52}$$

$$B_{jin}^{st} = \frac{(x_j - x_i^I)t_{yj} - (y_j - y_i^I)t_{xj}}{j\eta_o \rho_{ji}^I} H_n'^{(2)}(k_o \rho_{ji}^I) sin(n\phi_{ji}) \tag{2.53}$$

$$B_{jin}^{sz} = H_n^{(2)}(k_o \rho_{ji}^I) sin(n\phi_{ji}) \tag{2.54}$$

$$\mathbf{P}_i = \begin{bmatrix} P_0 \\ P_1 \\ \vdots \\ P_{N_i} \end{bmatrix} \qquad \mathbf{Q}_i = \begin{bmatrix} Q_1 \\ Q_2 \\ \vdots \\ Q_{N_i} \end{bmatrix} \tag{2.55}$$

Having chosen the number of multipoles and the corresponding truncation order, the unknown expansion coefficients would be $M = \sum_{i=1}^{N^I}(2N_i^I + 1)$. Therefore, the number of matching points should be $N^C \geq M$, $\mathbf{A}$ is a matrix of order (N^C x M), $\mathbf{K}$ is a column vector of order M and $\mathbf{V}$ is a column vector of order N^C. Then by formulating the matrix equation in (2.45), the unknowns expansion coefficients can be solved for using the least-square error method given by (2.24)

2.6 Far-Scattered Field

In the far-field region, the scattering pattern of the cylinder can be obtained by employing the asymptotic expansion for the Hankel function and taking[18]

$$\lim_{k\rho_i \to \infty} \rho_i^I = \rho - x_i^I cos\phi - y_i^I sin\phi \tag{2.56}$$

where ρ and ϕ are the polar coordinates of the distant observation point and ρ_i is the distance from the i^{th} source inside the cylinder to the distant observation point. Therefore, the far-scattered field is given by

$$H^s = -\frac{k_o}{4\eta_o}\sqrt{\frac{2j}{\pi k_o \rho}} e^{-jk_o\rho} \sum_{i=1}^{N^I} K_i^I e^{jk_o(x_i^I cos\phi + y_i^I sin\phi)} \tag{2.57}$$

The scattering cross section per unit length, *i.e.*, the echo width, σ is defined by

$$\sigma(\phi) = \lim_{\rho \to \infty} 2\pi\rho \left| \frac{H^s(\rho,\phi)}{H^i} \right|^2 \tag{2.58}$$

From (2.57) and (2.58), the echo width is given by

$$\sigma(\phi) = -\frac{k_o}{4\eta_o^2 |H^i|^2} \left| \sum_{i=1}^{N^I} K_i^I e^{jk_o(x_i cos\phi + y_i sin\phi)} \right|^2 \tag{2.59}$$

2.7 Solution for TM case

Let the cylinder, shown in Fig.2.1, be immersed in an incident transverse magnetic wave (TM). The solution proceeds, similar to the TE problem, line for line. The sources are now electric current filaments or multipole line sources I_i. Using the Duality theorem [41], the field equations can be obtained by systematically interchanging the symbols $(H_z, E_\phi, \epsilon, \mu, K)$ by $(E_z, -H_\phi, \mu, \epsilon, I)$ in the formulations presented for the (TE) case.

2.8 Selected Numerical Results and Discussion

Versatile computer programs have been developed using the formulations of the proceeding sections for the imperfectly conducting and dielectric cylinders. Some representative computations obtained with these programs are given in this section. The validity of the formulations can be verified in various ways. One important method is to compare the results obtained for the specific case of imperfectly conducting and dielectric circular cylinders with exact results, which can be obtained by an analytical method. Exact formulas for the scattering by a homogeneous dielectric circular cylinder is given in [41]. Also, an analytical solution for a circular cylinder with constant surface impedance is given in [23]. The solution for other geometries, such as elliptic and rectangular cylinders, can be compared against results obtained using method of moments solutions [18] and [19].

2.8.1 Results for Circular and Elliptic Cylinders

Figures 2.4 and 2.5 compare the results for an imperfectly conducting circular cylinder of $k_o a = 3.33$, where a is the radius of the cylinder, for TE and TM problems respectively. The cylinder of permittivity $\epsilon_r = 1 - j11.3$ is excited by an incident plane wave with $\phi^i = 180^o$. These figures compare the scattered echo width σ using the MFCM with IBCs for constant and curvature dependent surface impedance $Z_c(\rho)$ with the exact analytical solution [41] . For the present formulation, a set of $N = 18$ filament sources is placed on a circular surface of radius $r^I = 0.5a$ and the number of the matching points $N^c = N$ is used. The sources and the matching points are evenly spaced on their respective surfaces. The agreement in Figs. 2.4 and 2.5 between results based on the exact analytic solution and the numerical method for both TE and TM problems is excellent, indicating the high accuracy of

the present numerical method.

Figures 2.6 and 2.7 compare the forward scattering and backscattering echo widths, respectively, versus the normalized penetration depth δ/a using MFCM with IBCs, with both constant and curvature dependent surface impedance $Z_c(\rho)$, with the exact analytical solution [41]. The results are for an imperfectly conducting circular cylinder with $\sigma_c = 0.5S/m$ immersed in a transverse electric TE wave with $\phi^i = 180°$. It is seen that the error in the scattered field obtained using the MFCM-IBCs with constant surface impedance Z_c increases by increasing the normalized penetration depth δ/a. However, the curvature dependent $Z_c(\rho)$ solution gives very accurate results for all considered values of δ/a.

Figure 2.8 shows the normalized total magnetic field $(E_z^i + E_z^s)$ evaluated at the surface of a circular cylinder of $k_o a = \pi$ and $\epsilon_r = 1 - j12$. The figure shows good agreement between the exact analytical solution and the MFCM with IBC.

Figure. 2.9 compares the results for the scattering echo width of an imperfectly conducting elliptic cylinder using the MFCM-IBCs and the method of moments (MoM) [19]. The result is for an elliptic cylinder with $k_o a = 3$, $a/b = 2$, $\epsilon_r = 1 - j9.63$, and $\delta/a = 8.7\%$, and excited by an incident plane wave of $\phi^i = 0°$. The result shows good agreement between the (MoM) solution and the present method using a constant surface impedance Z_w and better agreement is obtained when the curvature dependent $Z_c(\rho)$ is used. The number of sources used is $N = 23$ for this method, and 90 for the MoM solution.

Figures 2.10, 2.11 and 2.12 compare the scattered field from a circular cylinder using analytical solution based on IBCs [40] and MFCM for TE and TM problems. The results are for circular cylinders with $k_o a = \pi$ and constant surface impedance Z_w of $j300$, $-j300$ *and* $(300 + j300)\Omega$, respectively. The cylinders are immersed in an incident plane wave with $\phi^i = 180°$. The plots show that the results obtained

using MFCM with IBCs, for different types of coating materials, are in excellent agreement with the analytical solution.

Finally, to study the effect of resistive coatings on the scattered fields Figs. 2.13 and 2.14 are included. These figures compare the scattered field from a circular cylinder using analytical solution based on IBCs [40] and MFCM for TE and TM problems, respectively. The results are for circular cylinders with $k_o a = \pi$ and constant real surface impedance Z_w of 300, 335 *and* 375Ω, respectively, and $\phi^i = 180^o$. Here, we notice the reduction in the amplitude of the backscattering corresponding to $\phi = 180^o$ by increasing the surface impedance.

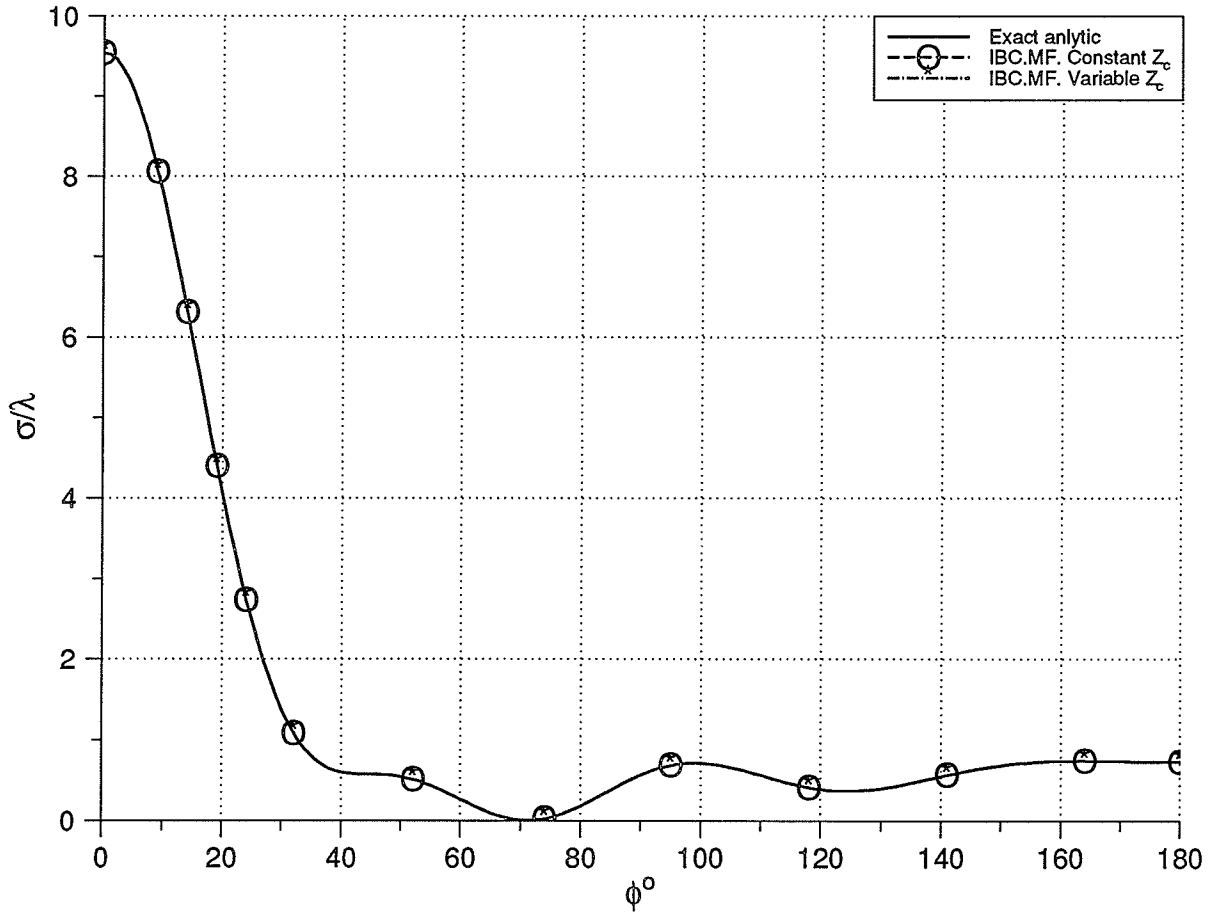

Figure 2.4: TE plot of the echo width versus ϕ for the case of a circular cylinder of $k_o a = 3.33$ $\epsilon_r = 1. - j11.3$ and $\delta/a = 12\%$

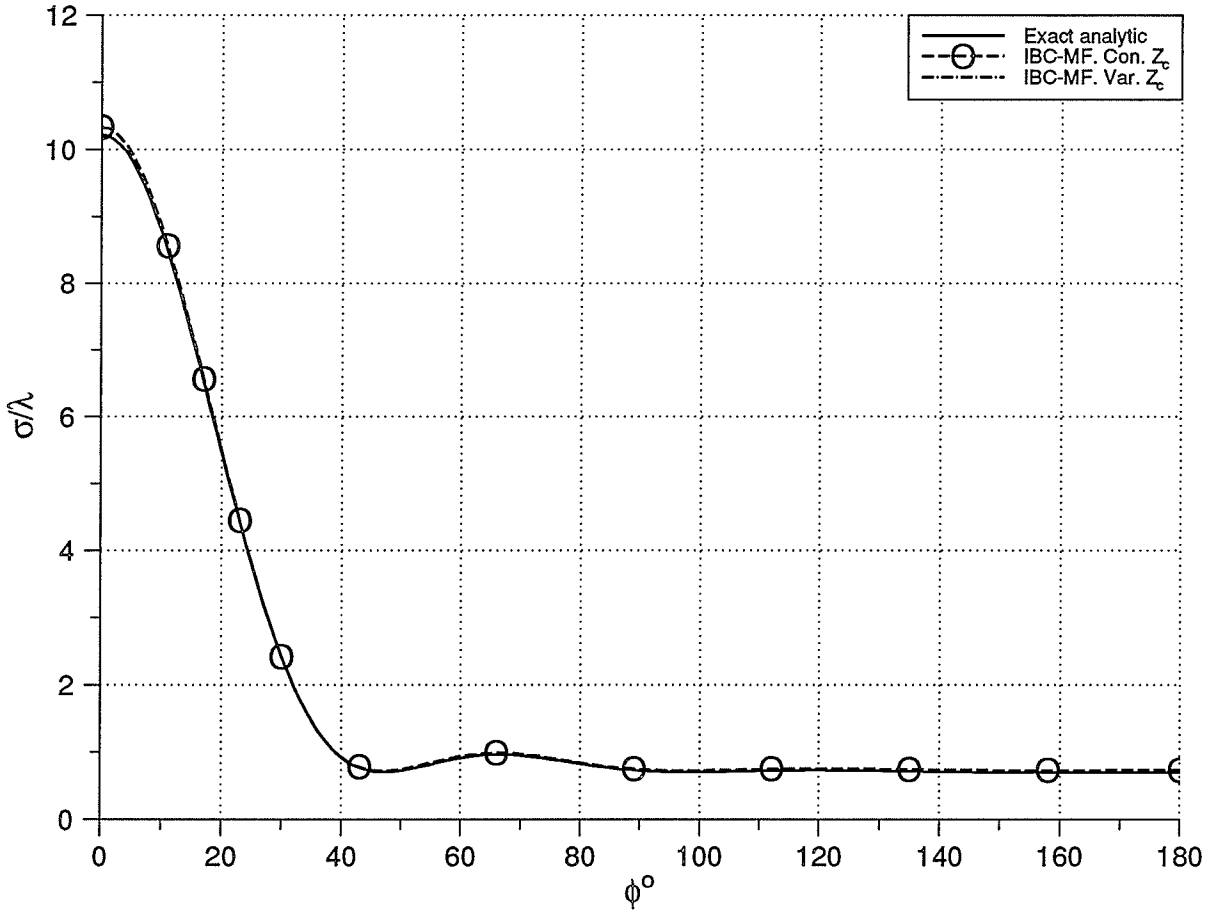

Figure 2.5: TM plot of the echo width versus ϕ for the case of a circular cylinder of $k_o a = 3.33$ $\epsilon_r = 1. - j11.3$ and $\delta/a = 12\%$

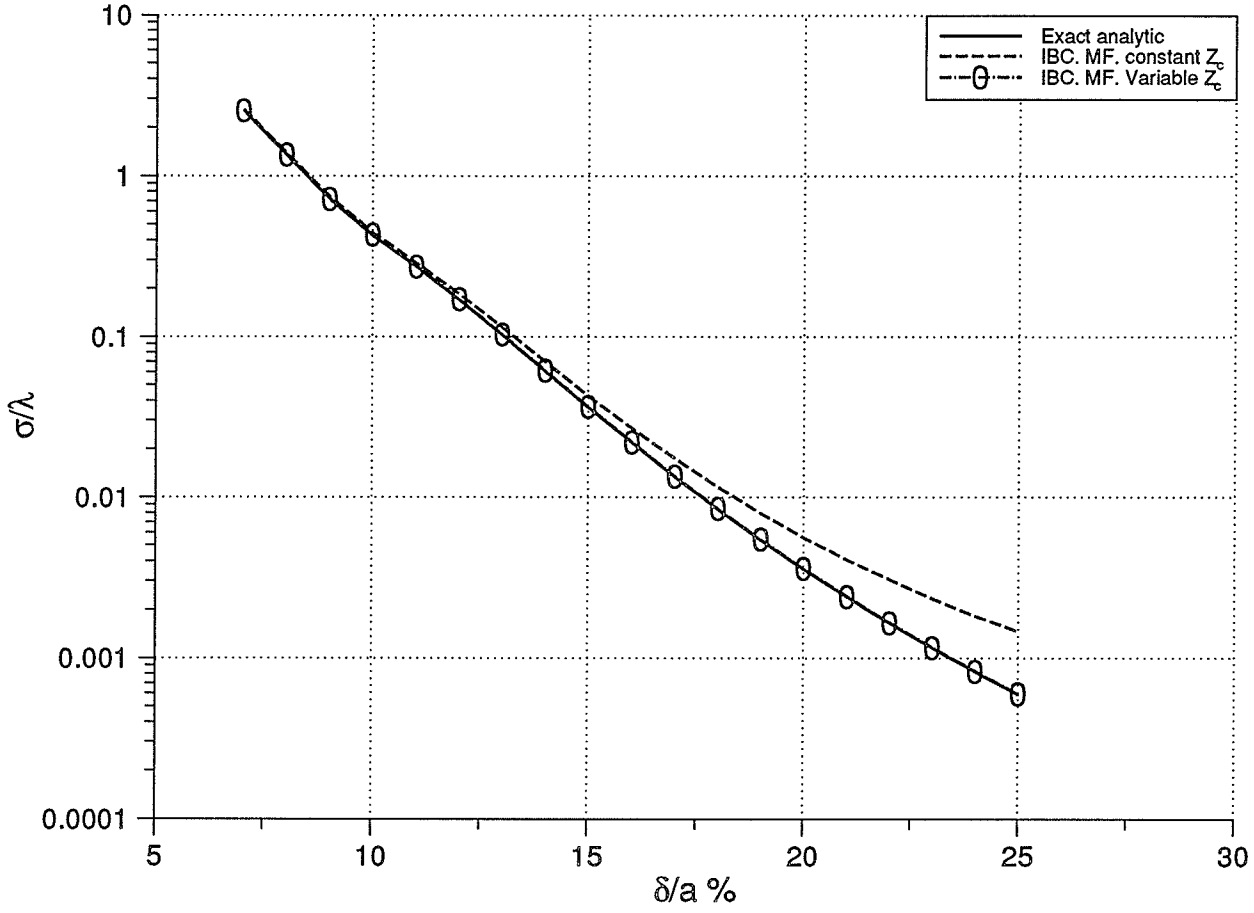

Figure 2.6: TE plot of the forward scattering versus δ for the case of a circular cylinder of $a = 1m$ and $\sigma_c = 0.5(S/m)$

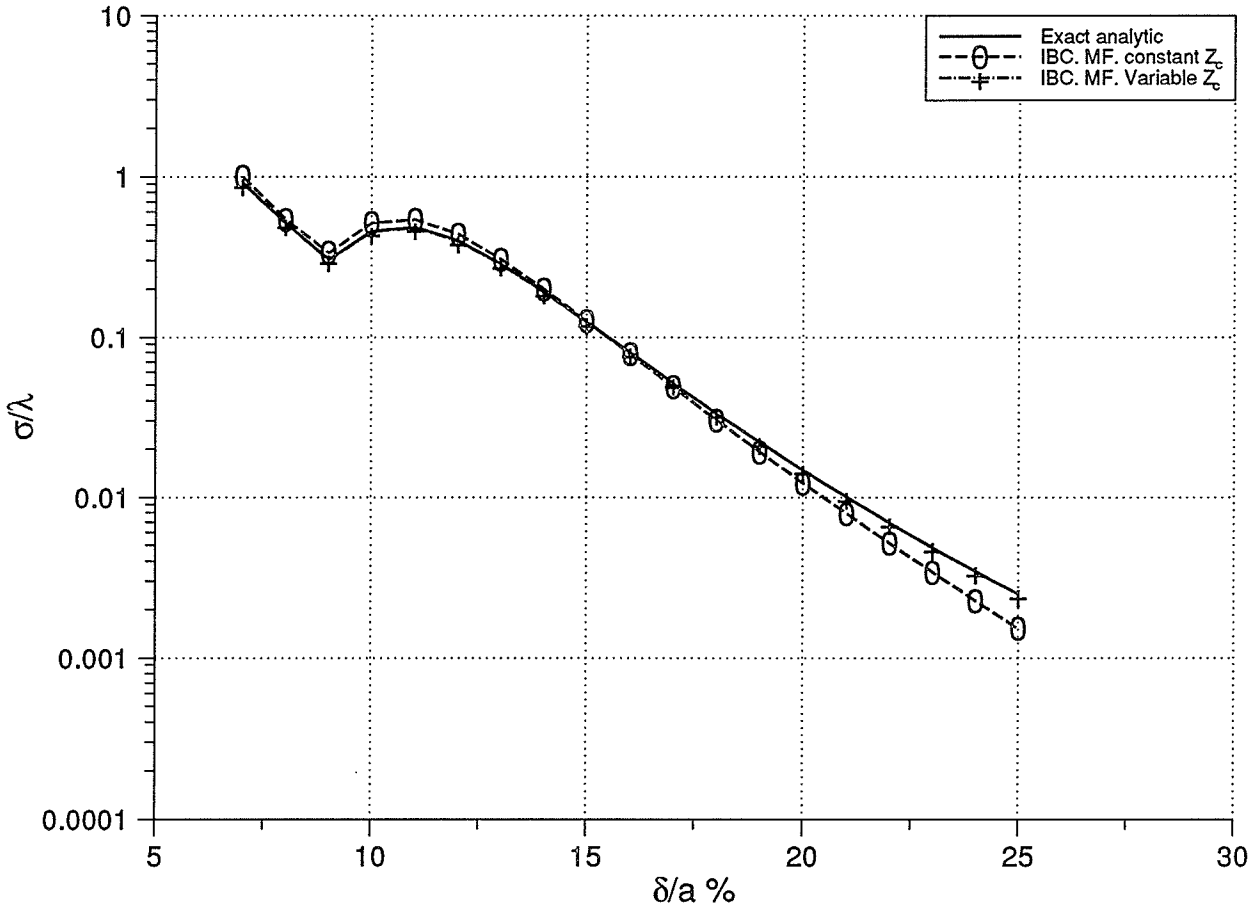

Figure 2.7: TE plot of the backscattering versus δ/a for the case of a circular cylinder of $a = 1m$ and $\sigma_c = 0.5(S/m)$

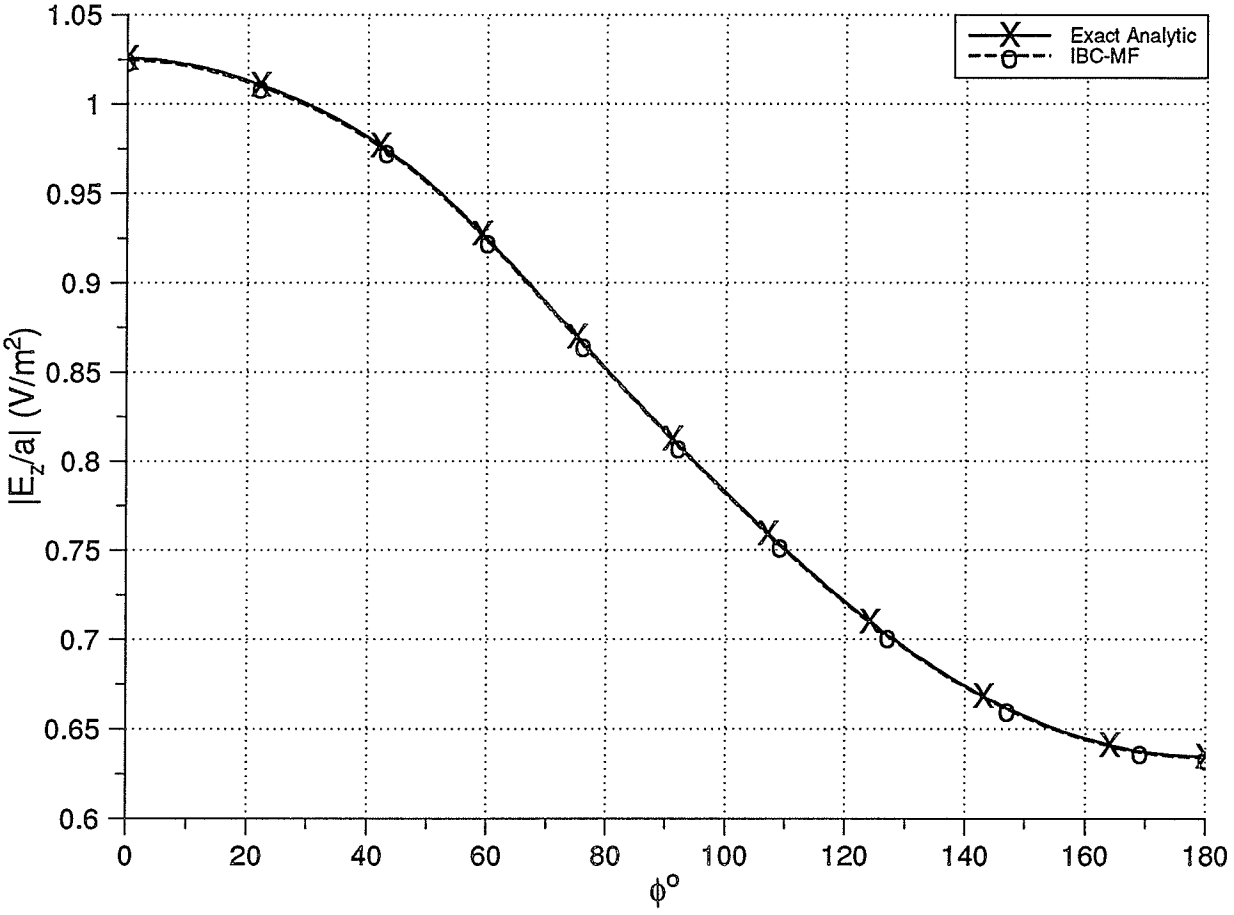

Figure 2.8: TM plots of the total normalized tangential electric field versus ϕ for the case of a circular cylinder of $k_o a = \pi$ and $\epsilon_r = 1. - j11.3$

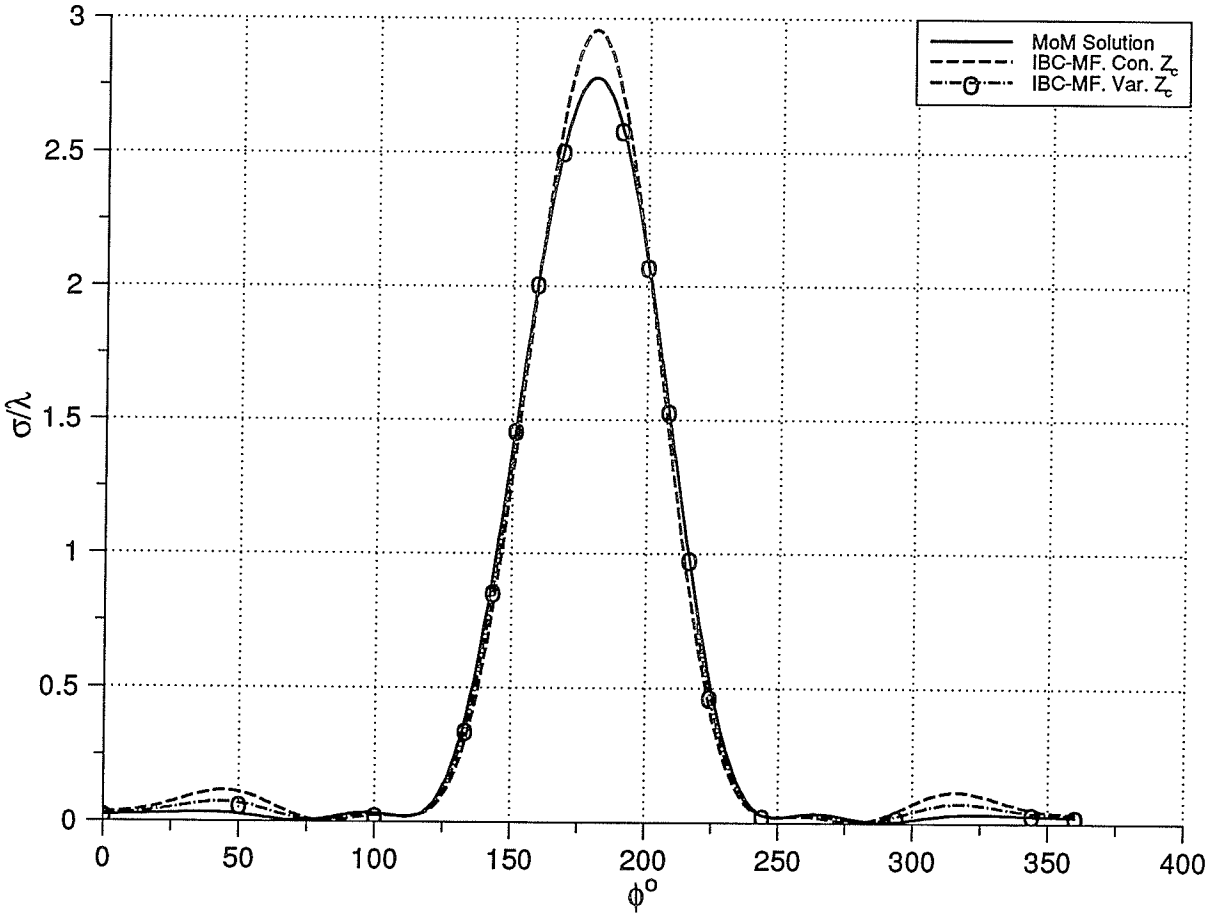

Figure 2.9: TE plot of the echo width versus ϕ for the case of a lossy elliptic cylinder of $k_o a = 3$, $a/b = 2$ $\epsilon = 1 - j9.63$ and $\phi^i = 0^o$

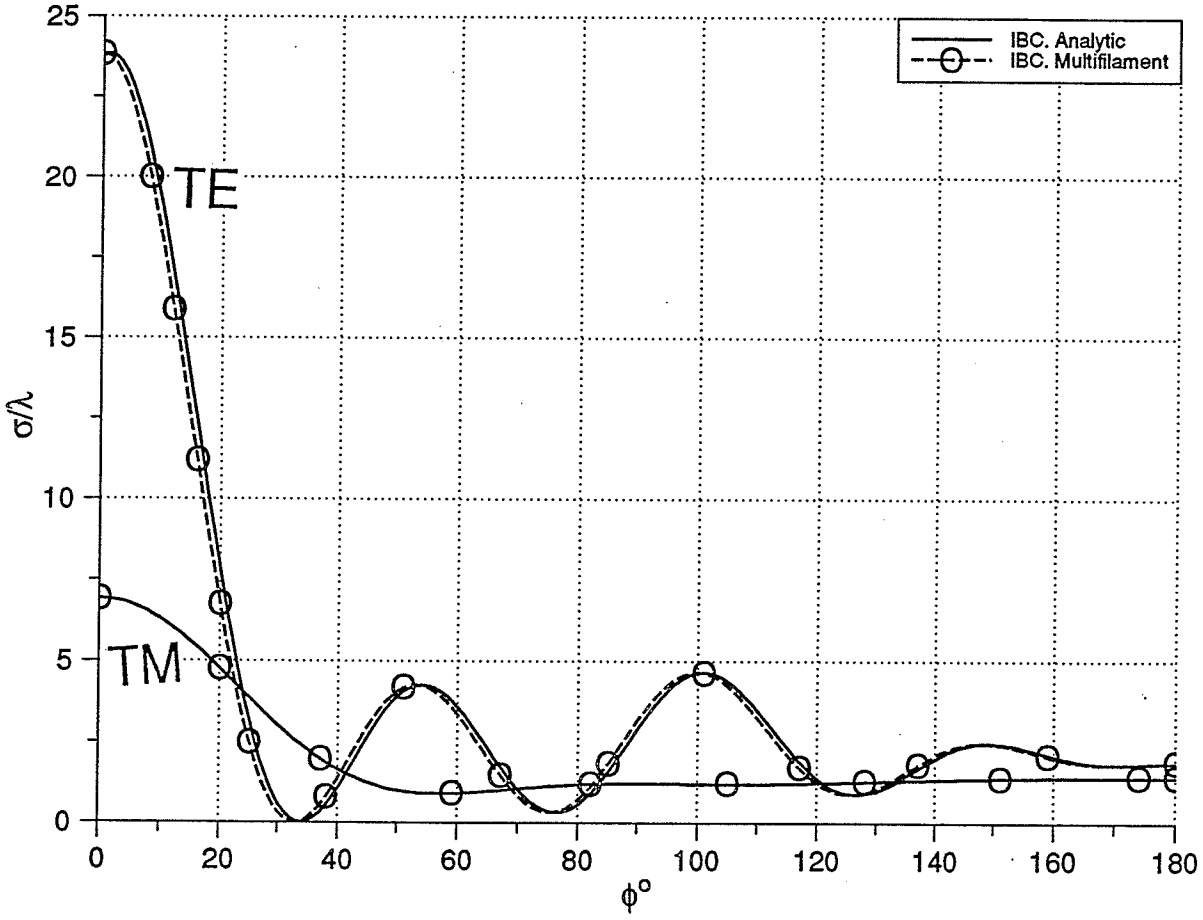

Figure 2.10: Echo width versus ϕ for the case of a circular cylinder of $k_o a = \pi$ and $Z_w = j300\Omega$

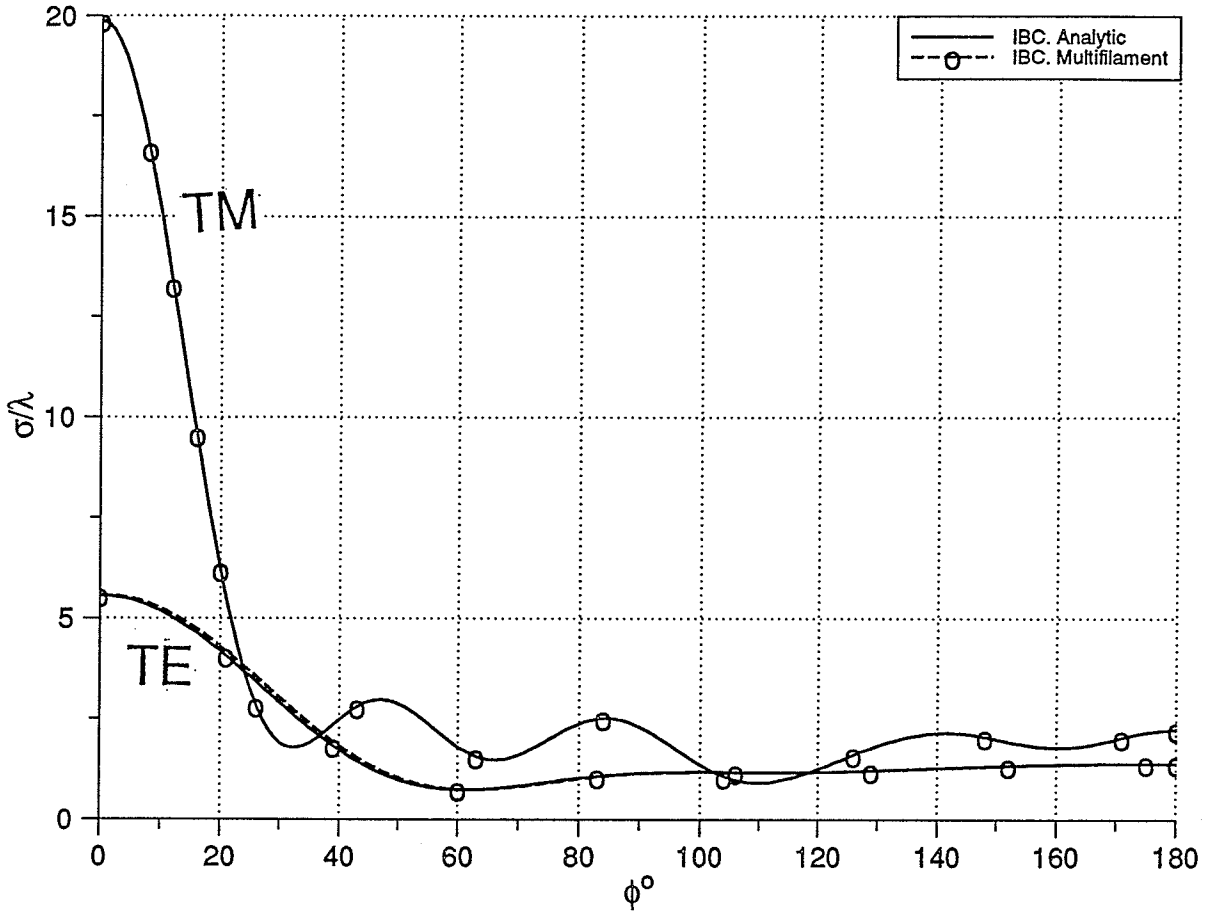

Figure 2.11: Echo width versus ϕ for the case of a circular cylinder of $k_o a = \pi$ and $Z_w = -j300\Omega$

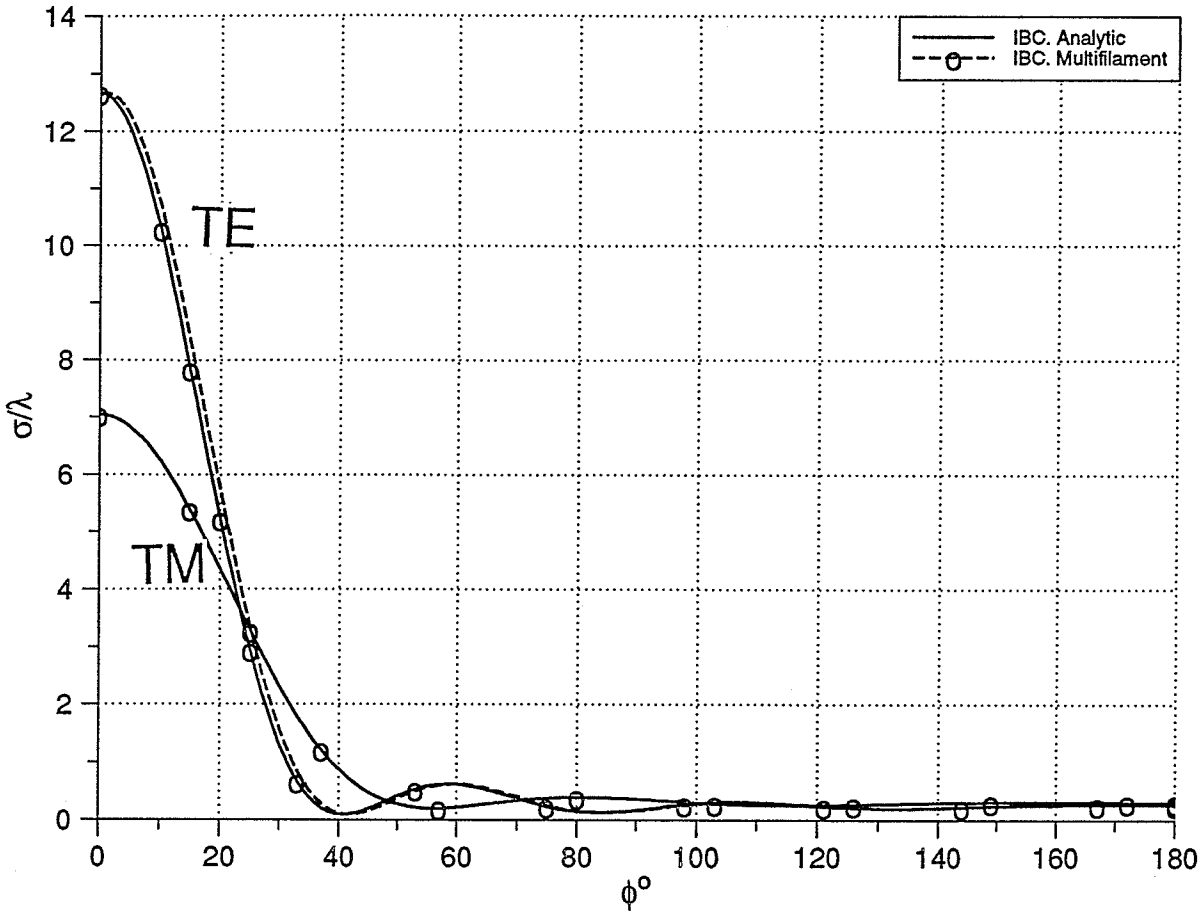

Figure 2.12: Echo width versus ϕ for the case of a circular cylinder of $k_o a = \pi$ and $Z_w = 300 + j300\Omega$

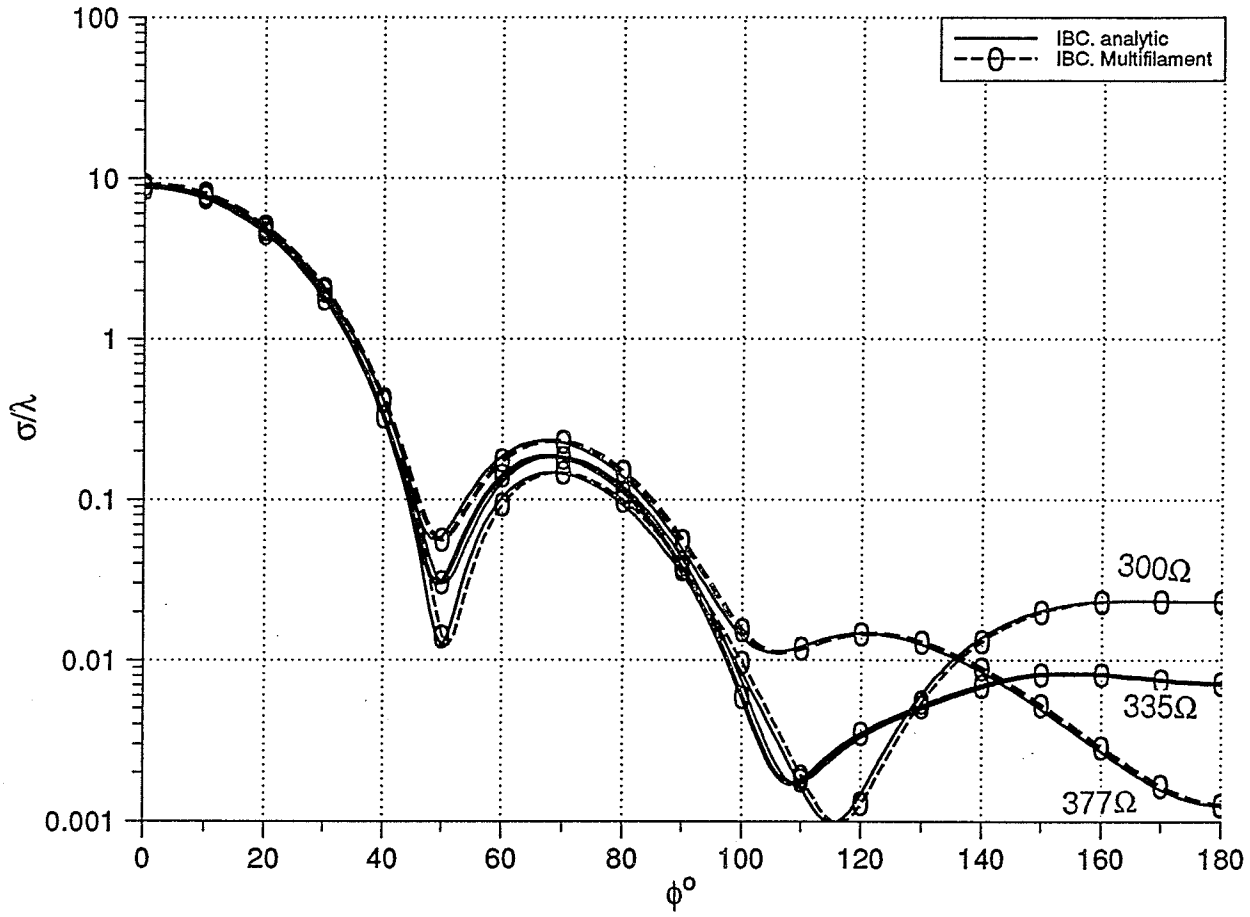

Figure 2.13: TE plots of the echo width versus ϕ for the case of circular cylinders of $k_o a = \pi$ and $Z_w = 300$, 335 and 377Ω

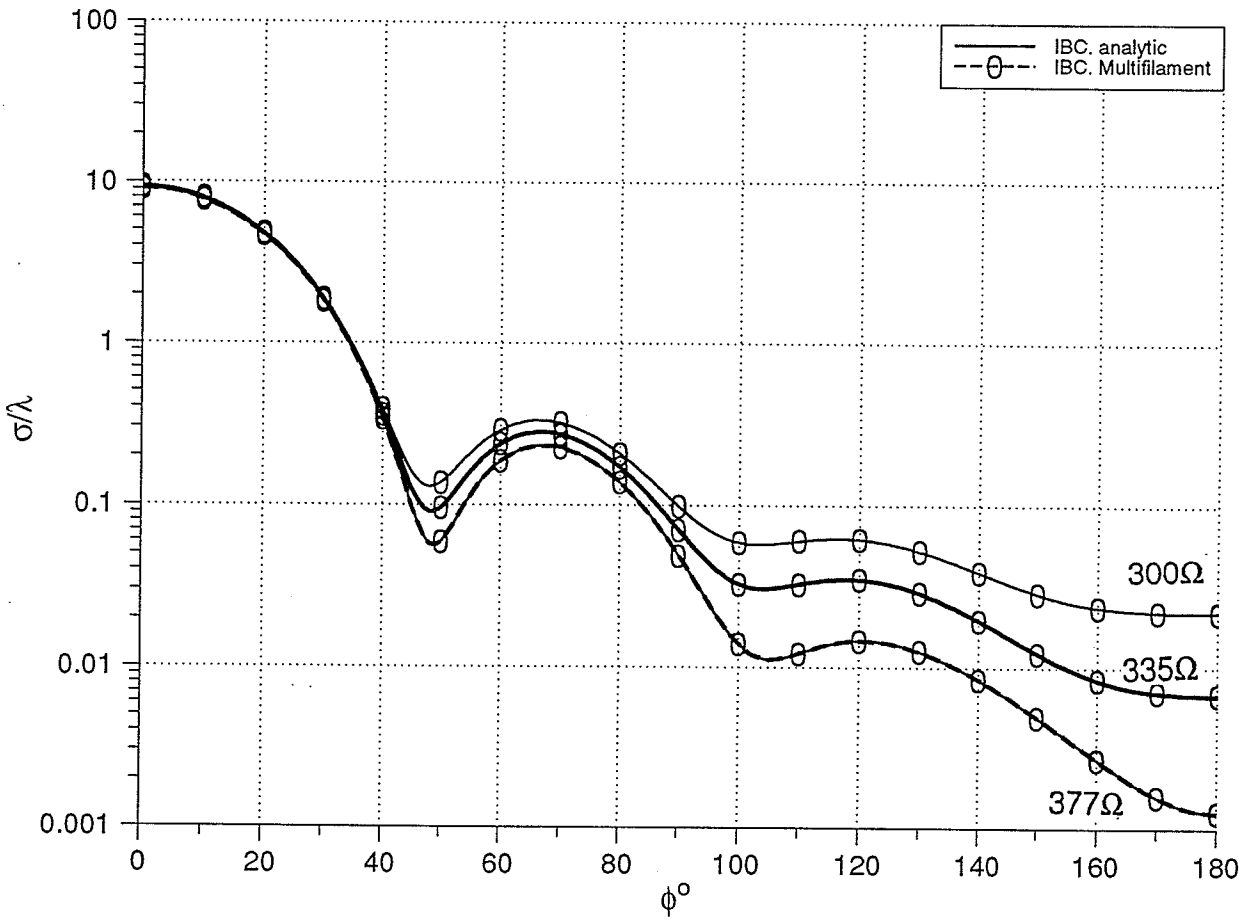

Figure 2.14: TM plots of the echo width versus ϕ for the case of circular cylinders of $k_o a = \pi$ and $Z_w = 300$, 335 and 377Ω

2.8.2 Numerical Consideration for Circular and Elliptic Cylinders

The special choice of equal number of sources N^I and matching points N^C which was used to obtain the preceding results was examined in other cases involving circular and elliptic cylinders of other radii and permittivities. It was found that the rate of convergence may be affected by the choice of the locations and the number of sources and matching points. According to studies done by Leviatan *et.al.* [21], [22] and the preceding results, the solution converges faster to a limiting value when the sources are placed on contours concentric with the cross section of the cylinder and of a shape similar to it. This implies that, for the circular cross section, the sources are placed on a circular surface of radius r^I. In addition, it was found that the selection of r^I between $0.05a$ and $0.95a$ have a comparable rate of convergence. Fig. 2.15 shows the convergence of the solution to the exact analytical solution for the case of a circular cylinder of $k_o a = \pi$ and $\epsilon_r = 2.6 - j5$. The sources are placed at $r^I = 0.95a$. The number of sources was increased from $N^I = 10$ to $N^I = 35$. The number of matching points was taken to be equal to the number of sources in each case. Furthermore, the option of imposing the boundary condition in the least square sense is also considered. It was found although in some cases the same accuracy can be obtained with fewer sources, thereby gaining the advantage of solving smaller matrices, in general this option is redundant for the case of circular cylinders. In addition, the solution should be tested by increasing the number of sources and matching points. The solution's convergence to a limiting value shouldn't be too sensitive to the change in the location of the sources within the range mentioned above. In any case, if the results are too sensitive to the change in the sources locations, the number of sources and matching points should be increased.

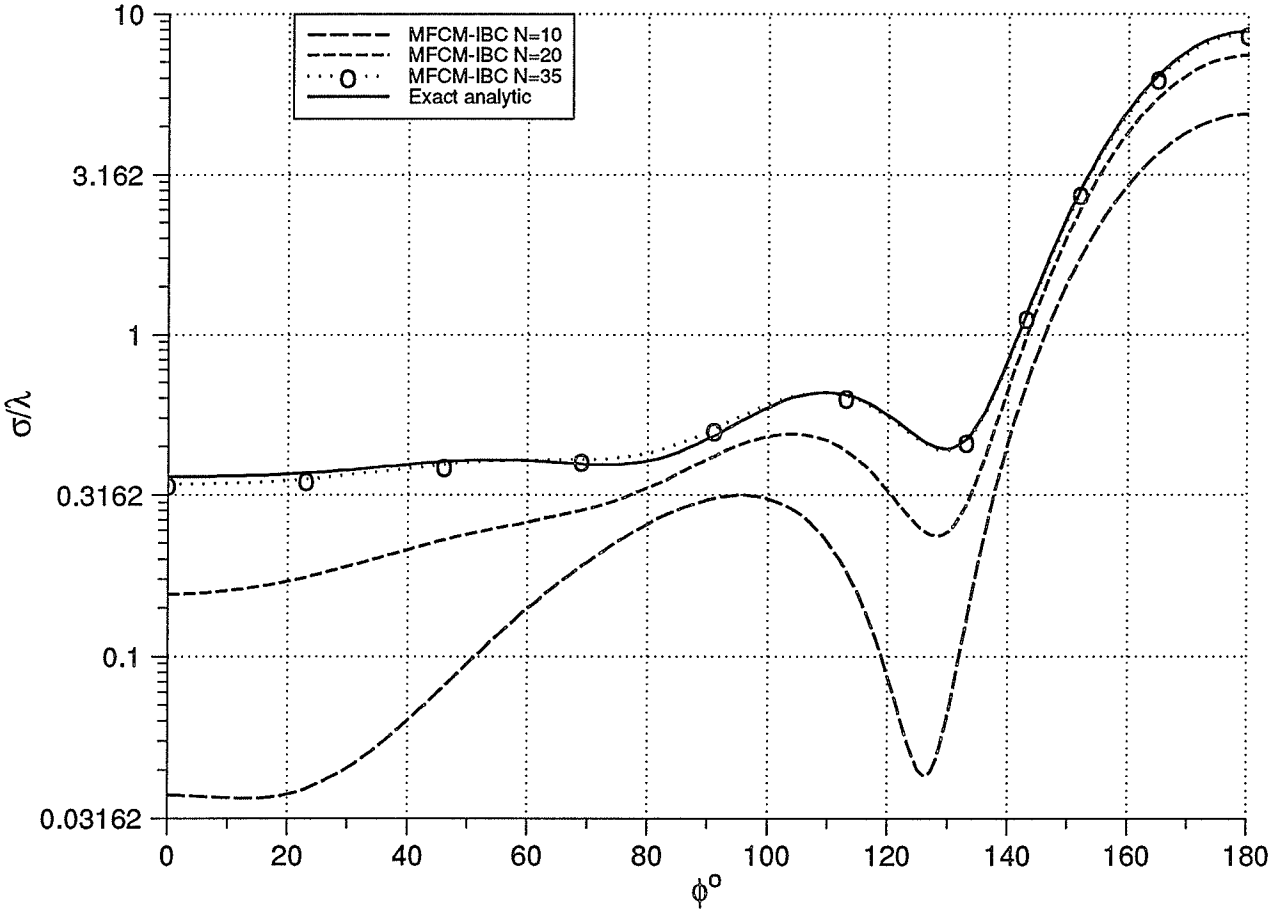

Figure 2.15: TM plot of the echo width versus ϕ for the case of a circular cylinder of $k_o a = \pi$ $\epsilon_r = 2.6 - j5$ for different number of sources

2.8.3 Results for Square Cylinders

Figure. 2.16 compares the results for a perfectly conducting square cylinder obtained using the multifilament current model, the generalized multiple multipoles technique and the moment of method solutions. The cylinder of $kl = 2\pi$, where l is the side length, and excited by an incident transverse magnetic TM plane wave with $\phi^i = -45^o$. For the MFCM solution, a technique developed by Eisler [42] is used to select the locations of the filamentary sources. The scattered field has been simulated by three sets of sources as shown in Fig. 2.18: (i) 48 filaments evenly spaced on a concentric square surface situated at a distance $d = 0.1\lambda$ from the boundary C; (ii) 16 filaments at a distance 0.01λ from the edges, 2 filaments on each side of each edge; and (iii) 24 filaments gradually connecting the former two sets. The number of matching point $N^C = N^I$ is used and distributed evenly on the boundary surface. For the GMMP solution, the scattered field has been simulated by two sets of multipoles line sources as shown in Fig. 2.19: (i) 36 multipoles of order zero evenly spaced on a concentric square surface situated at a distance $d = 0.1\lambda$ from the boundary C; (ii) a set of 4 multipoles of order one, one multipole situated at each corner at a distance 0.01λ from the boundary. In this case, the number of unknown expansion coefficients is $M = \sum_{i=1}^{N^I}(2N_i^I + 1) = 48$. The number of the matching point $N^C = 3M$ is used. As shown in Fig 2.16, the agreement between results based on the MFCM solution, the GMMP and the MoM is excellent.

Figure. 2.17 shows the results for a perfectly and imperfectly conducting square cylinder obtained using the generalized multiple multipoles technique. The cylinders of $kl = 2\pi$, where l is the side length, and $\epsilon_r = 10.0 - j3.0$ for the imperfectly conducting. The cylinders are excited by an incident transverse magnetic TM plane wave with $\phi^i = -0^o$. The selection of the sources and matching points are the same ones used to obtain Fig. 2.16.

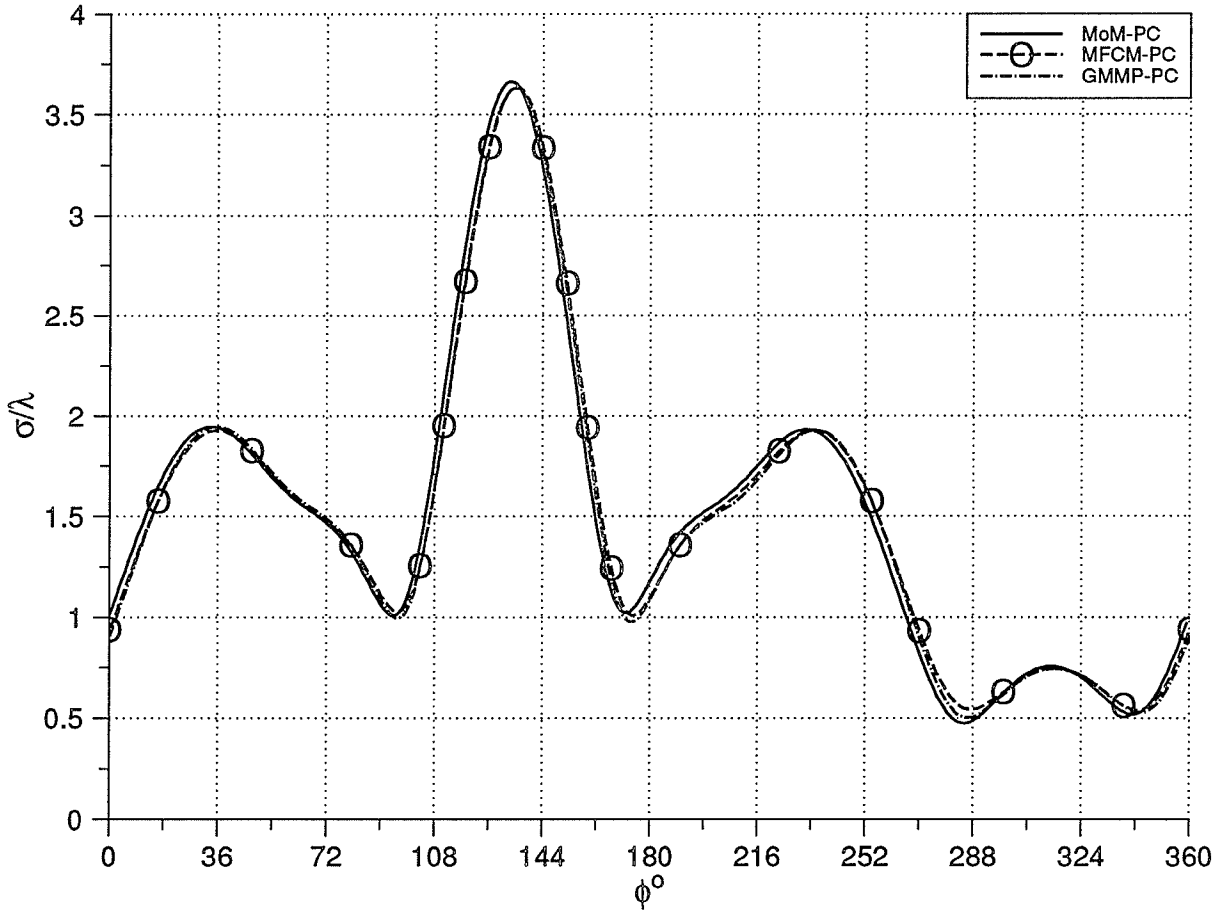

Figure 2.16: TM plots of the echo width versus ϕ for the case of a square cylinder of $k_o l = 2\pi, \phi^i = -45^o$

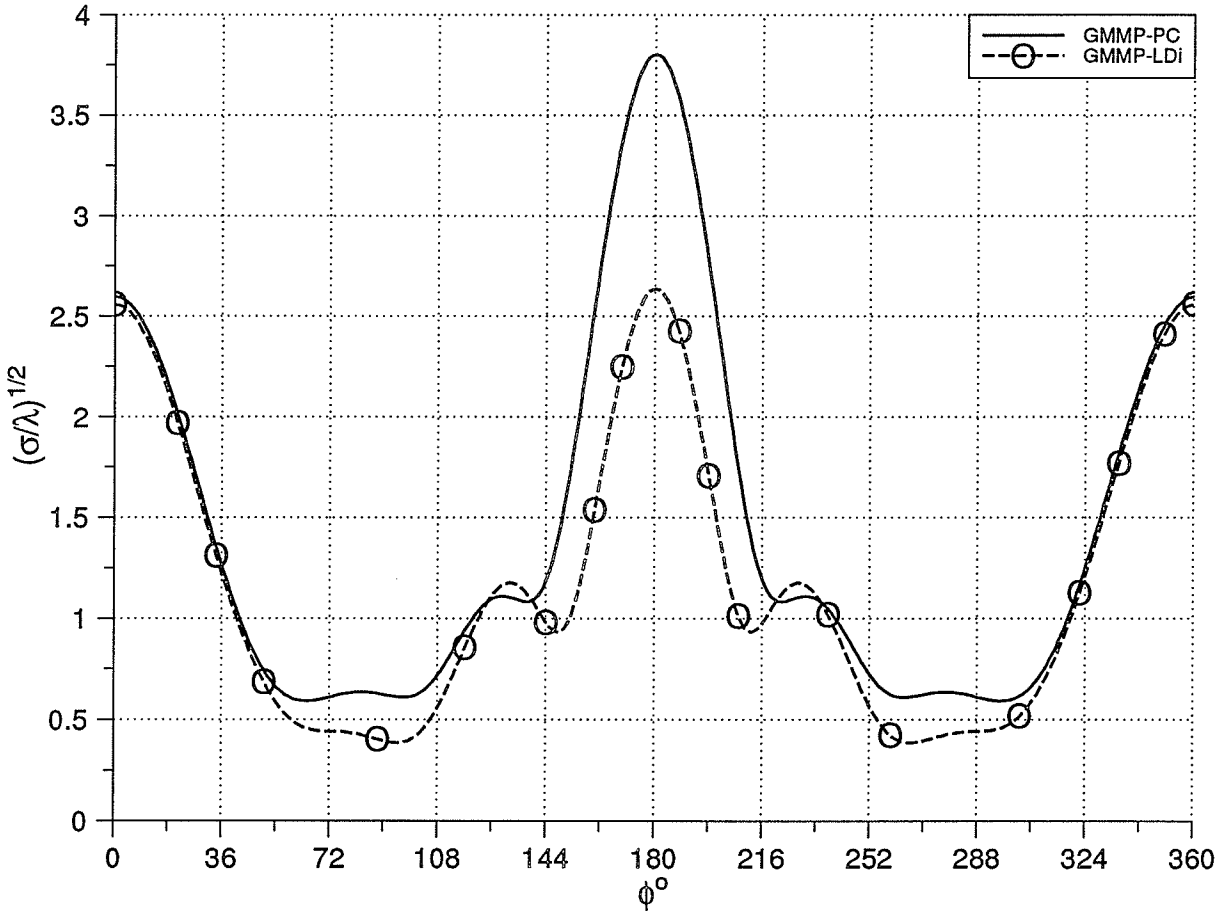

Figure 2.17: TM plots of the echo width versus ϕ for the case of a square cylinder of $k_o l = 2\pi$, $\phi^i = 0^o$

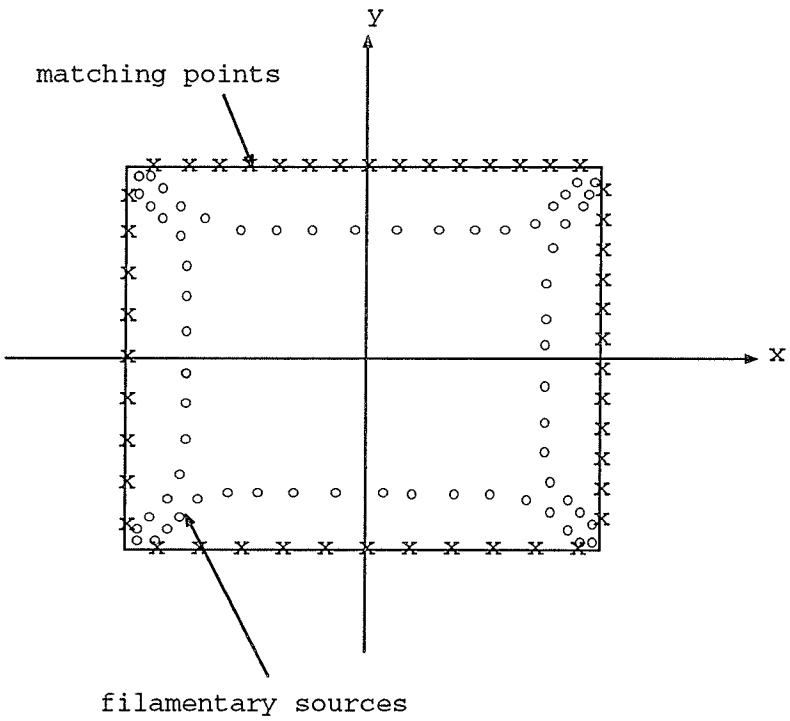

Figure 2.18: Locations of the filamentary sources and matching points

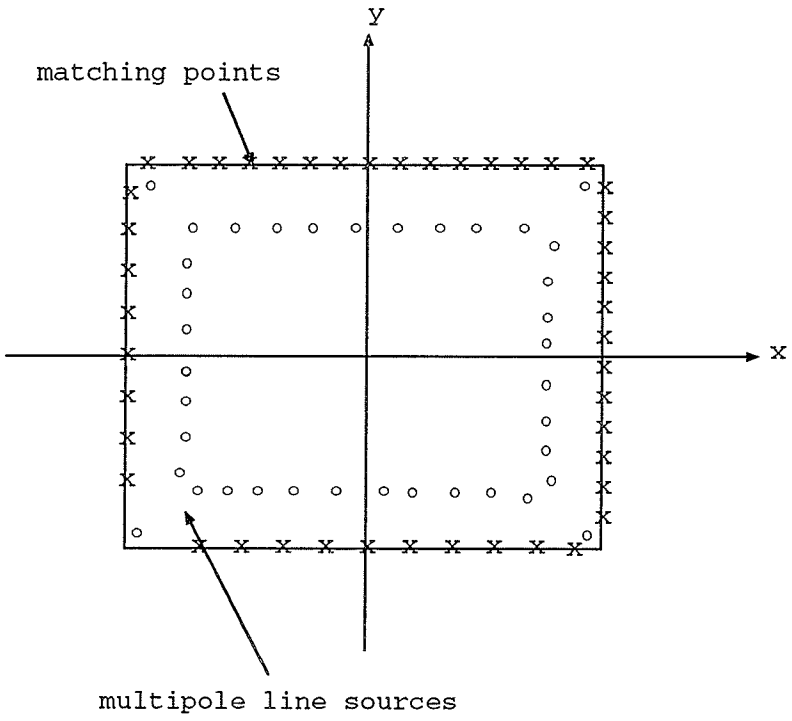

Figure 2.19: Locations of the multipole line sources and matching points

2.8.4 Numerical Consideration for Square Cylinders

As for the cylinders of smooth cross section, the rate of convergence may be affected by the choice of the sources locations, number of unknowns and number of matching points. Since, for the rectangular cylinders , the fields near the edges are inherently singular, the errors are expected to be higher than the rest of the surface. Therefore special consideration should be given to the edges. The MFCM and the GMMP simulations differ in the method by which they treat the singularity of the fields in the edges. Fig. 2.18 illustrates the distribution of the filamentary sources inside a square cylinder. This choice of locations reduces the errors in the boundary conditions and gives accurate results for the square cylinders. Furthermore, the accuracy of the solution can be improved by increasing the number of sources and the number of matching points.

Figure 2.19 illustrates the distribution of the multipoles line sources inside a square cylinder. In this configuration, all distance of multipoles along the straight line have constant values. Since the field near the edges is rapidly changing, one multipole is placed very close to the boundary in each corner of the rectangular cross section. According to Hafner [3], the fields of higher order multipoles are much more concentrated around its origin than the fields of lower order multipoles. Therefore, the multipoles close to the edges must be of higher order to allow the domain of the greatest influence of the multipole to cover that part of the boundary around the edges. The domain of the greatest influence of the multipoles is a circle around its origin with radius R which is the minimum distance d from the boundary multiplied by a factor of $\sqrt{2}$. Fig. 2.20 shows the effect of changing the locations of the first order multipoles on the convergence of the solution. It is seen that the closer the higher order multipoles to the boundary the more accurate solution is obtained. No other multipoles should be inside the domain of great influence of any

multipoles in order to avoid the dependency between the multipoles, hence avoiding an ill conditioned matrix. The numerical accuracy can be improved by controlling the number of the multipoles, the corresponding truncation order and the number of matching points. It was found that the over-determined system of linear equations gives a more accurate result and the solution converges faster than the case of a well determined system. Good results may be obtained when three times as many equations as unknowns are used. Again, it is evident and understandable that a large cylinder of high permittivity will require more sources and matching points than a smaller one of lower permittivity in order to achieve the same level of accuracy. In addition, the solution should be tested by increasing the number of sources and matching points. The convergence of the solution to a limiting value shouldn't be too sensitive to the location of the sources. In any case, if the results are too sensitive to the change in the location of sources, the number of sources and matching points should be increased.

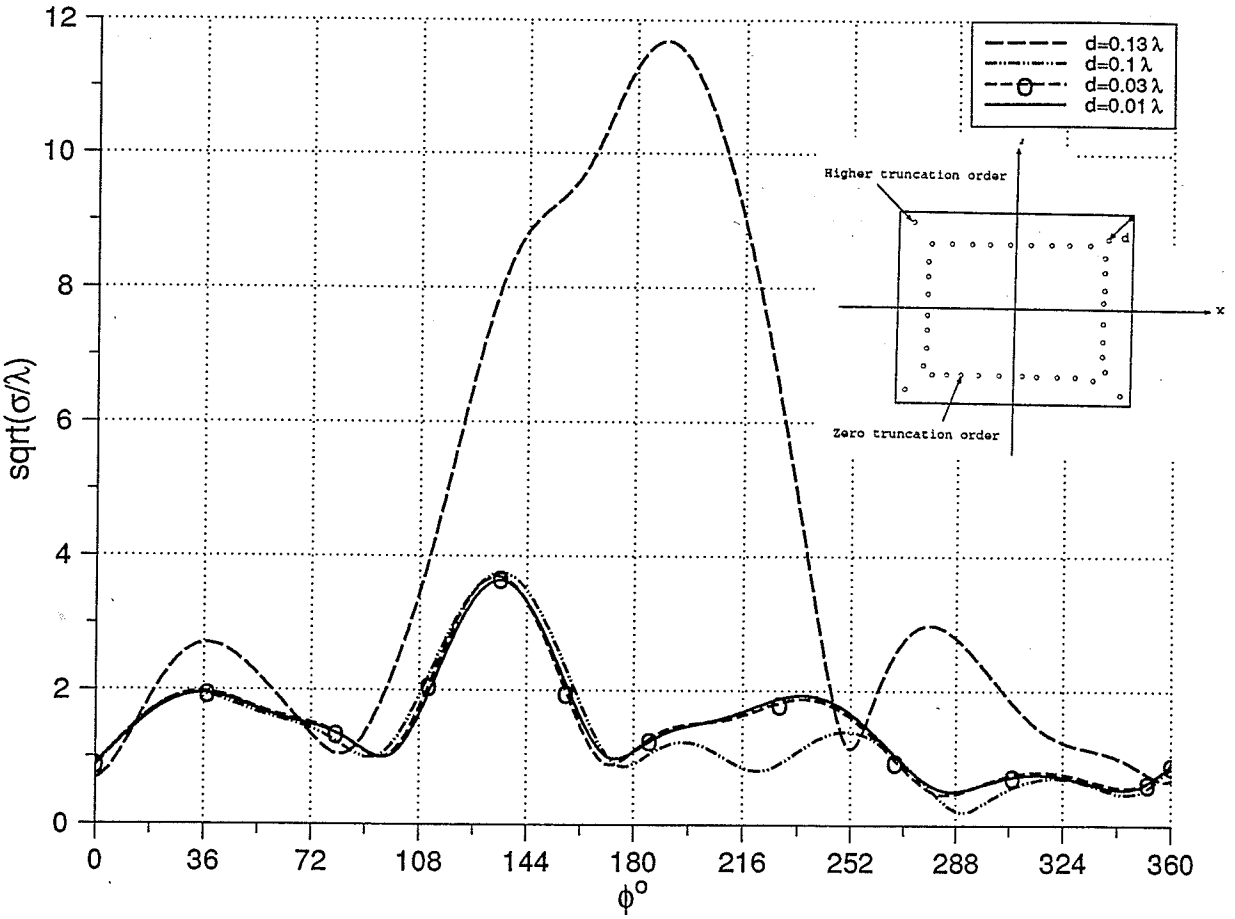

Figure 2.20: TM plots of the echo width versus ϕ for the case of a square cylinder of $k_o l = 2\pi$ with different location of sources

CHAPTER 3

Multiple Scattering by Parallel Cylinders

3.1 Introduction

In this chapter, the multifilament current model [21], [22] is used to solve the problem of multiple scattering by parallel cylinders of arbitrary cross sections. The problem is classified into two parts; transverse magnetic (TM) and transverse electric (TE) according to the type of excitation. For each excitation type, the formulation is carried out for the problems of homogeneous dielectric and imperfectly conducting cylinders. For the case of homogeneous dielectric cylinders, the problem is formulated using two sets of fictitious filamentary sources to simulate the fields of each cylinder. For each cylinder, one set of sources is placed inside it to simulate its scattered fields. The other set of sources is placed outside each cylinder to simulate the fields inside the respective cylinder. Application of the boundary conditions yields a system of linear equations which can be solved for the unknown filamentary currents .

For imperfectly conducting cylinders, as stated in chapter 2, the surface impedance boundary conditions (IBC) simplify the formulation by eliminating the need for the inclusion of the interior field [40]. Therefore, only one set of filamentary sources is needed to simulate the fields of each cylinder. This set of sources is placed inside each cylinder to simulate its scattered field. Again, application of the IBC results in a system of linear equations which can be solved for the unknown filamentary currents. The case of perfectly conducting cylinders can be handled as a

special case of the imperfectly conducting cylinders by setting the surface impedance to zero. Once the strengths of the filamentary currents are computed, the scattered field and other parameters of interest can be obtained. In the following sections, the formulation will be carried out in details for homogeneous dielectric and imperfectly conducting cylinders, for the TM case. The solution for the TE case will be discussed in a later section. Results for the normalized echo width for selected geometries of arbitrary cross sections and of various parameters are presented.

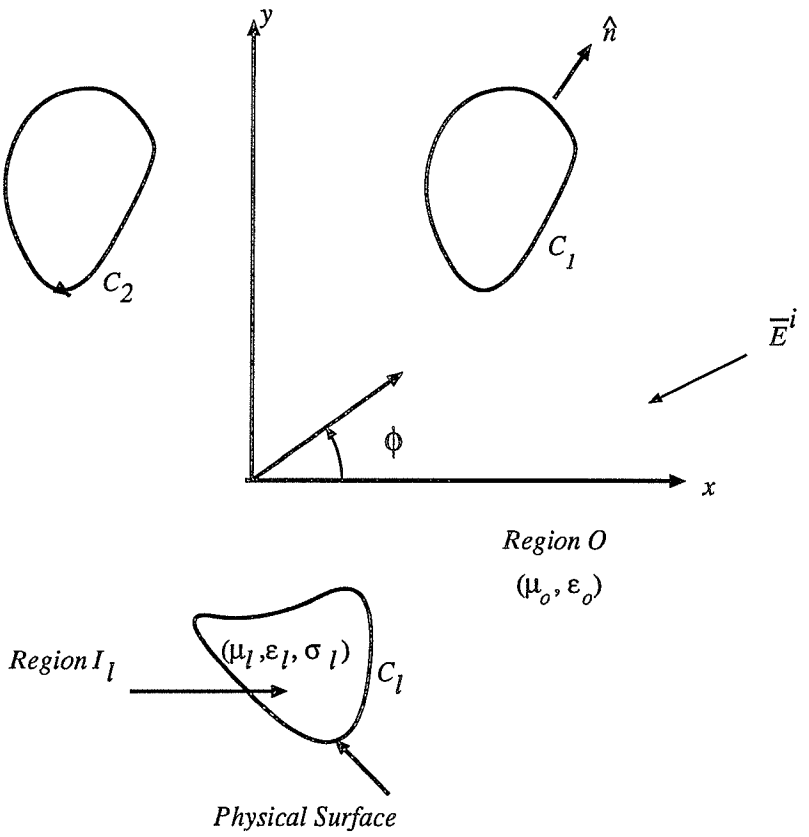

Figure 3.1: Geometry of the problem

3.2 Description of the Problem for TM case

The scattering geometry considered is shown in Fig. 3.1. Consider M parallel cylinders of arbitrary cross sections whose axes are taken to be parallel to the $z-$ axis of a rectangular coordinate system. The l^{th} cylinder is composed of a homogeneous dielectric material of permittivity ε_l, permeability μ_l, and conductivity σ_l, where $l = 1, 2...M$. The region surrounding the cylinders is free space of permittivity ε_o and permeability μ_o.

Let the cylinders be immersed in an incident transverse magnetic plane wave (TM) characterized by

$$\bar{E}^i = \hat{u}_z E_z^i \tag{3.1}$$

$$\bar{H}^i = \hat{u}_x H_x^i + \hat{u}_y H_y^i \tag{3.2}$$

where the time dependent $e^{j\omega t}$ is understood. Here, $\hat{u}_x$, $\hat{u}_y$, and $\hat{u}_z$ denote the unit vectors in the x, y, and z directions, respectively, and

$$E_z^i = e^{jk_o(xcos\phi^i + ysin\phi^i)} \tag{3.3}$$

$$H_x^i = -\frac{1}{\eta_o} sin\phi^i e^{jk_o(xcos\phi^i + ysin\phi^i)} \tag{3.4}$$

$$H_y^i = \frac{1}{\eta_o} cos\phi^i e^{jk_o(xcos\phi^i + ysin\phi^i)} \tag{3.5}$$

where η_o and k_o are, respectively, the intrinsic impedance and the wave number in free space, and ϕ^i is the angle of incidence. The problem is a two-dimensional one and can be worked out in some z =constant plane because $\bar{E}^i$ is $z-$directed and independent of z and the cylinders cross section is uniform along the z direction.

3.3 Homogeneous Dielectric Cylinders

For homogeneous dielectric cylinders, the objective is to calculate the fields scattered by the cylinders, and the fields transmitted inside the cylinders. Therefore, we set two simulated equivalent situation to the original ones in regions O and I_l shown in Fig. 3.1. In the simulated equivalence for region O, shown in Fig. 3.2, the field scattered by the l^{th} cylinder is simulated by the field of a set of fictitious electric current filaments placed on a closed surface enclosed by C_l, where C_l is the surface of the l^{th} cylinder and $l = 1, 2, 3...M$. These filaments are z directed, infinite

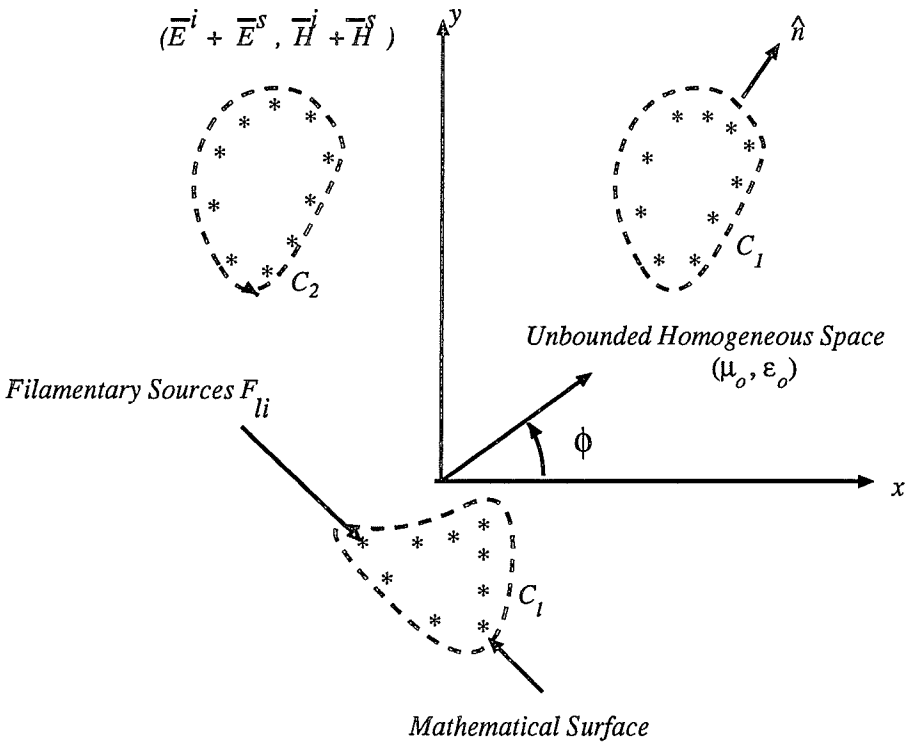

Figure 3.2: Simulated equivalence situation for region O

in extent and carry, yet undetermined, constant currents $F_{li}, i = 1, 2, 3..N_l^F$, where N_l^F is the number of sources inside the l^{th} cylinder. They are treated as electric current sources radiating in free space. In Fig. 3.2, (E^s, H^s) are the electromagnetic

scattered fields due to all fictitious current filaments inside all the cylinders and (E^i, H^i) are the fields of the incident wave as given by (3.1)- (3.5). The total fields $(E^s + E^i, H^s + H^i)$ in the region O are approximations of the fields in region (O) in the original situation. Similarly, in the simulated equivalence for the interior regions I_l, shown in Fig. 3.3, the transmitted fields inside each cylinder are simulated by the fields of M sets of fictitious electric current filaments. The l^{th} set of filament is placed on a closed surface enclosing C_l. Again, these filaments are z directed,

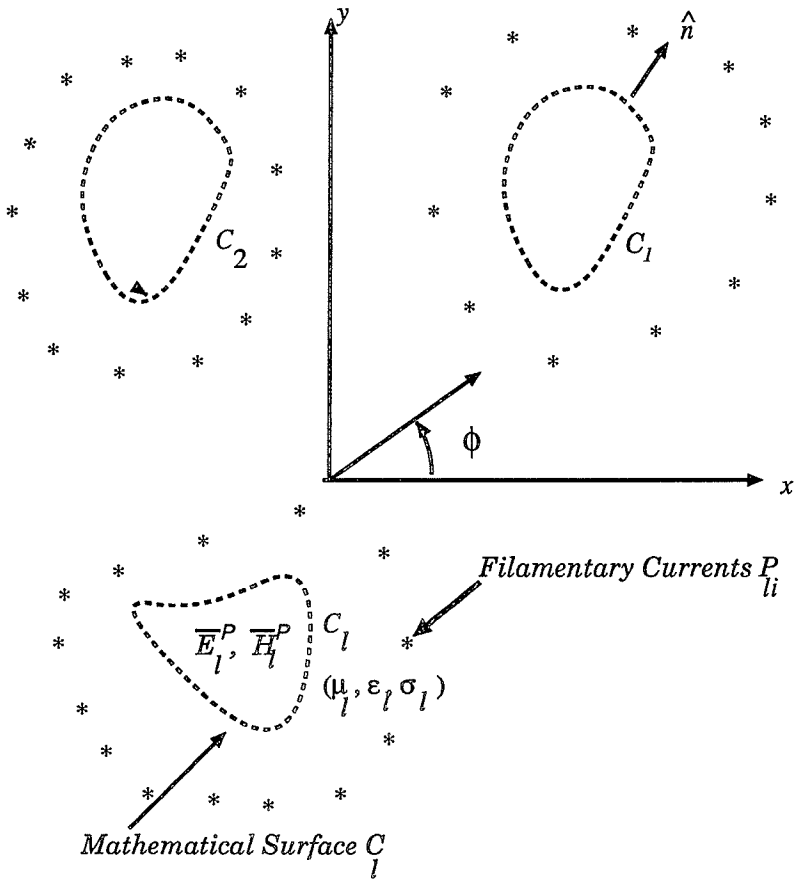

Figure 3.3: Simulated equivalence situation for region I_l

infinite in extent and carry, yet undetermined, constant currents $P_{li}, i = 1, 2, 3..N_l^P$, where N_l^P is the number of filaments surrounding the l^{th} cylinder. The l^{th} set is treated as electric current sources radiating in a space filled with homogeneous

material identical to the material composing the l^{th} cylinder. The fields (E_l^P, H_l^P) due to the fictitious current filaments P_{li} are approximations of the fields in region I_l in the original situation. The relationship between the electromagnetic fields $(E^s + E^i, H^s + H^i)$ and (E_l^P, H_l^P) in the simulated equivalent situations shown in Figs. 3.2 and 3.3, respectively, is dictated by the boundary conditions at the surface of the l^{th} cylinder shown in Fig. 3.1. Specifically, the continuity of the tangential electric and magnetic field components across C_l.

3.3.1 Expressions for E^s and H^s

The scattered fields (E^s, H^s) at an observation point (x, y) in some z =constant plane due to the current filaments $F_{li}, i = 1, 2, 3, ...N_l^F$ and $l = 1, 2, 3, ...M$ radiating in an unbounded free space are given by

$$\bar{E}^s = \hat{u}_z \sum_{l=1}^{M} \sum_{i=1}^{N_l^F} E_{z_{li}}^s \tag{3.6}$$

$$\bar{H}^s = \hat{u}_x \sum_{l=1}^{M} \sum_{i=1}^{N_l^F} H_{x_{li}}^s + \hat{u}_y \sum_{l=1}^{M} \sum_{i=1}^{N_l^F} H_{y_{li}}^s \tag{3.7}$$

where $E_{z_{li}}^s, H_{x_{li}}^s$ and $H_{y_{li}}^s$ are, respectively, the scattered electric and magnetic field components at an observation point (x, y) in region O due to the i^{th} electric current filament F_{li} of the l^{th} cylinder, situated at (x_i^F, y_i^F) inside C_l and are given by

$$E_{z_{li}}^s = -\frac{k_o \eta_o F_{li}}{4} H_o^{(2)}(k_o \rho_i^F) \tag{3.8}$$

$$H_{x_{li}}^s = -\frac{k_o F_{li}(y - y_i^F)}{4j\rho_i^F} H_1^{(2)}(k_o \rho_i^F) \tag{3.9}$$

$$H_{y_{li}}^s = \frac{k_o F_{li}(x - x_i^F)}{4j\rho_i^F} H_1^{(2)}(k_o \rho_i^F) \tag{3.10}$$

Here $H_o^{(2)}$ and $H_1^{(2)}$ are the second kind Hankel functions of zero order and first order, respectively, and

$$\rho_i^F = \sqrt{(x - x_i^F)^2 + (y - y_i^F)^2} \tag{3.11}$$

is the radial distance between the i^{th} source point located inside the l^{th} cylinder and the observation point under consideration.

3.3.2 Expressions for E^P and H^P

The electromagnetic fields (E_l^P, H_l^P) at an observation point (x, y) in region I_l due to the current filaments $P_{li}, i = 1, 2, 3, ...N_l^P$ radiating in an unbounded homogeneous dielectric space is given by

$$\bar{E}^P = \hat{u}_z \sum_{l=1}^{M} \sum_{i=1}^{N_l^P} E_{z_{li}}^P \tag{3.12}$$

$$\bar{H}^P = \hat{u}_x \sum_{l=1}^{M} \sum_{i=1}^{N_l^P} H_{x_{li}}^P + \hat{u}_y \sum_{l=1}^{M} \sum_{i=1}^{N_l^P} H_{y_{li}}^P \tag{3.13}$$

where $E_{z_{li}}^P$, $H_{x_{li}}^P$ and $H_{y_{li}}^P$ are, respectively, the electric and magnetic field components at an observation point (x, y) in region I_l due to an electric current filament P_{li} situated at (x_i^P, y_i^P) outside C_l and are given by

$$E_{z_{li}}^P = -\frac{k_l \eta_l P_{li}}{4} H_o^{(2)}(k_l \rho_i^P) \tag{3.14}$$

$$H_{x_{li}}^P = -\frac{k_l P_{li}(y - y_i^P)}{4j\rho_i^P} H_1^{(2)}(k_l \rho_i^P) \tag{3.15}$$

$$H_{y_{li}}^P = \frac{k_l P_{li}(x - x_i^P)}{4j\rho_i^P} H_1^{(2)}(k_l \rho_i^P) \tag{3.16}$$

Here η_l and k_l are, respectively, the intrinsic impedance and the wave number of the l^{th} cylinder, and

$$\rho_i^P = \sqrt{(x - x_i^P)^2 + (y - y_i^P)^2} \tag{3.17}$$

is the radial distance between the i^{th} source point located outside the l^{th} cylinder and the observation point under consideration.

3.3.3 Evaluation of the Unknown Currents F_{li} and P_{li}

For a dielectric object, the tangential components of the electric and magnetic fields must be continuous across the boundary. This leads to the operator equations on $C_l, l = 1, 2, 3, ...M$.

$$\hat{n}\mathrm{x}(\bar{E}^s - \bar{E}^P) = -\hat{n}\mathrm{x}\bar{E}^i \tag{3.18}$$

$$\hat{n}\mathrm{x}(\bar{H}^s - \bar{H}^P) = -\hat{n}\mathrm{x}\bar{H}^i \tag{3.19}$$

where $\hat{n}$ is a unit vector normal to the cylinder surface and pointing toward region O as shown in Fig. 3.1. Selecting N_l^C matching points on the surface of each cylinder and enforcing the boundary condition (3.18) and (3.19) at the matching points result in a system of linear equations. These equations can be written in a matrix form

$$\mathbf{AI} = \mathbf{V} \tag{3.20}$$

where

$$\mathbf{A} = \begin{bmatrix} \mathbf{A}_{11}^{s_e} & \mathbf{A}_{12}^{s_e} & \ldots & \mathbf{A}_{1M}^{s_e} & -\mathbf{A}_{11}^{P_e} & -\mathbf{A}_{12}^{P_e} & \ldots & -\mathbf{A}_{1M}^{P_e} \\ \mathbf{A}_{11}^{s_h} & \mathbf{A}_{12}^{s_h} & \ldots & \mathbf{A}_{1M}^{s_h} & -\mathbf{A}_{11}^{P_h} & -\mathbf{A}_{12}^{P_h} & \ldots & -\mathbf{A}_{1M}^{P_h} \\ \mathbf{A}_{21}^{s_e} & \mathbf{A}_{22}^{s_e} & \ldots & \mathbf{A}_{2M}^{s_e} & -\mathbf{A}_{21}^{P_e} & -\mathbf{A}_{22}^{P_e} & \ldots & -\mathbf{A}_{2M}^{P_e} \\ \mathbf{A}_{21}^{s_h} & \mathbf{A}_{22}^{s_h} & \ldots & \mathbf{A}_{2M}^{s_h} & -\mathbf{A}_{21}^{P_h} & -\mathbf{A}_{22}^{P_h} & \ldots & -\mathbf{A}_{2M}^{P_h} \\ \ldots & \ldots & \ldots & \ldots & \ldots & \ldots & \ldots & \ldots \\ \ldots & \ldots & \ldots & \ldots & \ldots & \ldots & \ldots & \ldots \\ \mathbf{A}_{M1}^{s_e} & \mathbf{A}_{M2}^{s_e} & \ldots & \mathbf{A}_{MM}^{s_e} & -\mathbf{A}_{M1}^{P_e} & -\mathbf{A}_{M2}^{P_e} & \ldots & -\mathbf{A}_{MM}^{P_e} \\ \mathbf{A}_{M1}^{s_h} & \mathbf{A}_{M2}^{s_h} & \ldots & \mathbf{A}_{MM}^{s_h} & -\mathbf{A}_{M1}^{P_h} & -\mathbf{A}_{M2}^{P_h} & \ldots & -\mathbf{A}_{MM}^{P_h} \end{bmatrix} \tag{3.21}$$

$$\mathbf{I} = \begin{bmatrix} \mathbf{F}_{1i} \\ \mathbf{F}_{2i} \\ \vdots \\ \mathbf{F}_{Mi} \\ \mathbf{P}_{1i} \\ \mathbf{P}_{2i} \\ \vdots \\ \mathbf{P}_{Mi} \end{bmatrix} \qquad \mathbf{V} = \begin{bmatrix} -\mathbf{V}_1^e \\ -\mathbf{V}_1^h \\ -\mathbf{V}_2^e \\ -\mathbf{V}_2^h \\ \vdots \\ -\mathbf{V}_M^e \\ -\mathbf{V}_M^h \end{bmatrix} \tag{3.22}$$

Here, $\mathbf{A}_{(M_1,M_2)}$ is the generalized impedance matrix, where $M_1 = 2\sum_{l=1}^{M} N_l^C$ and $M_2 = \sum_{l=1}^{M}(N_l^F + N_l^P)$. $\mathbf{A}_{lq}^{s_e}$ is an $(N_l^C \mathrm{x} N_q^F)$ matrix whose elements are the electric field intensity $E_{z_{ji}}^s$ due to the i^{th} filament of unit current inside the q^{th}, $q = 1, 2...M$, cylinder evaluated at the j^{th} matching point on C_l. Similarly, $\mathbf{A}_{lq}^{P_e}$ is an $(N_l^C \mathrm{x} N_q^P)$ matrix whose elements are the electric field intensity $E_{z_{ji}}^P$ due to the i^{th} filament of unit current outside the q^{th} cylinder evaluated at the j^{th} matching point on C_l. $\mathbf{A}_{lq}^{s_h}$ is an $(N_l^C \mathrm{x} N_q^F)$ matrix whose elements are the tangential magnetic field intensity $H_{z_{ji}}^s$ due to the i^{th} filament of unit current inside the q^{th} cylinder evaluated at the j^{th} matching point on C_l. $\mathbf{A}_{lq}^{P_h}$ is an $(N_l^C \mathrm{x} N_q^P)$ matrix whose elements are the tangential magnetic field intensity $H_{z_{ji}}^P$ due to the i^{th} filament of unit current outside the q^{th} cylinder evaluated at the j^{th} matching point on C_l. $\mathbf{I}_{(\sum_{l=1}^{M}(N_l^F+N_l^P))}$ is the generalized unknown current vector. $\mathbf{V}_{(2\sum_{l=1}^{M} N_l^C)}$ is the generalized voltage source vector. $\mathbf{V}_{l(N_l^C)}^e$ and $\mathbf{V}_{l(N_l^C)}^h$are column vectors whose elements are, respectively, the incident electric field and the incident tangential magnetic field intensities evaluated at the matching point under consideration.

Having formulated the matrix equation (3.20), the unknown current vector $\mathbf{I}$ can be solved for by inversion or elimination if the boundary conditions are enforced at $N_l^C = N_l^F = N_l^P$ selected points on C_l. On the other hand, if the BCs are enforced

at $N_l^C > N_l^F$ or N_l^P selected points on C_l the least-square error solution to (3.20) may be used [21]. This solution minimizes the standard norm of the vector $\mathbf{AI}-\mathbf{V}$ and is known to be

$$\mathbf{I} = (\tilde{\mathbf{A}}^*\mathbf{A})^{-1}\tilde{\mathbf{A}}^*\mathbf{V} \tag{3.23}$$

where $\tilde{\mathbf{A}}$ is the transpose of $\mathbf{A}$ and the asterisk denotes complex conjugate.

3.4 Imperfectly Conducting Cylinders

Consider M lossy dielectric cylinders of arbitrary cross section whose axes are taken to be parallel with the $z-$axis of a rectangular coordinate system, see Fig. 3.1. The material of each imperfectly conducting cylinder can be represented by a surface impedance $Z_c(\rho)$. For imperfectly conducting cylinders, the surface impedance boundary conditions (IBC) eliminate the need for the inclusion of the interior field [40]. Therefore, only one set of filamentary sources is needed to simulate the fields of each cylinder. In the simulated equivalence for region O, shown in Fig. 3.2, the fields scattered by the l^{th} cylinder are simulated by the fields of a set of fictitious electric current filaments placed on a closed surface enclosed in C_l, where C_l is the surface of the l^{th} cylinder and $l = 1, 2, 3...M$. These filaments are z directed, infinite in extent and carry, yet undetermined, constant currents $F_{li}, i = 1, 2, 3..N_l^F$, where N_l^F is the number of sources inside the l^{th} cylinder. They are treated as electric current sources radiating in free space. In Fig. 3.2, (E^s, H^s) are the electromagnetic scattered fields due to all fictitious current filaments inside all the cylinders and (E^i, H^i) are the fields of the incident wave as given by (3.1)-(3.5). The total fields $(E^s + E^i, H^s + H^i)$ in the region O are approximations of the field in region O in the original situation. Selecting N_l^C matching points on the surface of each cylinder and enforcing the IBC at all the matching points result in a system of linear equations

which can be solved for the unknown filamentary currents. The expressions for the incident and the scattered fields are given by (3.1)–(3.11).

3.4.1 Expression for the IBC

For objects with IBC the total electric and magnetic fields, on the surface C, are related by [40]

$$\bar{E} - (\hat{n} \cdot \bar{E})\hat{n} = Z_c(\rho)(\hat{n} \times \bar{H}) \tag{3.24}$$

$$Z_c(\rho) = Z_w(1 + q(\rho)) \tag{3.25}$$

with

$$Z_w = \begin{cases} \sqrt{\frac{j\omega\mu}{j\omega\epsilon+\sigma_c}} & \text{for a lossy dielectric region} \\ 0.0 & \text{for a perfectly conducting region} \end{cases} \tag{3.26}$$

$$q(\rho) = \frac{1}{4}(1-j)\delta k_u(\rho) - k_v(\rho) \tag{3.27}$$

where σ_c is the conductivity of the material, δ is the skin depth, Z_w is the wave impedance within the object and $k_u(\rho)$ and $k_v(\rho)$ are the principle curvatures of C at ρ. For small signal penetration, or for objects with large radii of curvature, $Z_c(\rho)$ can be assumed constant and equals to Z_w.

The impedance boundary condition in (3.12) can be reduced to

$$E_z = Z_c(\rho)H_t \tag{3.28}$$

where E_z is the total tangential electric field component in the exterior region and, H_t is the total tangential magnetic field component in that region.

3.4.2 Evaluation of the Unknown Electric Currents F_{li}

Selecting N_l^C matching points on the surface of each cylinder and enforcing the boundary condition in (3.28) at the j^{th}, $j = 1, 2, ...N_l^C$, matching point on the l^{th} cylinder, we get

$$(E^s_{z_{lj}} + E^i_{z_{lj}}) = Z_c(\rho_{lj})(H^s_{t_{lj}} + H^i_{t_{lj}}) \tag{3.29}$$

where $E^s_{z_{lj}}$ and $H^s_{t_{lj}}$ are, respectively, the scattered tangential electric and magnetic field components evaluated at the j^{th} matching point of the l^{th} cylinder. $E^i_{z_{lj}}$, $H^i_{t_{lj}}$ are the incident tangential electric and magnetic field components evaluated at the same point, and $Z_c(\rho_{lj})$ is the curvature dependent surface impedance evaluated at the j^{th} matching point of the l^{th} cylinder. Enforcing (3.29) at all matching points results in a set of linear equations which can be written in a matrix form in which the various matrices are interpreted in terms of generalized network parameters. The result is

$$\mathbf{AF} = \mathbf{V} \tag{3.30}$$

where

$$\mathbf{A} = \begin{bmatrix} \mathbf{A}^{s_e}_{11} + Z_c(\rho_1)A^{s_h}_{11} & \mathbf{A}^{s_e}_{12} + Z_c(\rho_1)A^{s_h}_{12} & ..... & \mathbf{A}^{s_e}_{1M} + Z_c(\rho_1)A^{s_h}_{1M} \\ \mathbf{A}^{s_e}_{21} + Z_c(\rho_2)A^{s_h}_{21} & \mathbf{A}^{s_e}_{22} + Z_c(\rho_2)A^{s_h}_{22} & ..... & \mathbf{A}^{s_e}_{2M} + Z_c(\rho_2)A^{s_h}_{2M} \\ ..... & ..... & ... & ..... \\ \mathbf{A}^{s_e}_{M1} + Z_c(\rho_M)A^{s_h}_{M1} & \mathbf{A}^{s_e}_{M2} + Z_c(\rho_M)A^{s_h}_{M2} & ... & \mathbf{A}^{s_e}_{MM} + Z_c(\rho_M)A^{s_h}_{MM} \end{bmatrix} \tag{3.31}$$

$$\mathbb{F} = \begin{bmatrix} F_{1i} \\ F_{2i} \\ \vdots \\ F_{Mi} \end{bmatrix} \tag{3.32}$$

$$\mathbf{V} = \begin{bmatrix} (-E^i_{z1} + Z_c(\rho_1)H^i_{t_1}) \\ (-E^i_{z_2} + Z_c(\rho_2)H^i_{t_2}) \\ \vdots \\ (-E^i_{z_M} + Z_c(\rho_M)H^i_{t_M}) \end{bmatrix} \tag{3.33}$$

Here, $\mathbf{A}_{(M_1,M_2)}$ is the generalized impedance matrix, where $M_1 = \sum_{l=1}^{M} N_l^C$ and $M_2 = \sum_{l=1}^{M} N_l^F$. $(\mathbf{A}^{se}_{lq} + Z_c(\rho_M)\mathbf{A}^{sh}_{lq})$ is an $(N_l^C \mathrm{x} N_q^F)$ matrix, where A^{se}_{lq} and A^{sh}_{lq} are, respectively, the electric field and the tangential magnetic field intensities due to the i^{th} filament inside the q^{th} cylinder of unit current evaluated at the j^{th} matching point on C_l. $\mathbf{I}_{(\sum_{l=1}^{M} N_l^F)}$ is the generalized unknown current vector. $\mathbf{V}_{(\sum_{l=1}^{M} N_l^C)}$ is the generalized voltage source vector.

Having formulated the matrix equation (3.20), the unknown current vector $\mathbf{F}$ can be solved for by inversion or elimination if the IBC are enforced at $N_l^C = N_l^F$ selected points on each C_l. On the other hand, if the IBC are enforced at $N_l^C > N_l^F$ selected points on C_l the least-square error solution given by (3.23)may be used

3.5 Far-Scattered Field

In the far-field region, the multiple scattering pattern of the cylinders can be obtained by employing the asymptotic expansion for the Hankel function and taking [18]

$$\rho_{li} = \rho - x_{li}cos\phi - y_{li}sin\phi \tag{3.34}$$

where ρ and ϕ are the polar coordinates of the distant observation point and ρ_{li} is the distance from the i^{th} source of the l^{th} cylinder to the distant observation point. Therefore, the far-scattered field is given by

$$E_z^s = -\frac{k_o\eta_o}{4}\sqrt{\frac{2j}{\pi k_o\rho}}e^{-jk_o\rho}\sum_{l=1}^{M}\sum_{i=1}^{N_l^F}F_{li}e^{jk_o(x_{li}cos\phi+y_{li}sin\phi)} \tag{3.35}$$

The scattering cross section per unit length, *i.e.*, the echo width, σ is defined by

$$\sigma(\phi) = \lim_{\rho\to\infty} 2\pi\rho\left|\frac{E_z^s(\rho,\phi)}{E_z^i}\right|^2 \tag{3.36}$$

From (3.34) and (3.35), the echo width is given by

$$\sigma(\phi) = \frac{k_o\eta_o^2}{4|E^i|^2}\left|\sum_{l=1}^{M}\sum_{i=1}^{N_l^F}F_{li}e^{jk_o(x_{li}cos\phi+y_{li}sin\phi)}\right|^2 \tag{3.37}$$

3.6 Solution for TE Problem

Let the M cylinders, shown in Fig. 3.1., be immersed in an incident transverse electric wave TE, the solution proceeds, similar to the TM problem, line for line. The sources are now magnetic current filaments, F_{li} and P_{li}. Using the Duality theorem [41], the field equations can be obtained by systematically interchanging the symbols $(E_z, -H_\phi, \epsilon, \mu)$ by $(H_z, E_\phi, \mu, \epsilon)$ in equations (3.1) through (3.37). As for the TM problem, the boundary conditions should be enforced at selected matching points at all the cylinders surfaces which result in a system of matrix equation similar to (3.19). By solving this system of matrix equation, the values for the unknowns F_{li} and P_{li} can be obtained.

3.7 Selected Numerical Results.

The validity of the multifilament current model (MFCM) solution for multiple scattering problems has been verified by comparison against results obtained for different geometries using the method of moments (MoM) solutions. A program based on Richmond's formulation for a single scatterer [18] has been modified to solve for the multiple scattering by parallel cylinders. The agreement between results based on the MoM solution and the forgoing method is excellent, indicating the high accuracy of the present numerical method. The convergence of the MFCM was confirmed by increasing the number of sources and matching points, changing the location of the sources and by interchanging the direction of the incidence and the observation points. The square root of the normalized scattered echo width $\sqrt{(\frac{\sigma}{\lambda})}$ is obtained for all cases considered in this section. The results are presented for multiple scattering by only two cylinders although the analysis is carried out and similar results can be generated for arbitrary number of cylinders.

Figure 3.4 illustrates the results for two identical dielectric circular cylinders of radius $k_o a = \pi$ placed along the Y-axis and their axes are separated by a distance $k_o d = 6\pi$. The cylinders of permittivity $\epsilon_r = 2.6$ are excited by an incident transverse magnetic TM plane wave with $\phi^i = 0^o$. For the MFCM, a set $N_1^F = N_2^F = 25$ filament sources is placed on a circular surface of radius $r^F = 0.75a$ inside each cylinder and another set $N_1^P = N_2^P = 25$ filament sources is placed on a circular surface of radius $r^P = 1.5a$ outside each cylinder. The number of the matching points $N_1^C = N_2^C = N_1^F$ is used. The sources and the matching points are evenly spaced on their respective surfaces. For the MoM solution, the matrix size is (200 x 200).

Figures 3.5 and 3.6 compare the normalized forward scattering and backscatter-

ing echo width $\sqrt{(\frac{\sigma}{\lambda})}$, respectively, versus the angle of incidence ϕ^i using the MFCM solution against the MoM solution. The results are for the two cylinders considered in Fig. 4 with the same locations and number of sources and matching points.

Figure 3.7 compare the results for two identical perfectly conducting elliptic cylinders ($Z_w = 0.0$), each of a semi-major axis $k_o a_e = 2\pi$ along the Y-axis and an axial ratio of 4.0. The cylinders are located along the Y-axis and their centers are separated by $k_o d = 8\pi$. The cylinders are excited by an incident transverse magnetic TM plane wave with $\phi^i = 0°$. For the MFCM, a set of $N_l^F = 32$ filament sources is placed inside each cylinder on an elliptical surface of major axis $0.975a_e$ and an axial ratio of 4.0 . The number of matching points $N_1^C = N_2^C = N^F$ is used. The sources and the matching points are again evenly spaced on their respective surfaces.

To check the accuracy of the impedance boundary conditions, the results based on the MFCM combined with IBC are compared with those of the MoM with exact boundary conditions. Fig. 3.8 compares the results for a perfectly conducting circular cylinder of radius $k_o a = \pi$ and a lossy dielectric circular cylinder of radius $k_o a = \pi$ and complex permittivity $\epsilon_r = 4 - j5$. The center of the dielectric cylinder is located along the positive X-axis at a distance $k_o d = 6\pi$ from the center of the perfectly conducting cylinder. The cylinders are excited by an incident transverse magnetic TM plane wave with $\phi^i = 180°$. For the MFCM, a set $N_l^F = 25$ filament sources is placed inside each cylinder on a circular surface of radius $r^F = 0.75a$. The number of matching points $N_1^C = N_2^C = N^F$ is used. The sources and matching points are evenly spaced on their respective surfaces.

Figure 3.9 compares the results for a perfectly conducting elliptic cylinder with semi-major axis $k_o a_e = \pi$ along the Y-axis and an axial ratio of 2.0 and a dielectric circular cylinder of radius $k_o a = \pi$ and permittivity $\epsilon_r = 2.6 - j2$. The center of the

circular cylinder is located along the positive direction of the X-axis at a distance $k_o d = 6\pi$ from the center of the elliptic cylinder. The cylinders are excited by an incident transverse magnetic TM plane wave with $\phi^i = 90^o$. For MFCM, a set of $N_1^F = 32$ filament sources is placed inside the elliptic cylinder on an elliptical surface of major axis $0.975a_e$ and an axial ratio of 2.0. Another set of $N_2^F = 25$ filament sources is placed inside the circular cylinder on a circular surface of radius $r^F = 0.75a$. The numbers of the matching points $N_1^C = N_1^F$ and $N_2^C = N_2^F$ are used. The sources and the matching points are evenly spaced on their respective surfaces. The impedance boundary condition with constant surface impedance is enforced at the matching points for the MFCM.

Figure 3.10 compares the results for two identical perfectly conducting square cylinders of side length $k_o a_l = \pi$. The axes of the cylinders are located on the X-axis and separated by a distance $k_o d = 6\pi$. The cylinders are excited by an incident transverse magnetic TM plane wave with $\phi^i = 0^o$. For rectangular cylinders, a technique developed by Eisler and Leviatan [42] is used to select the locations of the filamentary sources. The scattered field has been simulated by three sets of sources: (i) 28 filaments evenly spaced on a concentric square surface situated at a distance $d = 0.1\lambda$ from the boundary C^l; (ii) 16 filaments at a distance 0.01λ from the edges, 2 filaments on each side of each edge; and (iii) 12 filaments gradually connecting the former two sets. The number of the matching points $N_1^C = N_2^C = N^F$ is used and distributed evenly on the boundary surface. As shown in Fig 3.10, the agreement between results based on the MoM solution and the forgoing method is excellent.

Finally, figure 3.11 illustrates the results for two dielectric circular cylinders of radii $a_1 = 0.1\lambda_o$ and $a_2 = 0.2\lambda_o$, respectively. The axes of the cylinders are separated by a distance 0.4λ and placed along the X-axis. The cylinders of permittivity $\epsilon_{r_1} = \epsilon_{r_2} = 2$ and are excited by an incident transverse electric TE or TM plane wave

with $\phi^i = 0^o$. Two sets $N_1^F = 17$ and $N_2^F = 30$ of filamentary sources are placed on a circular surface of radius $r^F = 0.5a_1$ and $r^F = 0.5a_2$, respectively, inside the cylinders. Another two sets $N_1^P = 17$ and $N_2^P = 30$ of filamentary sources are placed on a circular surface of radius $r^P = 1.05a_1$ and $r^P = 1.05a_2$ outside the cylinders. The numbers of the matching points $N_1^C = N_1^F$ and $N_2^C = N_2^F$ are used. The sources and the matching points are evenly spaced on their respective surfaces. The accuracy of the results is confirmed by comparing the far scattered fields with results obtained by Elsherbeni and Kishk [43].

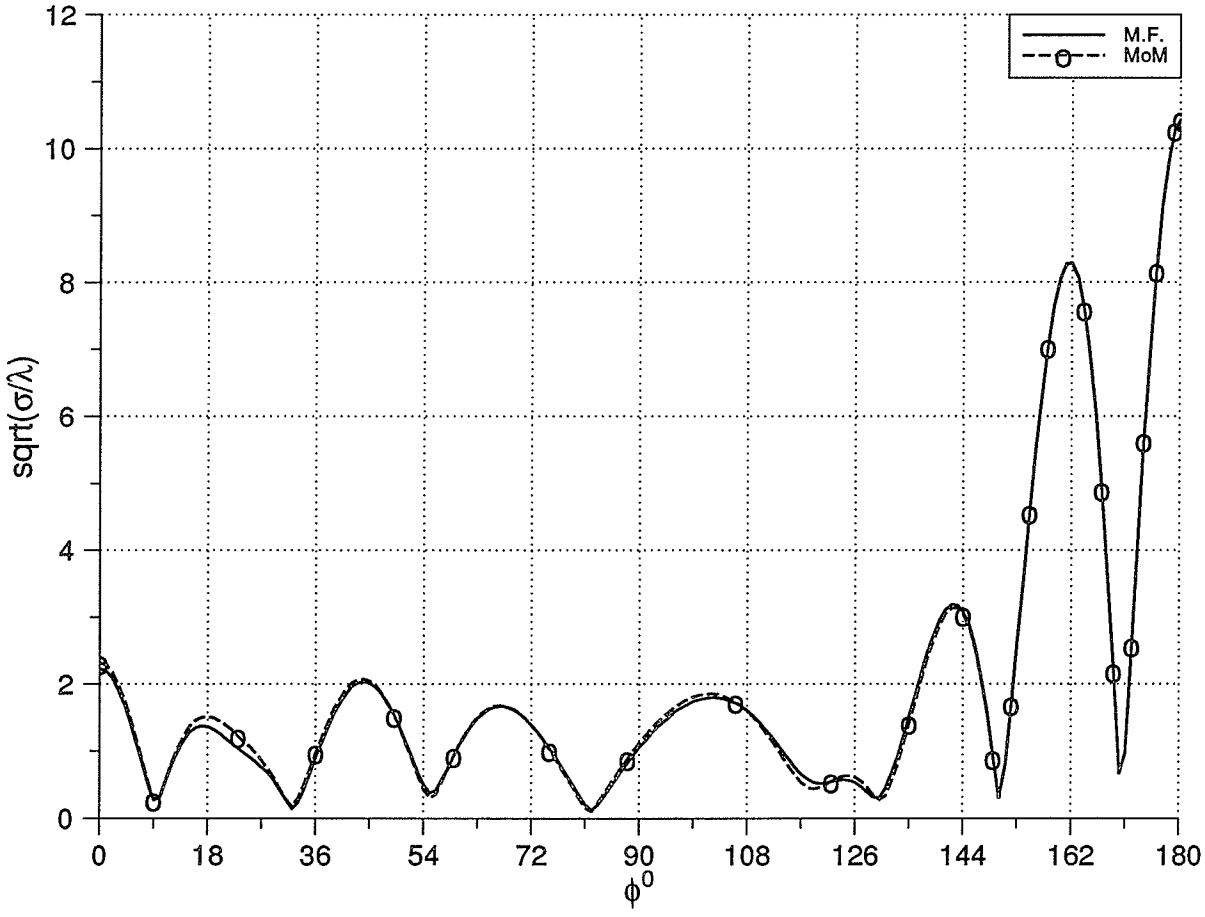

Figure 3.4: The normalized echo-width pattern for two circular cylinders.

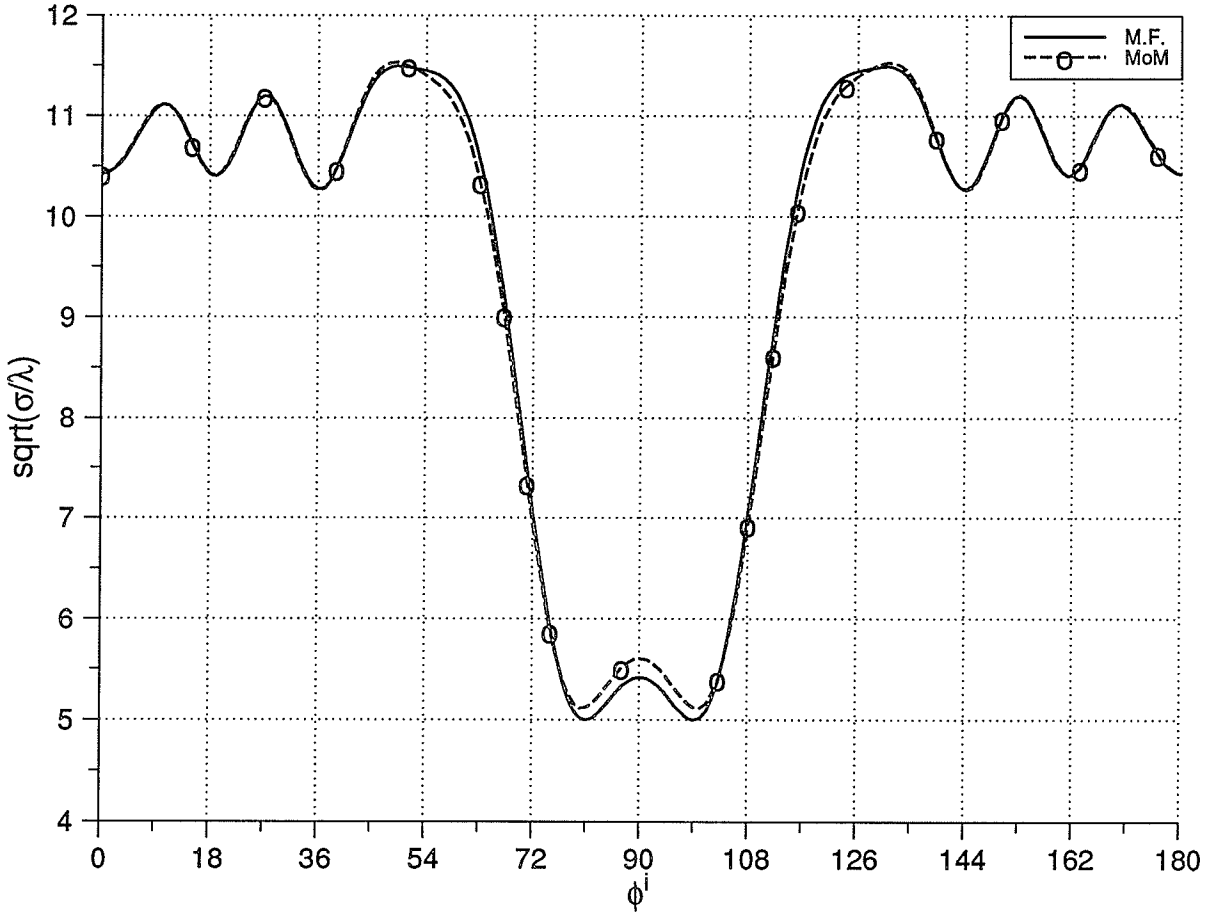

Figure 3.5: The normalized forward scattering echo width versus ϕ^i for two circular cylinders.

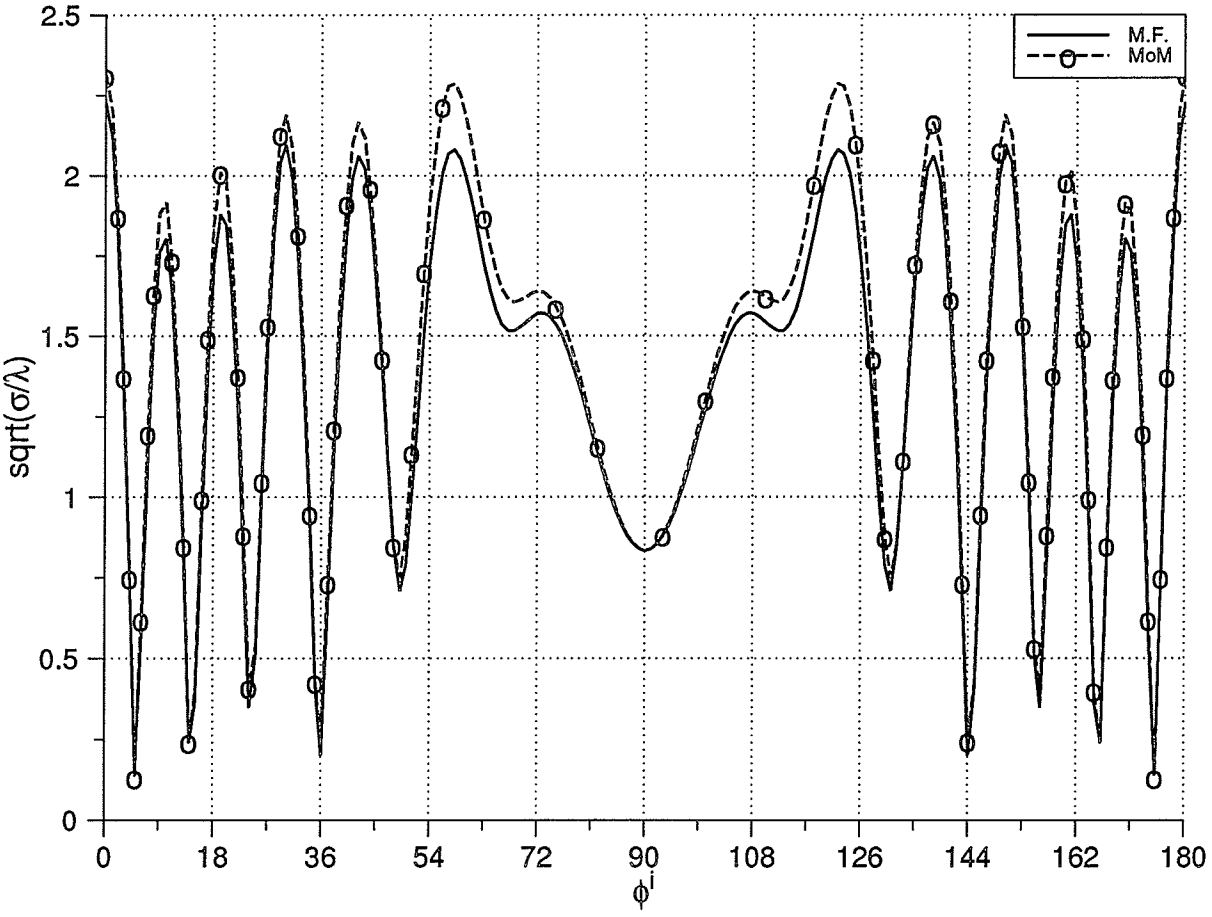

Figure 3.6: The normalized backscattering echo width versus ϕ^i for two circular cylinders.

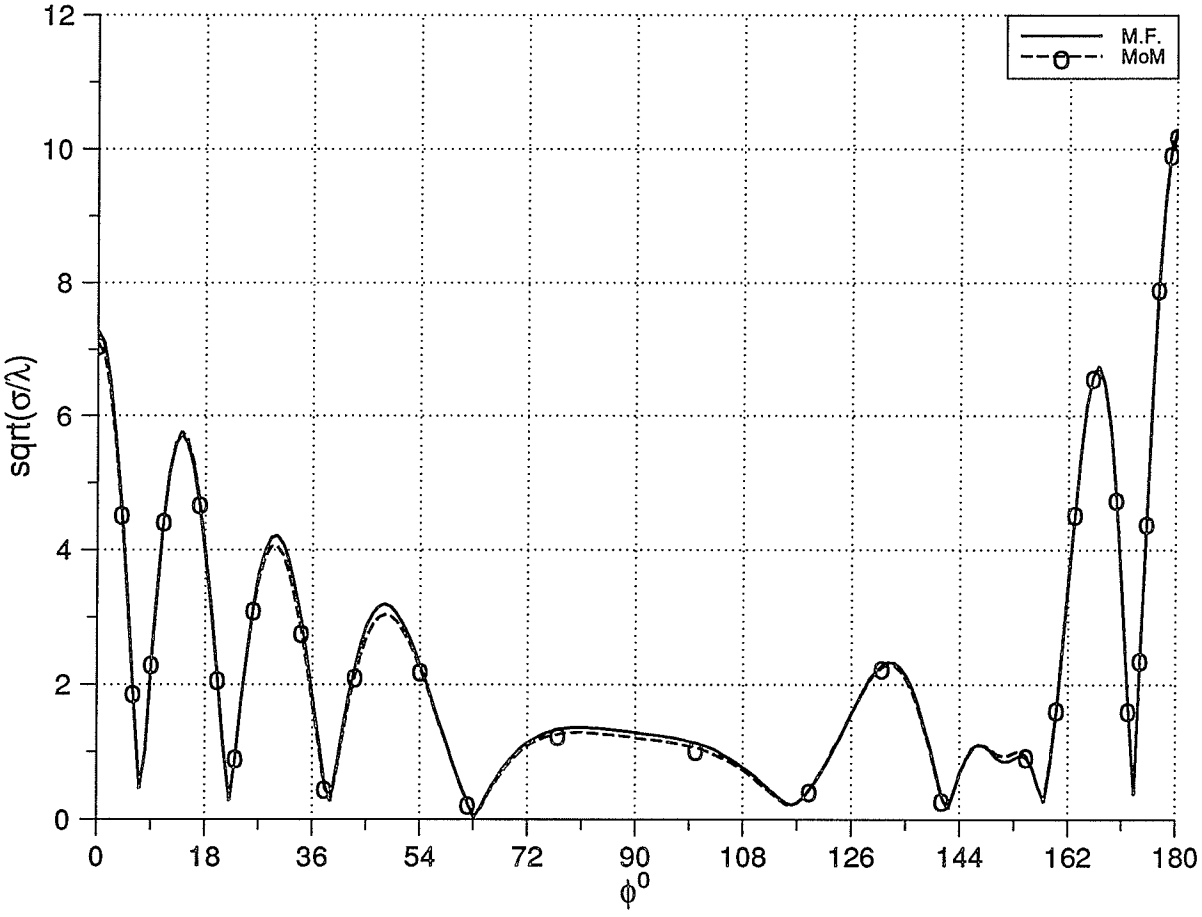

Figure 3.7: The normalized echo-width pattern for two perfectly conducting elliptic cylinders.

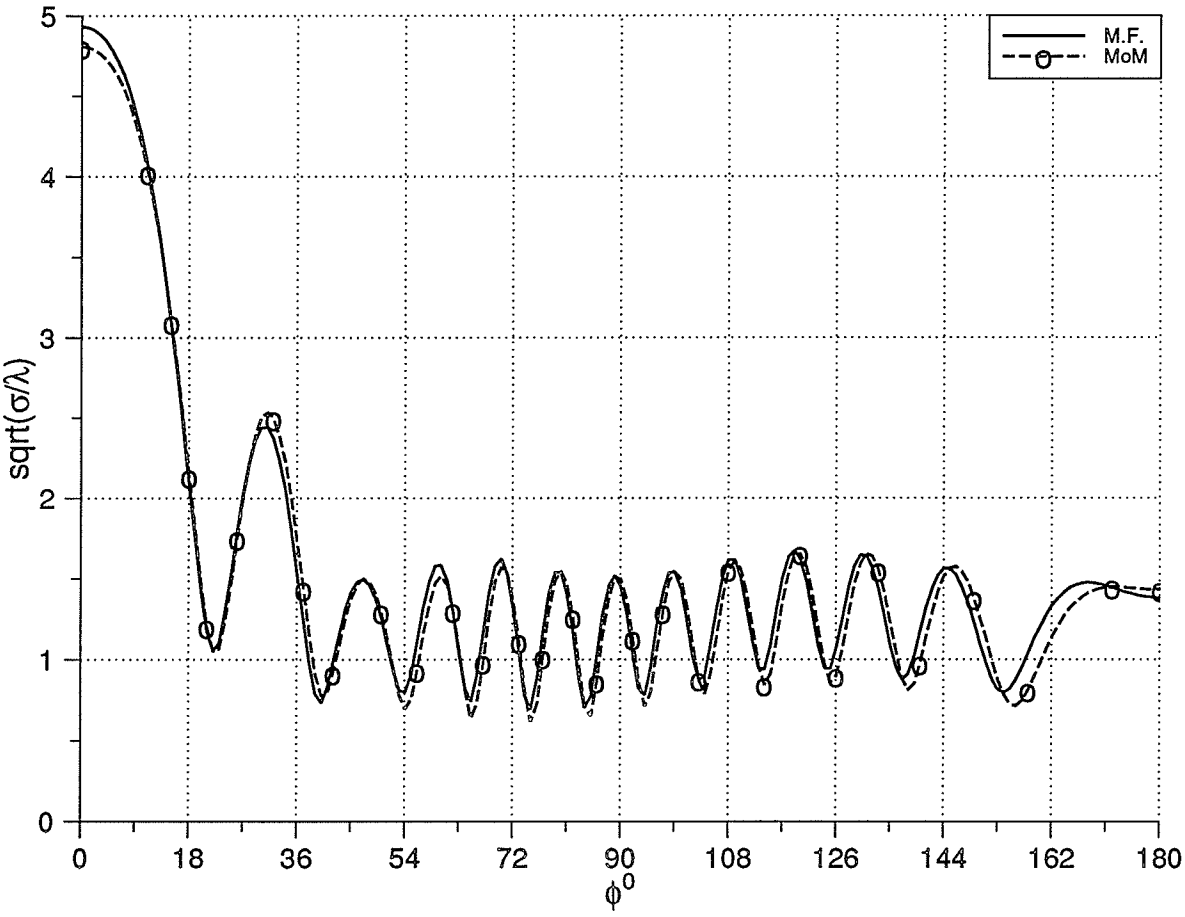

Figure 3.8: The normalized echo-width pattern for perfectly conducting and homogeneous dielectric circular cylinders.

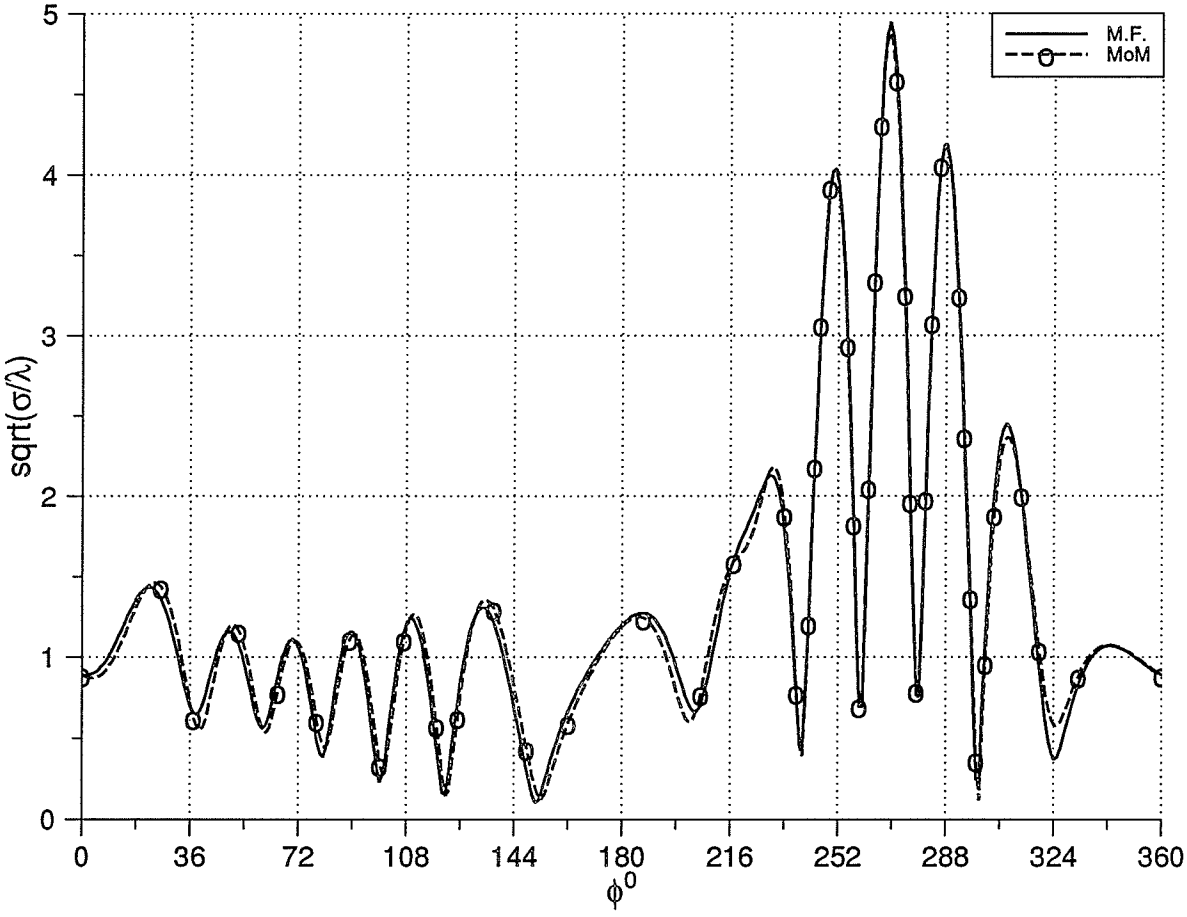

Figure 3.9: The normalized echo-width pattern for a perfectly conducting elliptic cylinder and a dielectric circular cylinder, (TM case.)

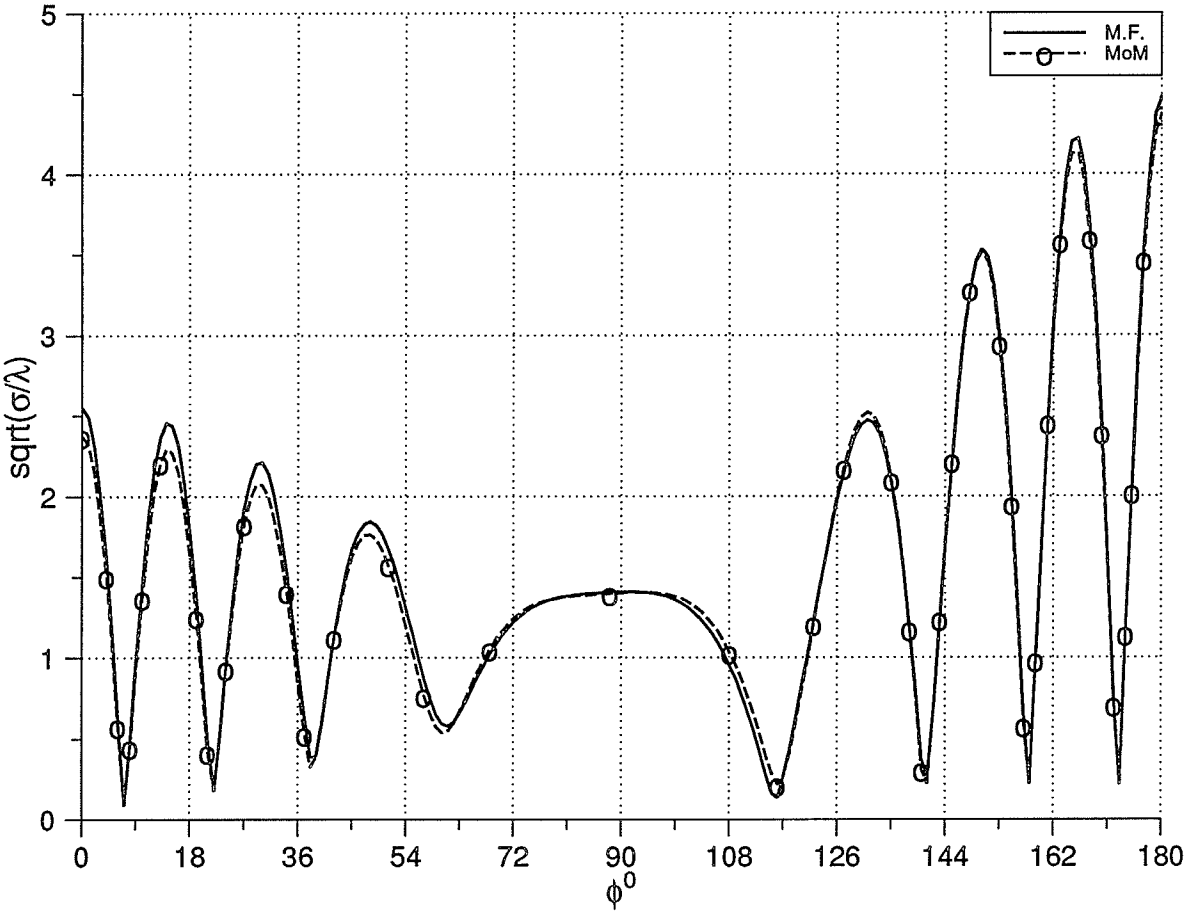

Figure 3.10: The normalized echo-width pattern for two perfectly conducting square cylinders.

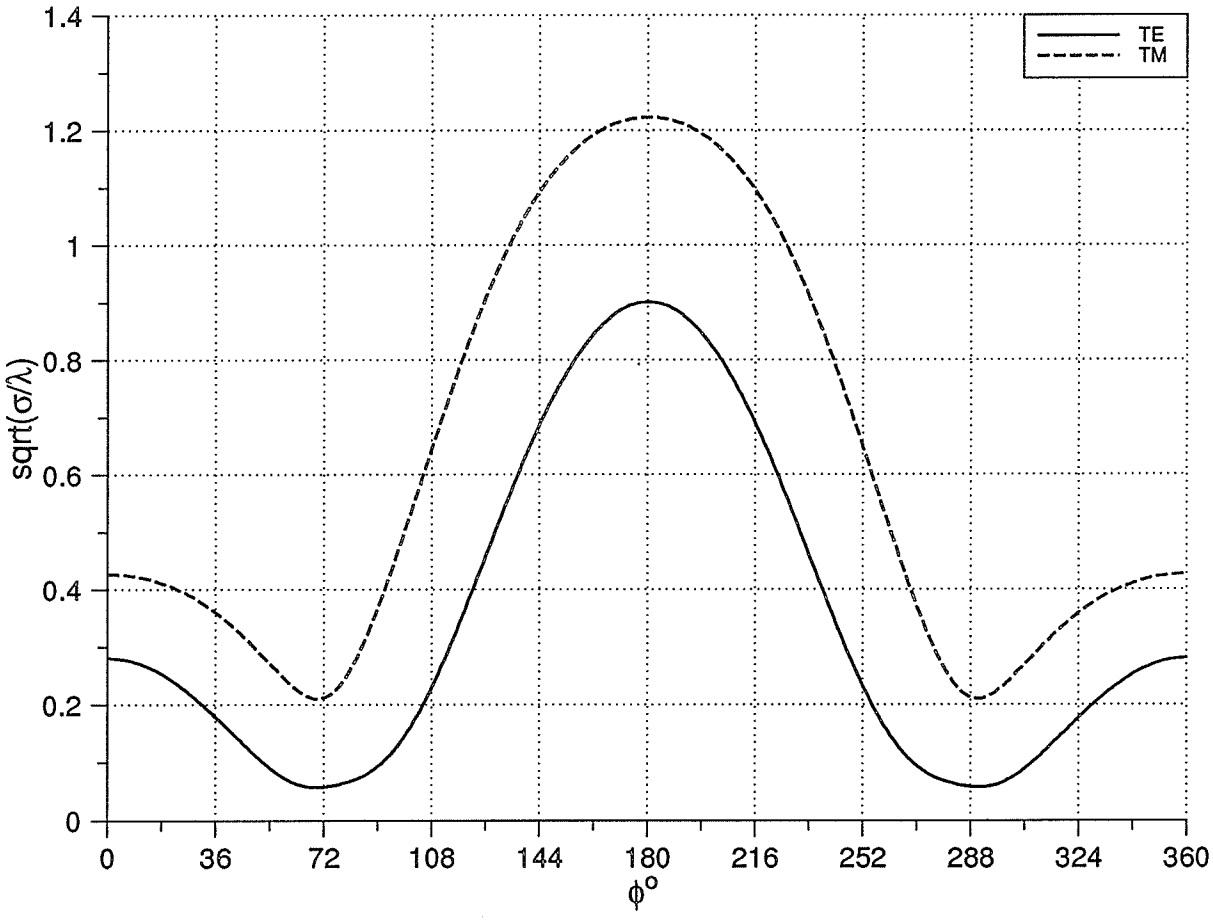

Figure 3.11: The normalized echo-width pattern for two circular cylinders, (TE and TM cases).

To study the behavior of the echo width backscattering versus the separation distance between two parallel cylinders, results for cylinders, located on the x-axis, of various parameters and cross sections for TM plane wave with $\phi^i = 0^o$ (endfire) and $\phi^i = 90^o$ (broadside) are included.

Figure 3.12 shows the broadside backscattering versus the separation distance $k_o d$ for two identical homogeneous dielectric circular cylinders of $k_o a = 0.5$ and permittivity $\epsilon_r = 2.25$. A set $N^F = 15$ filament sources is placed on a circular surface of radius $r^F = 0.75a$ inside each cylinder and another set $N^P = 15$ filament sources is placed on a circular surface of radius $r^P = 2a$ outside each cylinder. The number of the matching points $N^C = N^F$ is used. The sources and the matching points are evenly spaced on their respective surfaces. As shown in the figure, the oscillations decay with increasing the separation distance between the cylinders and the mean value is 0.395 which is about four times the value of the independent scattering from the single cylinder (0.0987). The wavelength of the oscillation is 2π. These results agree well with results obtained analytically by Olaofe [32].

Figure 3.13 shows the endfire backscattering versus the separation distance $k_o d$ for two identical homogeneous dielectric circular cylinders of $k_o a = 0.5$ and permittivity $\epsilon_r = 2.25$. The number and location of sources and the number of matching point are the same as for Fig. 3.12. As shown for all values of $k_o d$, the endfire backscattering is below four times the corresponding value for the single cylinder (0.174). The wavelength of the oscillations is π. The amplitude of the oscillations of each is almost constant, non-negligible, and almost completely independent of separation. Again, these results agree well with results obtained analytically by Olaofe [32].

Figure 3.14 shows the broadside backscattering versus the separation distance $k_o d$ for three sets of two identical imperfectly conducting circular cylinders of $k_o a =$

1.0. The cylinders have a constant surface impedance of $Z_c = 200\Omega$, $Z_c = 300\Omega$ and $Z_c = 370\Omega$. A set $N_1^F (= N_2^F) = 20$ filament sources is placed on a circular surface of radius $r^F = 0.75a$ inside each cylinder. The number of the matching point $N_1^C = N_1^F$ is used to obtain the results of each curve. The sources and the matching points are evenly spaced on their respective surfaces. As shown in the figure, for the three curves, the oscillations decay with increasing the separation distance between the cylinders; they have mean value corresponding to four times the value of the independent scattering from the single cylinder. The wavelength of the oscillation is 2π. Also, the mean value of the oscillation decreases by increasing the value of the surface impedance which agrees with the results shown in Fig. 2.14.

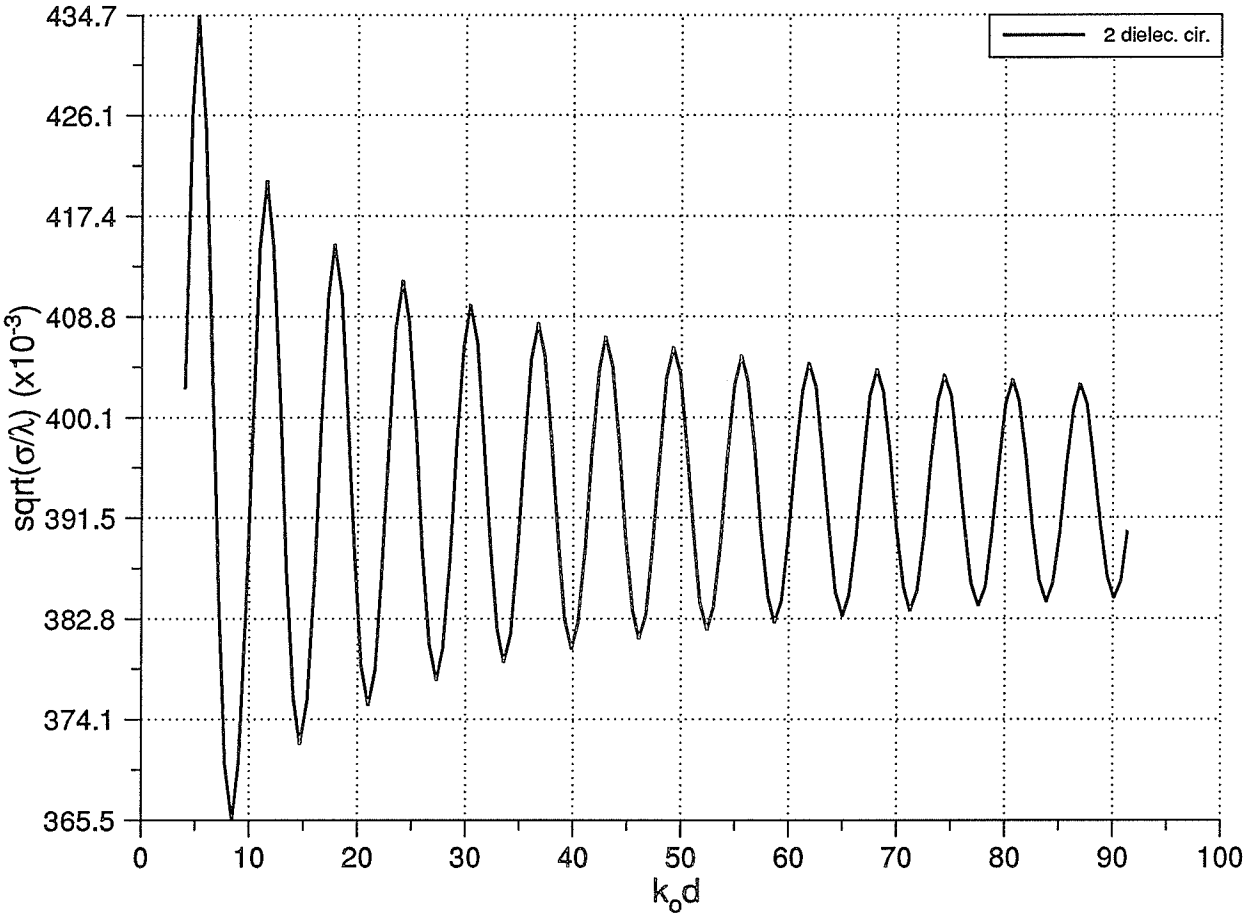

Figure 3.12: The normalized echo-width pattern versus the separation distance for two circular cylinders, $\phi^i = 90^o$

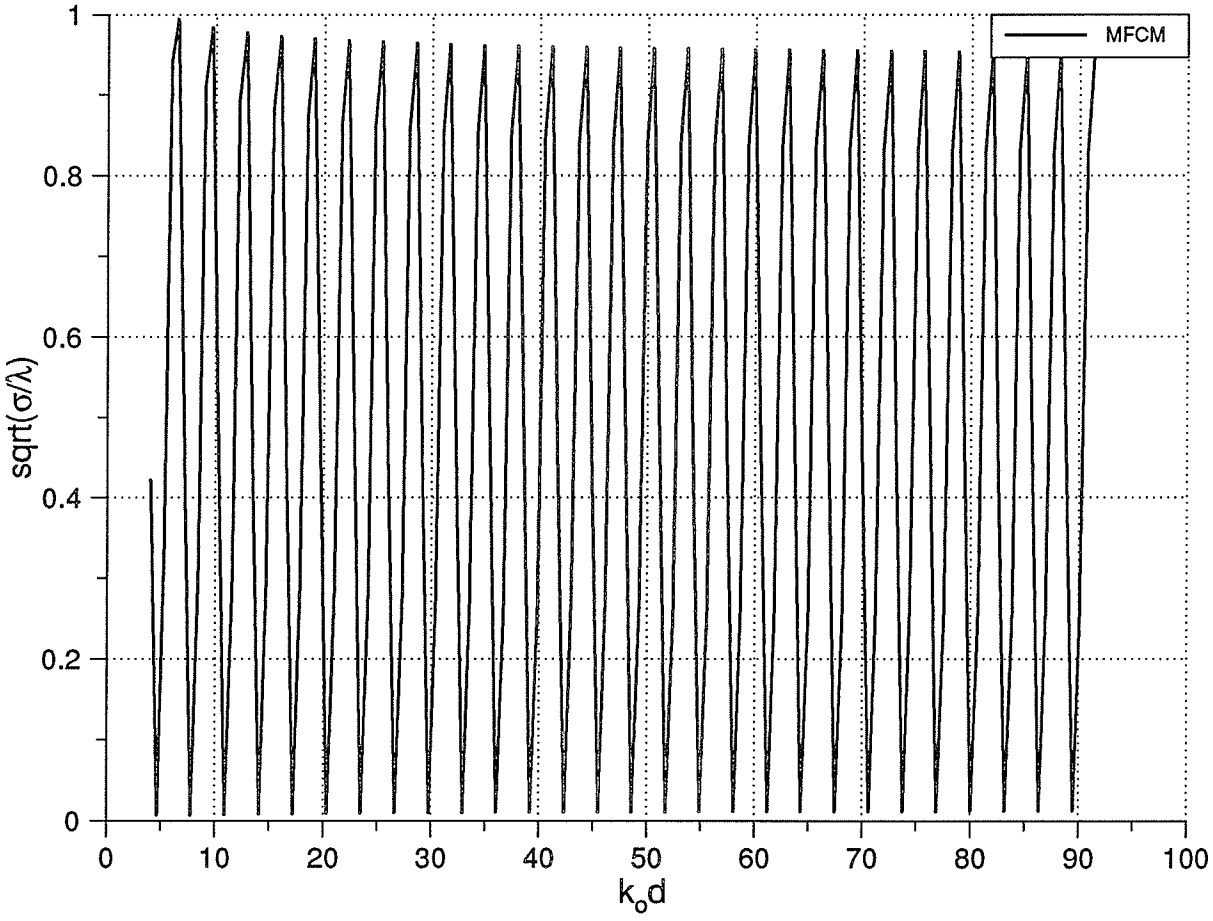

Figure 3.13: The normalized echo-width pattern versus the separation distance for two circular cylinders, $\phi^i = 0^o$

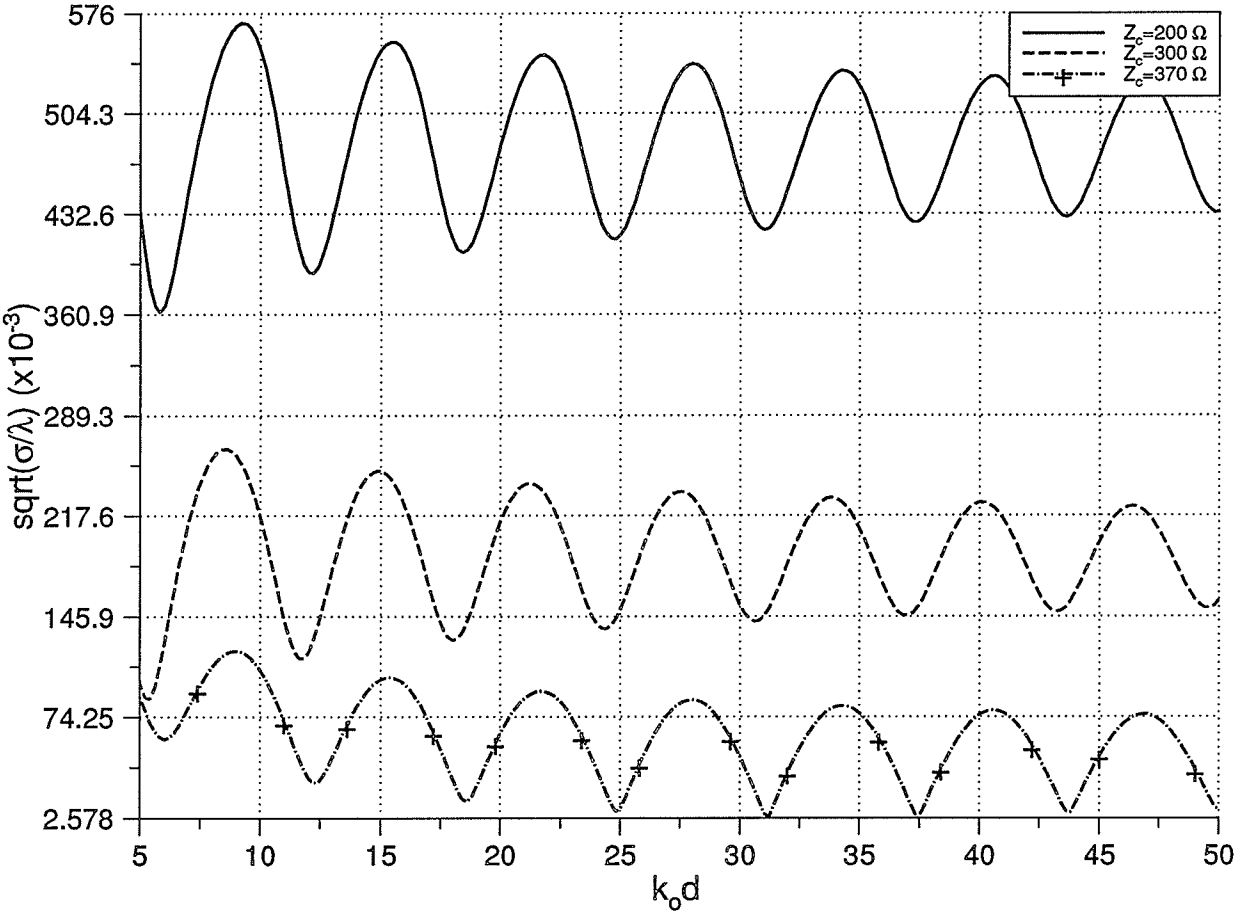

Figure 3.14: The normalized echo-width pattern versus the separation distance, $\phi^i = 0^o$

CHAPTER 4

Radiation From Axially-Slotted Cylinders

In this chapter, the multifilament current model and the generalized multiple multipole technique are used to solve the problems of electomagnetic radiation from axially-slotted cylinders of arbitrary cross sections. The exciting source is assumed to be either a prescribed aperture field distribution E_s on the slot or an electric line source placed inside the shell. In the following section, the formulation will be given for electomagnetic radiation from axially-slotted cylinders excited by E_s on the slot. The formulation is carried out using the multifilament current model (MFCM) and the generalized multiple multipole technique (GMMP). The formulation for the electomagnetic radiation from dielectric-loaded axially-slotted cylinders excited by an electric line source placed inside the shell will be given in a later section using the GMMP technique only. Results for circular cylinders of various parameters are given and compared with available analytical and numerical solutions.

4.1 Formulation for Known Aperture Field Distribution

4.1.1 Problem Specification

Figure. 4.1 shows an infinitely long slot-perforated cylindrical shell whose axis is taken to be parallel with the $z-$axis of a rectangular coordinate system. It is assumed that the shell is infinitesimally thin and made of perfect conductor. The shell is situated in free space of permittivity ε_o and permeability μ_o. The theory is given for TE axial slots.

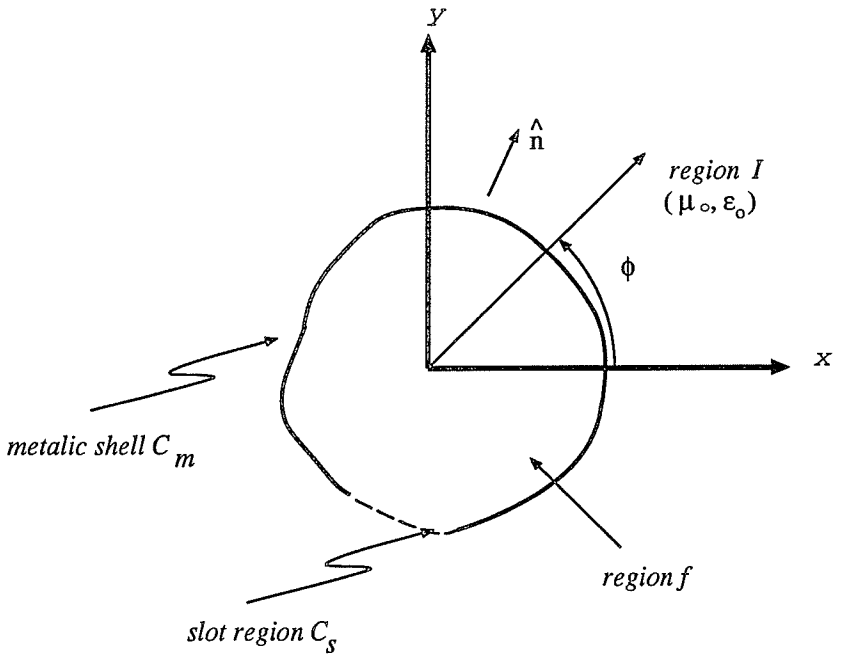

Figure 4.1: Geometry of the problem

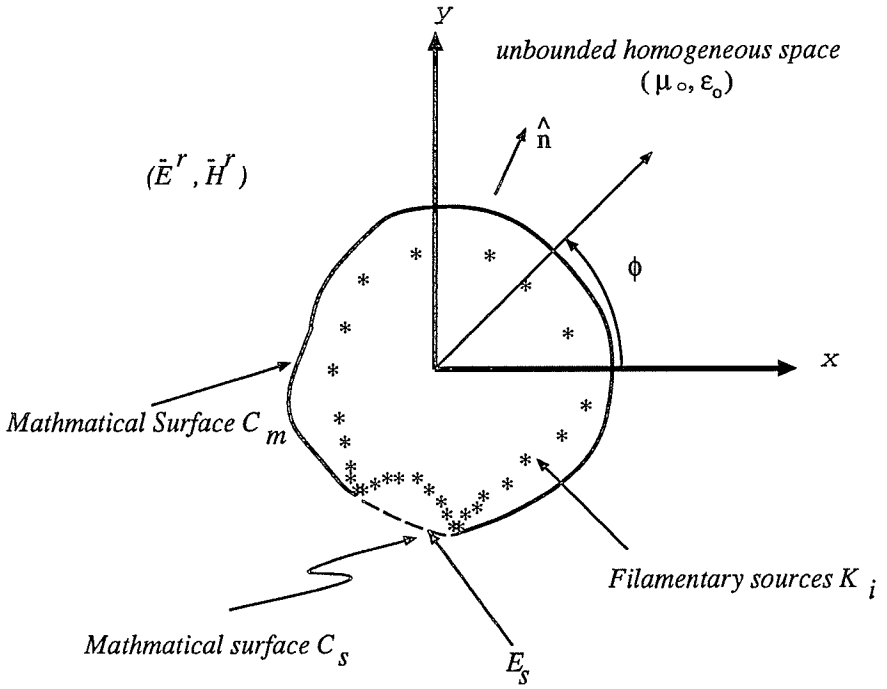

Figure 4.2: Simulated equivalence situation for region I

4.1.2 Multifilament Current Model

The multifilament current model simulation uses one set of filamentary sources to simulate the fields radiated by the cylinder. This set of sources is placed inside the cylinder at some distance from its surface to simulate its radiated fields. The sources carry, yet to be determined, constant complex currents. They generate smooth field functions capable of representing smooth fields in the boundary surface. The singular behavior of the fields near the edges of the slot can be approximated by locating some of the filamentary sources in the vicinity of the slot edge [39]. Application of the boundary conditions results in a system of linear equations which can be solved for the unknown filamentary currents. Fig. 4.2 shows the simulation of the field radiated by the cylinder, where the radiated field is simulated by the fields of a set of fictitious magnetic current filaments placed on a closed surface enclosed by C. These filaments are z directed, infinite in extent and carry, yet to be determined, constant currents $K_i^I, i = 1, 2, 3, ...N^I$. They are treated as magnetic current sources radiating in free space. In Fig. 4.2, (E^r, H^r) are the electromagnetic radiated fields due to all the fictitious current filaments and (E_s) is the field across the slot. The field (E^r) in the surrounding region in Fig. 4.2 is an approximation of the field in the surrounding region in the original situation. Note that the locations of the filaments inside C has not been specified. As far as the formulation is concerned, their locations can be arbitrary. The question of selecting filament locations suitable for a numerical solution will be dealt with later on.

4.1.2.1 Expression for E^r

The radiated field (E^r) at an observation point (x, y) in some z =constant plane due to the current filaments $K_i^I, i = 1, 2, 3, ...N^I$ radiating in an unbounded free space is given by

$$\bar{E}^r = \hat{u}_x \sum_{i=1}^{N^I} E^r_{xi} + \hat{u}_y \sum_{i=1}^{N^I} E^r_{yi} \tag{4.1}$$

where E^r_{xi} and E^r_{yi} are the radiated electric field components at an observation point (x, y) in the exterior region due to a magnetic current filament K^I_i situated at (x^I_i, y^I_i) inside C and are given by

$$E^r_{xi} = \frac{k_o K^I_i (y - y^I_i)}{4j\rho} H^{(2)}_1(k_o \rho^I_i) \tag{4.2}$$

$$E^r_{yi} = \frac{k_o K^I_i (x^I_i - x)}{4j\rho} H^{(2)}_1(k_o \rho^I_i) \tag{4.3}$$

$$\rho^I_i = \sqrt{(x - x^I_i)^2 + (y - y^I_i)^2} \tag{4.4}$$

where $H^{(2)}_0$ and $H^{(2)}_1$ are the second kind Hankel functions of zero order and first order, respectively and ρ^I_i is the radial distance between the source point and the observation point under consideration.

4.1.2.2 Evaluation of the Unknown Currents K^I_i

.

In order to compute the unknown magnetic currents, only the boundary conditions have to be fulfilled. Therefore, by enforcing the BC at a selected number of matching points we can evaluate K^I_i. The tangential electric field must vanish over the perfectly conducting surface and match the prescribed aperture field distribution in the slot, *i.e*,

$$\hat{n} \mathrm{x} \bar{E}^r = E_s \qquad \text{on } C_s \tag{4.5}$$

$$\hat{n} \mathrm{x} \bar{E}^r = 0 \qquad \text{on } C_m \tag{4.6}$$

where $\hat{n}$ is a unit vector normal to the cylinder surface and pointing outward as shown in Fig.4.1. Selecting N_s^C matching points on the metallic surface of the cylinder and N_m^C matching points on the slot and enforcing the boundary condition (4.5) and (4.6) at the j^{th}, $j = 1, 2, ...(N_s^C + N_m^C)$, matching point we get

$$E_{tj}^r = E_s \qquad \text{on } C_s \tag{4.7}$$

$$E_{tj}^r = 0 \qquad \text{on } C_m \tag{4.8}$$

where E_{tj}^r is E_t^r evaluated at the j^{th} matching point. Enforcing equation (4.7) at all the matching points on the metallic surface of the cylinder and enforcing equation (4.8) at all the matching points on the slot result in a set of linear equations which can be written in a matrix form in which the various matrices are interpreted in terms of generalized network parameters. The result is

$$\mathbf{A}\ \mathbf{K}\ =\ \mathbf{V} \tag{4.9}$$

where

$$\mathbf{A} = \begin{bmatrix} A_{11}^r & A_{12}^r & \cdots & A_{1N^I}^r \\ A_{21}^r & A_{22}^r & \cdots & A_{2N^I}^r \\ \cdots\cdots & \cdots\cdots & \cdots & \cdots\cdots \\ A_{N_s^C 1}^r & A_{N_s^C 2}^r & \cdots & A_{N_s^C N^I}^r \\ A_{11}^r & A_{12}^r & \cdots & A_{1N^I}^r \\ A_{21}^r & A_{22}^r & \cdots & A_{2N^I}^r \\ \cdots\cdots & \cdots\cdots & \cdots & \cdots\cdots \\ A_{N_m^C 1}^r & A_{N_m^C 2}^r & \cdots & A_{N_m^C N^I}^r \end{bmatrix} \tag{4.10}$$

$$\mathbb{K} = \begin{bmatrix} K_1 \\ K_2 \\ \vdots \\ K_{N^I} \end{bmatrix} \tag{4.11}$$

$$\mathbb{V} = \begin{bmatrix} E_{s1} \\ E_{s2} \\ \vdots \\ E_{sN_s^C} \\ 0 \\ 0 \\ \vdots \\ 0 \end{bmatrix} \tag{4.12}$$

with

$$A_{11}^r = -\frac{k_o(x_j - x_i^I)t_{yj} - (y_j - y_i^I)t_{tj}}{4j\rho_{ji}^I} H_1^{(2)}(k_o\rho_{ji}^I) \tag{4.13}$$

$$\rho_{ji}^I = \sqrt{(x_j - x_i^I)^2 + (y_j - y_i^I)^2} \tag{4.14}$$

Here, $\mathbf{A}_{(N_s^C+N_m^C,N^I)}$ is the generalized impedance matrix. $\mathbf{K}_{(N^I)}$ is the generalized unknown current vector, and $\mathbf{V}_{(N^C)}$ is the generalized voltage source vector. In (4.9), A_{ji}^r is the tangential electric field intensity due to a filament K_i^I of unit magnetic current evaluated at ρ_{ji}^I on C. In (4.11), E_{sj} is the electric field prescribed on the slot at the j^{th} matching point and ρ_{ji}^I is the radial distance between the i^{th} source and the j^{th} matching point. t_{xj} and t_{yj} are, respectively, the x and y components of the tangential unit vector evaluated at the j^{th} matching points.

Having formulated the matrix equation (4.9), the unknown current vector $\mathbf{K}$ can be solved for by inversion or elimination if the BCs are enforced at $N_s^C + N_m^C = N^I$ selected points on C. On the other hand, if the BCs are enforced at $N_s^C + N_m^C > N^I$ selected points on C the least-square error solution to (4.9) may be used [22]. This solution minimizes the standard norm of the vector $\mathbf{AK} - \mathbf{V}$ and is given by

$$\mathbf{K} = (\tilde{\mathbf{A}} * \mathbf{A})^{-1} \tilde{\mathbf{A}}^* \mathbf{V} \tag{4.15}$$

where $\tilde{\mathbf{A}}$ is the transpose of $\mathbf{A}$ and the asterisk denotes a complex conjugate.

4.1.3 Generalized Multiple Multipole Technique

The generalized multiple multipole technique (GMMP) represents the radiated fields by multiple expansions with different origins of outward cylindrical waves. The multiplicity of the origins for the outward waves can be interpreted as equivalent source locations within the boundary of the cylinder. Then, the total radiated fields are represented as a sum over the contribution from each origin. Furthermore, the source distribution at each origin generates a field represented as a sum over cylindrical waves, each of which is generated by a specific source component at that origin. The sources are multipoles which include monopoles, dipoles and higher order multipoles. As a result, we have a distribution of equivalent sources within the boundary which creates a field on the boundary that leads to the satisfaction of the boundary conditions. Applying the boundary conditions in the least square sense results in a system of linear equations which can be solved for the unknown expansion coefficients. The GMMP simulation for the fields radiated by the cylinder is similar to the multifilament current model simulation. However, the GMMP simulation uses a set of multipole line sources to simulate the fields radiated by the cylinder. Again, this set of multipoles is situated inside the cylinder to simulate its radiated fields. In this case, the singular behavior of the fields near the edges of the

slot can be approximated by locating some of the multipole line sources with higher truncation order in the vicinity of the slot edge. The procedure of the solution for the unknown expansion coefficients is exactly the same as the MFCM procedure. The simulation of the radiated fields is shown in Fig. 4.2 where the filamentary sources are replaced by multipoles line sources. The GMMP formulation is given in the following section.

4.1.3.1 Expression for E^r

The radiated field E^r at an observation point (x, y) in some z =constant plane due to the multipole source $K_i^I, i = 1, 2, 3, ...N^I$ radiating in an unbounded free space is given by [3]

$$\bar{E}^r = \hat{u}_x \sum_{i=1}^{N^I} E_{xi}^r + \hat{u}_y \sum_{i=1}^{N^I} E_{yi}^r \tag{4.16}$$

where E_{xi}^r and E_{yi}^r are the radiated electric field components at observation point (x, y) in the exterior region due to a multipole line source K_i^I situated at (x_i^I, y_i^I) inside C and are given by

$$E_{xji}^r(\rho_{ji}^I) = \frac{j(y_j - y_i^I)}{\eta_o \rho_{ji}^I} \left[\sum_{n=0}^{N_i^I} P_{in} H_n'^{(2)}(k_o \rho_{ji}^I) \cos(n\phi_{ji}) + \sum_{n=1}^{N_i^I} Q_{in} H_n'^{(2)}(k_o \rho_i^I) \sin(n\phi_i) \right] \tag{4.17}$$

$$E_{yji}^r(\rho_{ji}^I) = -\frac{j(x_j - x_i^I)}{\eta_o \rho_{ji}^I} \left[\sum_{n=0}^{N_i^I} P_{in} H_n'^{(2)}(k_o \rho_{ji}^I) \cos(n\phi_{ji}) + \sum_{n=0}^{N_i^I} Q_{in} H_n'^{(2)}(k_o \rho_{ji}^I) \sin(n\phi_i) \right] \tag{4.18}$$

where E_{xj}^r *and* E_{yj}^r are the radiated electric field components at an observation point (x_j, y_j) in the exterior region due to the i^{th} source K_i^I situated at (x_i^I, y_i^I) inside C,

N_i^I is the truncation order of the i^{th} source, P_{in} and Q_{in} are the unknown expansion coefficients and

$$\rho_{ji}^I = \sqrt{(x_j - x_i^I)^2 + (y_j - y_i^I)^2} \tag{4.19}$$

$$\phi_{ji} = \arctan\left((y_j - y_i^I)/(x_j - x_i^I)\right) \tag{4.20}$$

4.1.3.2 Evaluation of the Unknown Expansion Coefficients

In order to compute the unknown parameters, P_{in} and Q_{in} in the GMMP expansions, only the boundary conditions have to be fulfilled because the field equations are completely satisfied by the GMMP expansions. Selecting N_m^C matching points on the metallic surface and N_s^C matching points on the slot and enforcing the boundary conditions in (4.7) and (4.8) at all the matching points result in a set of linear equations which can be written in a matrix form as

$$\mathbf{A}\,\mathbf{K} = \mathbf{V} \tag{4.21}$$

where

$$\mathbf{A} = \begin{bmatrix} \mathbf{A}_{11} & \mathbf{A}_{12} & \dots & \mathbf{A}_{1N^I} & \mathbf{B}_{11} & \mathbf{B}_{12} & \dots & \mathbf{B}_{1N^I} \\ \mathbf{A}_{21} & \mathbf{A}_{22} & \dots & \mathbf{A}_{2N^I} & \mathbf{B}_{21} & \mathbf{B}_{22} & \dots & \mathbf{B}_{2N^I} \\ \dots & \dots & \dots & \dots & \dots & \dots & \dots & \dots \\ \mathbf{A}_{N_s^C 1} & \mathbf{A}_{N_s^C 2} & \dots & \mathbf{A}_{N_s^C N^I} & \mathbf{B}_{N_s^C 1} & \mathbf{B}_{N_s^C 2} & \dots & \mathbf{B}_{N_s^C N^I} \\ \mathbf{A}_{11} & \mathbf{A}_{12} & \dots & \mathbf{A}_{1N^I} & \mathbf{B}_{11} & \mathbf{B}_{12} & \dots & \mathbf{B}_{1N^I} \\ \mathbf{A}_{21} & \mathbf{A}_{22} & \dots & \mathbf{A}_{2N^I} & \mathbf{B}_{21} & \mathbf{B}_{22} & \dots & \mathbf{B}_{2N^I} \\ \dots & \dots & \dots & \dots & \dots & \dots & \dots & \dots \\ \mathbf{A}_{N_m^C 1} & \mathbf{A}_{N_m^C 2} & \dots & \mathbf{A}_{N_m^C N^I} & \mathbf{B}_{N_m^C 1} & \mathbf{B}_{N_m^C 2} & \dots & \mathbf{B}_{N_m^C N^I} \end{bmatrix} \tag{4.22}$$

$$\mathbf{K} = \begin{bmatrix} \mathbf{P}_1 \\ \mathbf{P}_2 \\ \vdots \\ \mathbf{P}_{N^I} \\ \mathbf{Q}_1 \\ \mathbf{Q}_2 \\ \vdots \\ \mathbf{Q}_{N^I} \end{bmatrix} \qquad \mathbf{V} = \begin{bmatrix} E_{s1} \\ E_{s2} \\ \vdots \\ E_{sN_s^C} \\ 0 \\ 0 \\ \vdots \\ 0 \end{bmatrix} \tag{4.23}$$

with

$$\mathbf{A}_{ji}^T = \begin{bmatrix} A_{ji0}^{r_t} \\ A_{ji1}^{r_t} \\ \vdots \\ A_{jiN_i}^{j_t} \end{bmatrix} \qquad \mathbf{B}_{ji}^T = \begin{bmatrix} B_{ji1}^{j_t} \\ B_{ji2}^{j_t} \\ \vdots \\ B_{jiN_i}^{j_t} \end{bmatrix} \tag{4.24}$$

$$A_{jin}^{r_t} = \frac{(x_j - x_i^I)t_{yj} - (y_j - y_i^I)t_{xj}}{j\eta_o \rho_{ji}^I} H_n'^{(2)}(k_o \rho_{ji}^I) cos(n\phi_{ji}) \tag{4.25}$$

$$B_{jin}^{r_\phi} = \frac{(x_j - x_i^I)t_{yj} - (y_j - y_i^I)t_{xj}}{j\eta_o \rho_{ji}^I} H_n'^{(2)}(k_o \rho_{ji}^I) sin(n\phi_{ji}) \tag{4.26}$$

$$\mathbf{P}_i = \begin{bmatrix} P_0 \\ P_1 \\ \vdots \\ P_{N_i} \end{bmatrix} \qquad \mathbf{Q}_i = \begin{bmatrix} Q_1 \\ Q_2 \\ \vdots \\ Q_{N_i} \end{bmatrix} \tag{4.27}$$

Having chosen the number of multipoles and the corresponding truncation order, the unknown expansion coefficients would be $M = \sum_{i=1}^{N^I}(2N_i^I + 1)$. Therefore, the number of matching points is $N_s^C + N_m^C \geq M$. Thus, the order of the matrix $\mathbf{A}$ is ($N_s^C + N_m^C$ x M) and that of column vectors $\mathbf{K}$ and $\mathbf{V}$ are, respectively, M and $N_s^C + N_m^C$. The unknown expansion coefficients can then be solved for using the least-square error method given by (4.15).

4.2 Formulation for an Electric Line Source

Figure 4.3 shows an infinitely long slot-perforate cylindrical shell whose axis is taken to be parallel with the $z-$axis of a rectangular coordinate system. It is assumed that the shell is made of perfect conductor and the slot is loaded with a homogeneous dielectric material of permittivity ε_r, permeability μ_r. The shell is situated in free space of permittivity ε_o and permeability μ_o. The excitation, in this case, is due to a line source (TM excitation) situated inside or outside the shell. In some cases, this geometry can provide a useful model to study electromagnetic coupling/interference/radiation from/into two dimensional structure.

The incident fields due to the electric line source, located at (x_o, y_o), are given by

$$E_z^i = I_o H_o(\rho_j) \tag{4.28}$$

$$H_x^i = -J\frac{I_o(y-y_o)}{(\eta_o \rho_j)} H_1(\rho_j) \tag{4.29}$$

$$H_y^i = J\frac{I_o(x-x_o)}{(\eta_o \rho_j)} H_1(\rho_j) \tag{4.30}$$

where I_o is the strength of the line source.

We set three simulated equivalent situations to the original ones in regions 1, 2 and 3 shown in Fig. 4.3. In the simulated equivalence for region 1, shown in Fig. 4.4, the fields in region 1 are simulated by the fields of a set of fictitious multipole sources placed on a closed surface enclosed by the shell. These sources are z directed, infinite in extent and carry, yet undetermined, constant currents. They are treated as electric current sources radiating in free space. Similarly, in the simulated equivalence for region 2, shown in Fig. 4.5, the fields in region 2 are simulated by the fields of a set of fictitious multipole sources placed on a closed

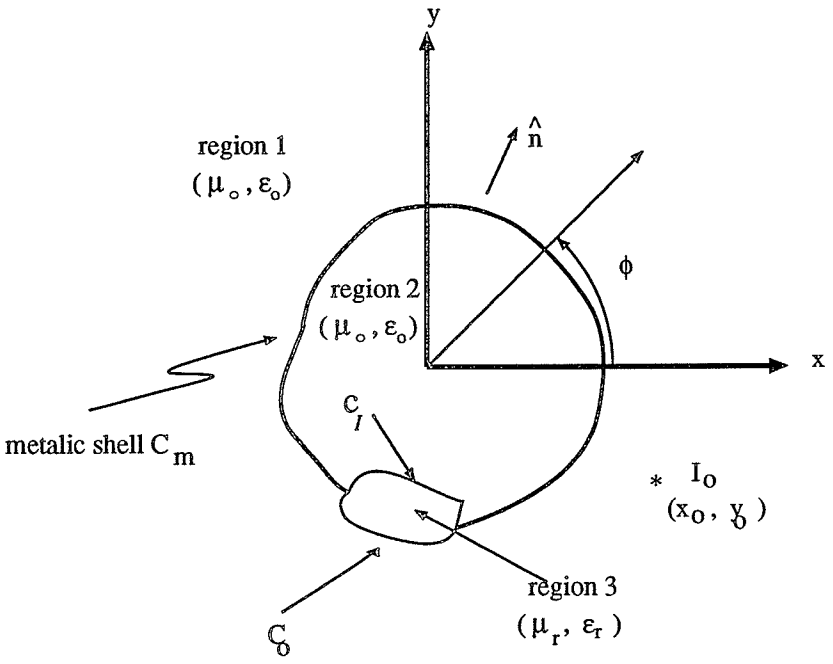

Figure 4.3: Cross section of a dielectric-loaded slot on a cylindrical shell

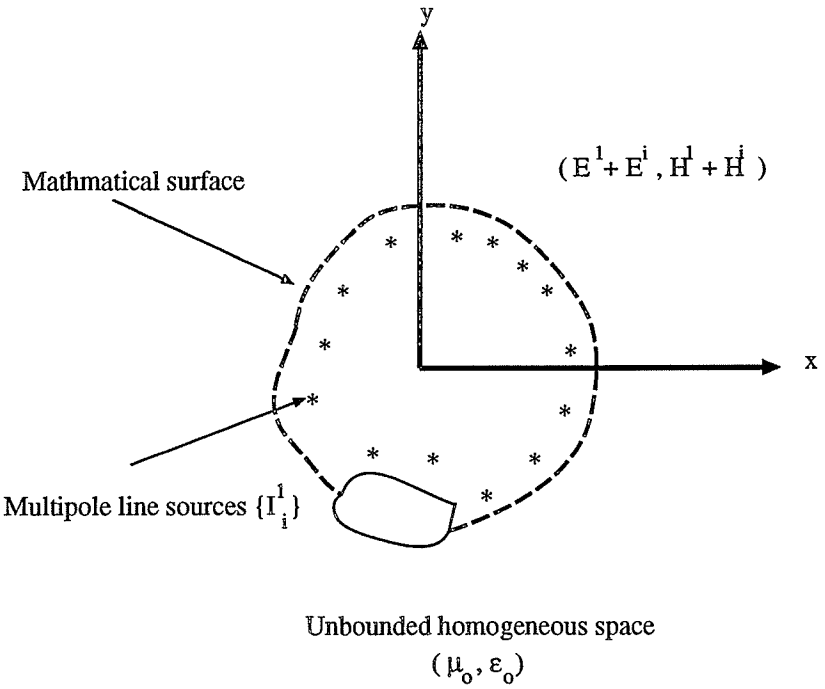

Figure 4.4: Simulated equivalence situation for region 1

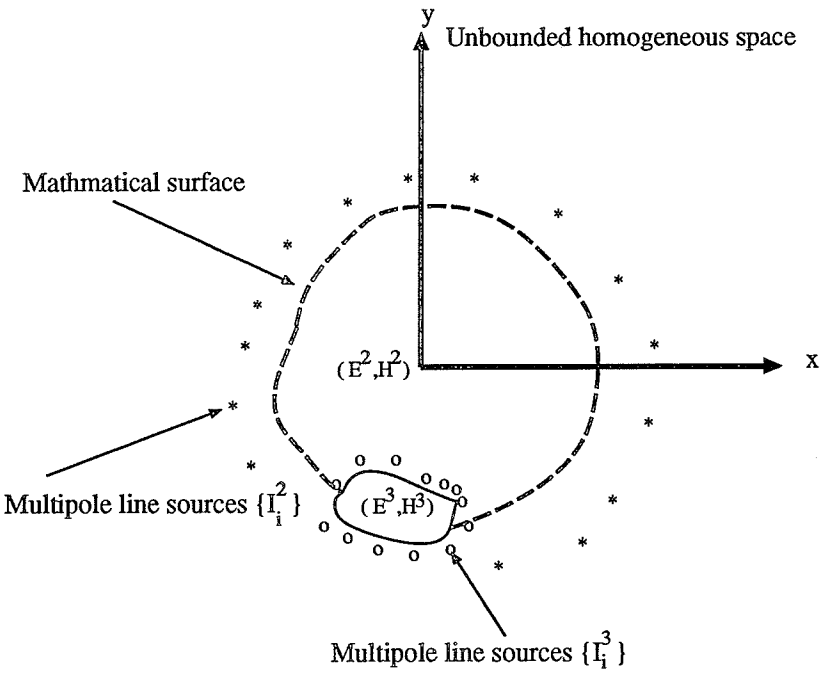

Figure 4.5: Simulated equivalence situation for region 2 (*) and 3 (o).

surface enclosing the shell. Again, these sources are z directed, infinite in extent and carry, yet undetermined, constant currents. They are treated as electric current sources radiating in a free space. Similarly, in the simulated equivalence for region 3, shown in Fig. 4.5, the fields in region 3 are simulated by the fields of a set of fictitious multipole sources placed on a closed surface enclosing the loading material. Again, these sources are z directed, infinite in extent and carry, yet undetermined, constant currents. They are treated as electric current sources radiating in a space filled with homogeneous material identical to the material filling the slot. The relationships between the electromagnetic fields $(E^1 + E^i, H^1 + H^i)$, (E^2, H^2) and (E^3, H^3) in the simulated equivalent situation shown in Figs. 4.4 and 4.4, respectively, are dictated by the boundary conditions in the original problem shown in Fig. 4.3.

4.2.1 Expression for E^1 and H^1

The scattered fields (E^1, H^1) at an observation point (x_j, y_j) in some z =constant plane due to the current sources $F_i, i = 1, 2, 3, ...N^1$ radiating in an unbounded free space are given by [3]

$$\bar{E}^1 = \hat{u}_z \sum_{i=1}^{N^1} E^s_{zji} \tag{4.31}$$

$$\bar{H}^1 = \hat{u}_x \sum_{i=1}^{N^1} H^s_{xji} + \hat{u}_y \sum_{i=1}^{N} H^s_{yji} \tag{4.32}$$

where $E^1_{z_i}, H^1_{x_i}$ and $H^1_{y_i}$ are, respectively, the scattered electric and magnetic field components at an observation point (x_j, y_j) in region 1 due to the i^{th} electric current source F_i situated at (x_i, y_i) inside C and are given by

$$E^1_{zji} = \sum_{n=0}^{N^1_i} P^1_{in} H^{(2)}_n(k_o \rho_{ji}) \cos(n\phi_{ji}) + \sum_{n=1}^{N^1_i} Q^1_{in} H^{(2)}_n(k_o \rho_{ji}) \sin(n\phi_{ji}) \tag{4.33}$$

$$H^1_{xji}(\rho^I_{ji}) = \frac{j(y_j - y^I_i)}{\eta_o \rho^I_{ji}} \left[\sum_{n=0}^{N^1_i} P^1_{in} H'^{(2)}_n(k_o \rho^I_{ji}) \cos(n\phi_{ji}) + \sum_{n=1}^{N^1_i} Q^1_{in} H'^{(2)}_n(k_o \rho^I_i) \sin(n\phi_i) \right] \tag{4.34}$$

$$H^1_{yji}(\rho^I_{ji}) = -\frac{j(x_j - x^I_i)}{\eta_o \rho^I_{ji}} \left[\sum_{n=0}^{N^1_i} P^1_{in} H'^{(2)}_n(k_o \rho^I_{ji}) \cos(n\phi_{ji}) + \sum_{n=0}^{N^1_i} Q^1_{in} H'^{(2)}_n(k_o \rho^I_{ji}) \sin(n\phi_i) \right] \tag{4.35}$$

where $E^1_{z_i}, E^1_{x_i}$ *and* $E^1_{y_i}$ are, respectively, the scattered electric and magnetic fields components at an observation point (x_j, y_j) in region 1 due to the i^{th} source situated at (x^1_i, y^1_i) inside region 2, N^1_i is the truncation number of the i^{th} source, P^1_{in} and Q^1_{in} are unknown coefficients and

$$\rho_{ji} = \sqrt{(x_j - x^1_i)^2 + (y_j - y^1_i)^2} \tag{4.36}$$

$$\phi_{ji} = \arctan\left((y_j - y^1_i)/(x_j - x^1_i)\right) \tag{4.37}$$

4.2.2 Expressions for E^2 and H^2

The electromagnetic fields (E^2, H^2) at an observation point (x_j, y_j) in region 2 due to the multipole sources $I_i^2, i = 1, 2, 3, ...N^2$ situated at (x_i^2, y_i^2) in region 2 and radiating in an unbounded homogeneous free space are given by equations (4.31) through (4.35) with the replacement of the superscript 1 by 2.

4.2.3 Expressions for E^3 and H^3

The electromagnetic fields (E^3, H^3) at an observation point (x_j, y_j) in region 3 due to the multipole sources $I_i^3, i = 1, 2, 3, ...N^3$ situated at (x_i^3, y_i^3) outside region 3 and radiating in an unbounded homogeneous dielectric space is given by

$$\bar{E}^3 = \hat{u}_z \sum_{i=1}^{N^3} E_{zji}^3 \tag{4.38}$$

$$\bar{H}^3 = \hat{u}_x \sum_{i=1}^{N^3} H_{xji}^3 + \hat{u}_y \sum_{i=1}^{N^3} H_{yji}^3 \tag{4.39}$$

where $E_{z_i}^3, H_{x_i}^3$ and $H_{y_i}^3$ are, respectively, the electric and magnetic fields components at an observation point (x, y) in region 3 due to a multipole line source situated at (x_i^3, y_i^3) outside the loading material and are given by equations (4.33), (4.34) and (4.35) with (k_o, η_o, P_{in}^1,Q_{in}^1) replaced by (k_l, η_l, P_{in}^3,Q_{in}^3), respectively.

4.2.4 Evaluation of the Unknown Expansion Coefficients.

In order to solve for the unknown expansion coefficients, only the boundary conditions has to be fulfilled because the field equations are completely satisfied by the GMMP expansions. The boundary conditions, for a line source located inside the boundary surface, are given by

$$\hat{n}\mathrm{x}(\bar{E}^1 - \bar{E}^3) = 0.0 \qquad \text{on } C_o \tag{4.40}$$

$$\hat{n}\mathrm{x}(\bar{H}^1 - \bar{H}^3) = 0.0 \qquad \text{on } C_o \tag{4.41}$$

$$\hat{n}\mathrm{x}(\bar{E}^2 - \bar{E}^3) = -\hat{n}\mathrm{x}\bar{E}^i \qquad \text{on } C_I \tag{4.42}$$

$$\hat{n}\mathrm{x}(\bar{H}^2 - \bar{H}^3) = -\hat{n}\mathrm{x}\bar{H}^i \qquad \text{on } C_I \tag{4.43}$$

$$\hat{n}\mathrm{x}\bar{E}^1 = 0 \qquad \text{on } C_m \tag{4.44}$$

$$\hat{n}\mathrm{x}\bar{E}^2 = -\hat{n}\mathrm{x}\bar{E}^i \qquad \text{on } C_m \tag{4.45}$$

Selecting N^C matching points on boundaries and enforcing the boundary conditions at all the matching points result in a system of linear equations. These equations can be written in a matrix form as

$$\mathbf{A}\ \mathbf{U} = \mathbf{V} \tag{4.46}$$

where

$$\mathbf{A} = \begin{bmatrix} \mathbf{A}_z^1 & 0.0 & -\mathbf{A}_z^3 \\ \mathbf{A}_t^1 & 0.0 & -\mathbf{A}_t^3 \\ 0.0 & \mathbf{A}_z^2 & -\mathbf{A}_z^3 \\ 0.0 & \mathbf{A}_t^2 & -\mathbf{A}_t^3 \\ \mathbf{A}_z^1 & 0.0 & 0.0 \\ 0.0 & \mathbf{A}_z^2 & 0.0 \end{bmatrix} \tag{4.47}$$

$$\mathbf{U} = \begin{bmatrix} \mathbf{P}_i^1 \\ \mathbf{Q}_i^1 \\ \mathbf{P}_i^2 \\ \mathbf{Q}_i^2 \\ \mathbf{P}_i^3 \\ \mathbf{Q}_i^3 \end{bmatrix} \qquad \mathbf{V} = \begin{bmatrix} -E_{zl}^i \\ -H_{tl}^i \\ 0.0 \\ 0.0 \\ -E_z^i \\ 0.0 \end{bmatrix} \tag{4.48}$$

where the quantities $\mathbf{A}_z^1$, $\mathbf{A}_z^2$, $\mathbf{A}_z^3$, $\mathbf{A}_t^1$ $\mathbf{A}_t^2$ and $\mathbf{A}_t^3$ of each element of the matrix $\mathbf{A}$ may be deduced using (4.33) through (4.39).

Having chosen the number of multipoles and the corresponding truncation order, the unknown expansion coefficients would be
$M = \sum_{i=1}^{N^1}(2N_i^1 + 1) + \sum_{i=1}^{N^2}(2N_i^2 + 1) + \sum_{i=1}^{N^3}(2N_i^3 + 1)$. Therefore, the number of matching points $2(N_o^C + N_I^C + N_m^C) \geq M$. Thus, the order of the matrix $\mathbf{A}$ is a $(2(N_o^C + N_I^C + N_m^C)$ x $M)$ and that of the column vectors $\mathbf{K}$ and $\mathbf{V}$ are, respectively, M and $2(N_o^C + N_I^C + N_m^C)$. The unknowns expansion coefficients can then be solved for using the least-square error method given by (4.15).

4.3 Selected Numerical Results and Discussion

Versatile computer programs have been developed using the formulations of the proceeding sections for the axially slotted cylinders. Some representative computations obtained using these programs for slotted circular cylinders are given in this section. For all the results given in this section, the slot is centered at $\phi = 0^o$ and has half angular width of ϕ_s. Thus, in terms of the cylindrical coordinates (ρ, ϕ), $(\rho = a, \phi_s \leq \phi \leq 2\pi - \phi_s)$ define the conducting part of the cylinder C_m while $(\rho = a, 0 \leq \phi \leq \phi_s) \cup (\rho = a, 2\pi - \phi_s \leq \phi \leq 2\pi)$ define the slot region C_s.

The treatment of the singular behavior of the fields near the edges of the slot differs between the two numerical solutions, the generalized multiple technique and the multifilament current model. In the GMMP simulation, we place multipole sources of higher order in the vicinity of the slot. Since the fields of higher order multipoles are much more concentrated around its origin than the fields of lower order multipoles, the singular behavior of field near the edges will be better approximated by the field of these sources. For the MFCM, additional sources are placed near the slot edges and some sources are gradually placed farther from $C_M \cup C_s$.

Source locations that obey this desired form for the circular cylinder under study are introduced by Leviatan and Haller [39].

In the simulation of the radiated fields using the MFCM, we assume a total of N^I sources comprising N_m^I sources in front of C_m and N_s^I sources in front of C_s. The i^{th} source in front of C_m is centered at $(\rho_m^I(i), \phi_m^I(i))$, where [39]

$$\rho_m^I(i) = \rho_m^{I_{max}} - (\rho_m^{I_{max}} - \rho_m^{I_{min}}) sin(\frac{\pi(i-1)}{N_m^I - 1}), \qquad 1 \leq i \leq N_m^I \tag{4.49}$$

$$\phi_m^I(i) = \pi - (\pi - \phi_0 - \Delta\phi_m^I) cos(\frac{\pi(i-1)}{N_m^I - 1}), \qquad 1 \leq i \leq N_m^I \tag{4.50}$$

where, $\rho_m^{I_{max}}$ and $\rho_m^{I_{min}}$ denote, respectively, the largest and the smallest radial distances among the radial distances to the sources in front of C_m. $\Delta\phi_m^I$ denotes a suitable selected angular shift in the azimuthal direction relative to the position of the slot edges. The specific choice of the parameters $\rho_m^{I_{max}}$, $\rho_m^{I_{min}}$ and $\Delta\phi_m^I$ clearly affects the layout of the sources, but they follow the above mentioned rule. The other sources are specified in a similar manner. The i^{th} source in front of C_s is centered at $(\rho_s^I(i), \phi_s^I(i))$, where

$$\rho_s^I(i) = \rho_s^{I_{max}} - (\rho_s^{I_{max}} - \rho_s^{I_{min}}) sin(\frac{\pi(i-1)}{N_s^I - 1}), \qquad 1 \leq i \leq N_s^I \tag{4.51}$$

and

$$\phi_s^I(i) = \begin{cases} (\phi_0 - \Delta\phi_s^I) cos(\frac{\pi(i-1)}{N_s^I - 1}), & 1 \leq i \leq \frac{N_m^I}{2} \\ 2\pi + (\phi_0 - \Delta\phi_s^I) cos(\frac{\pi(i-1)}{N_s^I - 1}), & \frac{N_m^I}{2} \leq i \leq N_s^I \end{cases} \tag{4.52}$$

where, $\rho_s^{I_{max}}$ and $\rho_s^{I_{min}}$ denote, respectively, the largest and the smallest radial distances among the radial distances to the sources in front of C_s. $\Delta\phi_s^I$ denotes a suitable selected angular shift in the azimuthal direction.

Figure 4.6 shows results obtained using the exact analytical solution [36], the MFCM and the GMMP. The results are for slotted circular cylinder of $k_0 a = 2$ and

$\phi_s = 1.5^o$. We assumed a uniform field $E_s = E_o$ with a unit amplitude on the slot. For the MFCM, we used for the number of sources and matching points: $N_m^I = 60$, $N_s^I = 10$, $N_m^C = 3N_m^I$ and $N_s^C = 3N_s^I$. And for the location of sources we set: $\rho_s^{Imax} = \rho_m^{Imax} = 0.99a$, $\rho_s^{Imin} = \rho_m^{Imin} = 0.75a$ and $\Delta\phi_m^I = \Delta\phi_s^I = 0.03^o$. For the GMMP, we set $N_s^I = 4$ with first order truncation located at $0.99a$, $N_m^I = 24$ with zero order truncation located at $0.8a$, $N_s^C = 30$ and $N_m^C = 100$. Also, the matching points are more dense near the edges of the slot in C_m. As shown in the figure, both numerical methods are in good agreement with the analytical solution, however, better agreement is obtained using the GMMP.

Figure 4.7 shows results obtained using the exact analytical solution [36], the MFCM and the GMMP. The results are for slotted circular cylinder of $k_0a = \pi$ and $\phi_s = 2.5^o$. We assumed a field of cosine distribution $E_s = E_o cos\pi\phi/\phi_s$ with a unit amplitude exists on the slot. For the MFCM, we used for the number of sources and matching points $N_m^I = 75$, $N_s^I = 15$, $N_m^C = 3N_m^I$ and $N_s^C = 3N_s^I$. And for the location of sources we set $\rho_s^{Imax} = \rho_m^{Imax} = 0.99a$, $\rho_s^{Imin} = \rho_m^{Imin} = 0.75a$ and $\Delta\phi_m^I = \Delta\phi_s^I = 0.065^o$. For the GMMP, we set $N_s^I = 6$ with truncation of order one located at $0.99a$, $N_m^I = 35$ with truncation of order zero located at $0.8a$, $N_s^C = 35$ and $N_m^C = 130$. Also, the matching points are more dense near the edges of the slot in C_m. As shown in the figure, both numerical methods are in good agreement with the analytical solution, however, better agreement is obtained using the GMMP.

Figure 4.8 shows results obtained using the exact analytical solution [36] and the GMMP. The results are for slotted circular cylinder of $k_0a = 4$ and $\phi_s = 2.5^o$. Two cases are shown for different field distributions with $E_o = 1V/m$. For the GMMP, we set $N_s^I = 6$ with truncation of order one located at $0.99a$, $N_m^I = 40$ with truncation of order zero located at $0.8a$, $N_s^C = 35$ and $N_m^C = 150$. Also, the matching points are more dense near the edges of the slot in C_m. As shown in the figure, good

agreement with the analytical solutions are obtained. The corresponding surface field distribution, computed using the GMMP, are shown in Fig. 4.9. As shown in the figure, the results are in reasonable agreement with the prescribed fields on the slot.

The effect of different dielectric filling a slot in a thick circular cylindrical shell on the radiated field is shown in Fig. 4.10. The inner and outer diameters of the shell are $a = 0.707\lambda_o$ and $b = 0.807\lambda_o$, respectively. The angular width of the slot is 60^o. The excitation source is an electric line source placed at the center of the shell. The results are obtained for dielectrics of permittivities $\epsilon_r = 3.0, 4.0, 5.0$ and 6.0. Three sets of sources are used to simulate the fields of the shell: The first set of $N^1 = 25$ with zero order truncation is located at $0.7a$, the second set of $N^2 = 25$ with zero order truncation is located at $2b$ and the third set of $N^3 = 10$ with first order truncation is placed around the slot at a distance $0.01\lambda_o$ from the boundary surface. The total number of matching points is 140. The results are in good agreement with results obtained by Arvas and Sarkar [44] using the MoM.

Figure 4.11 shows the effect of the unloaded and loaded slots opening on the far field. The inner and outer diameters of the shell are $a = 0.707\lambda_o$ and $b = 0.807\lambda_o$, respectively. The angular widths of the slots are $30^o, 60^o$ and 90^o. The excitation source is an electric line source placed at the center of the shell. The loaded dielectric material is of permittivity $\epsilon_r = 3.0$. Three sets of sources are used to simulate the fields of the shell: The first set of $N^1 = 25$ with zero order truncation is located at $0.7a$, the second set of $N^2 = 25$ with zero order truncation is located at $2b$ and the third set of $N^3 = 12$ with first order truncation is placed around the slot at a distance $0.01\lambda_o$ from the boundary surface. The total number of matching points is 150. These results agree well with those obtained by Arvas and Sarkar [44].

Figure 4.12 shows the aperture field amplitude versus ϕ in circular cylindrical

shell. The diameter of the shell is $a = 0.398\lambda_o$. The angular width of the slot is 60^o. The excitation source is a TM plane wave incident at $\phi^i = 0.0$. The aperture is covered internally by lossless dielectrics of permittivities $\epsilon_r = 1.0, 3.0$ and 5.0. The angular width of the dielectric strip is 78^o. The thickness of the dielectric is $0.039\lambda_o$. Three sets of sources are used to simulate the fields of the shell: A set of $N^1 = 15$ with zero order truncation is located at $0.7a$, the second set of $N^2 = 15$ with zero order truncation is located at $2a$ and the third set of $N^3 = 10$ with first order truncation is placed around the slot at a distance $0.01\lambda_o$ from the boundary surface. The total number of matching points is 120. The results are in good agreement with results obtained by Arvas and Sarkar [44].

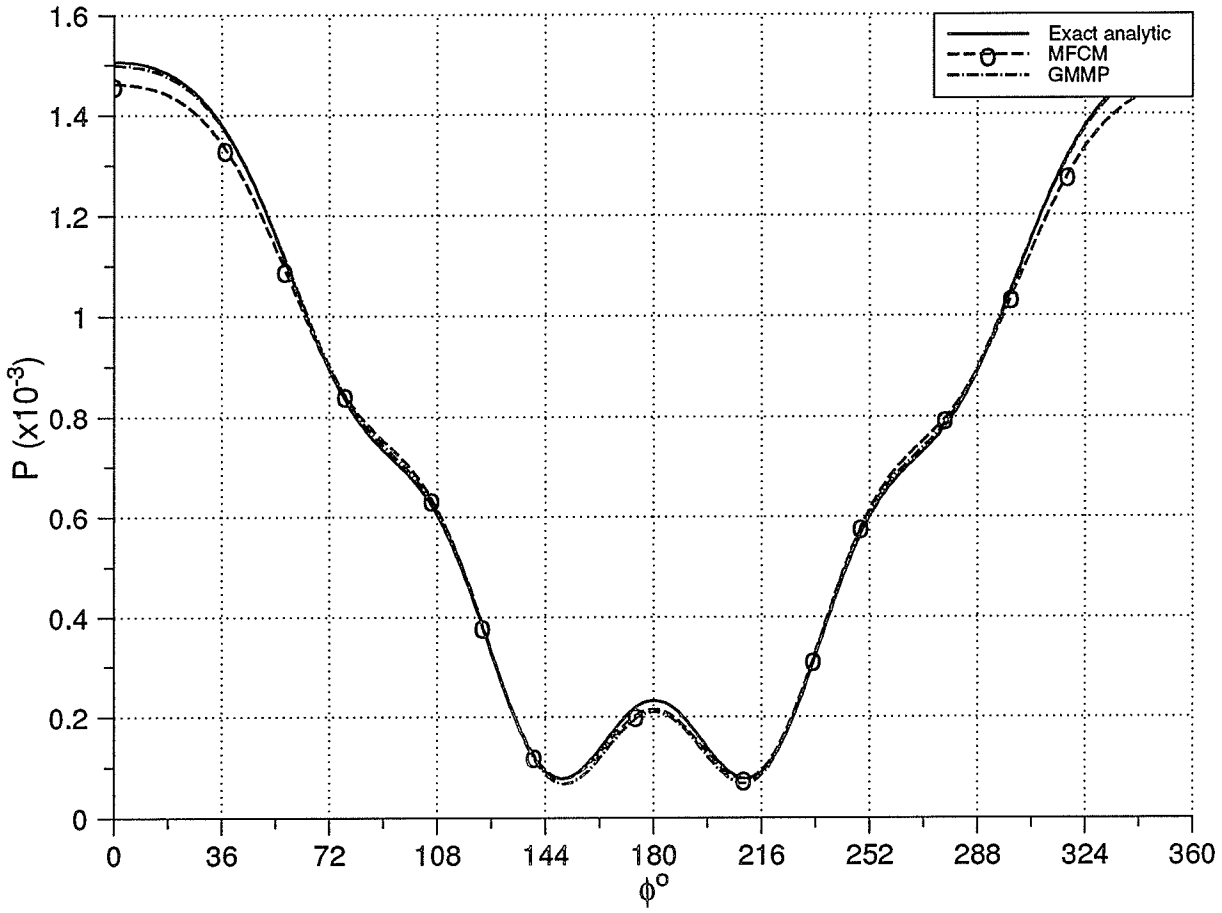

Figure 4.6: Radiated power versus ϕ for a slotted cylinder, $k_o a = 2$ and $\phi_s = 1.5°$ due to a uniform field $E_s = E_o$

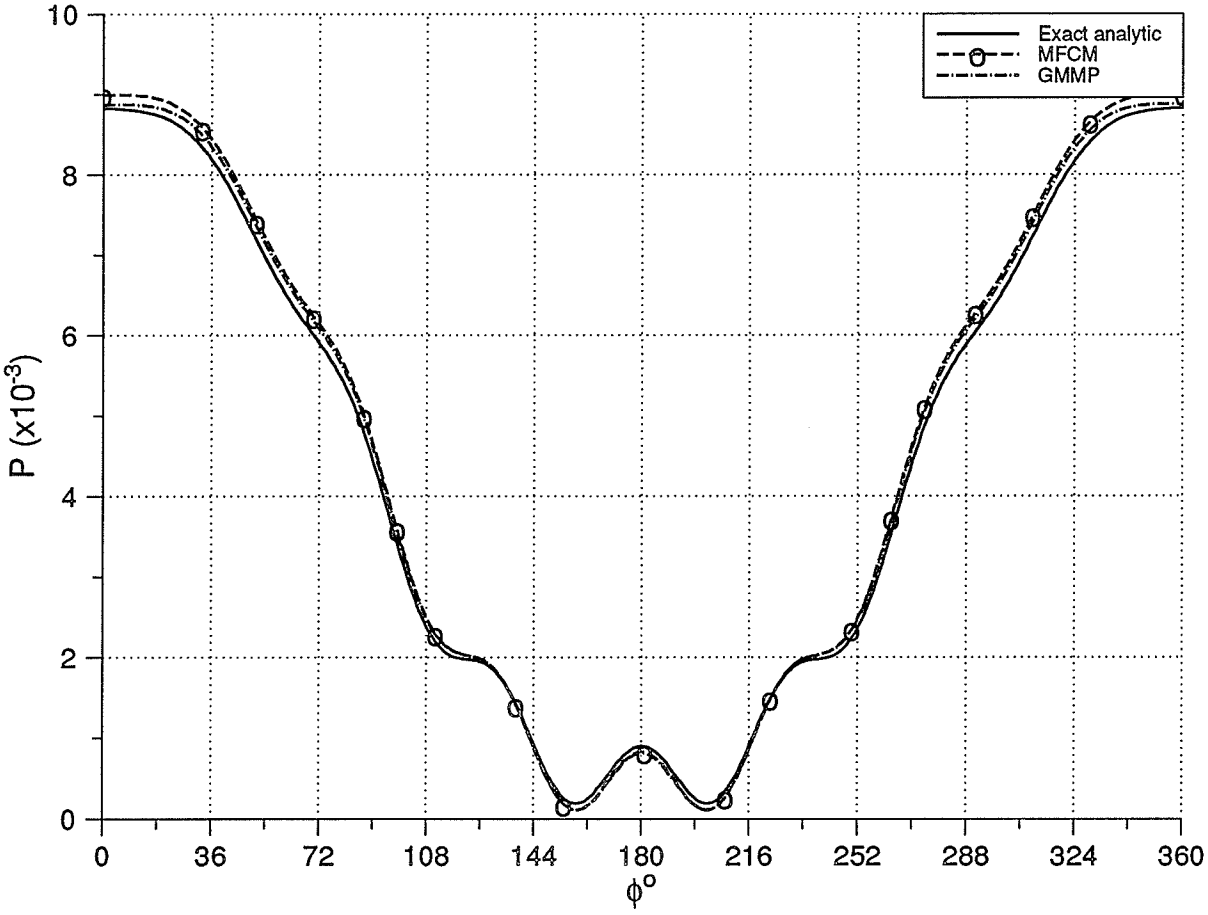

Figure 4.7: Radiated power versus ϕ for a slotted cylinder, $k_o a = \pi$ and $\phi_s = 2.5°$ due to a field $E_s = E_o cos\pi\phi/\phi_s$

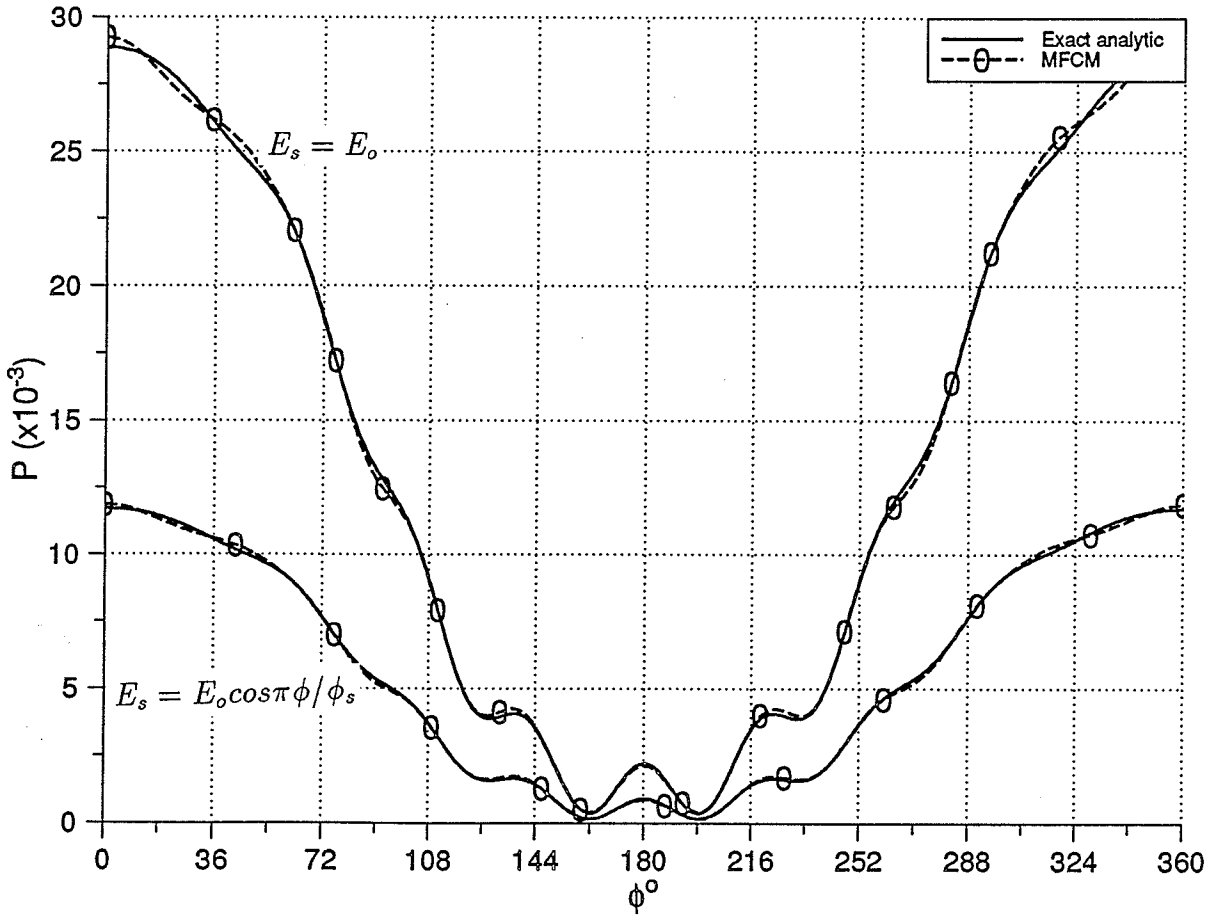

Figure 4.8: Radiated power versus ϕ for slotted cylinder $k_o a = 4$ and $\phi_s = 2.5°$.

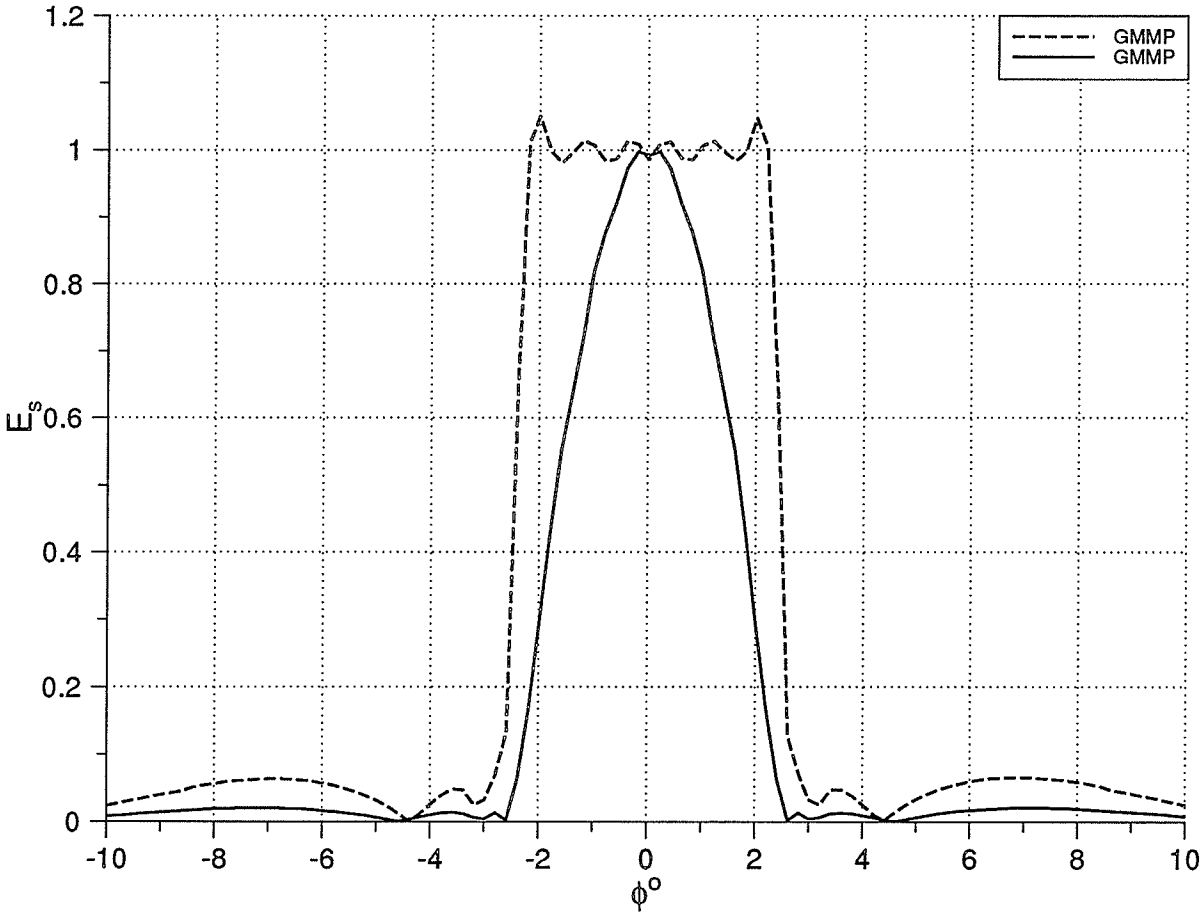

Figure 4.9: Radiated near field versus ϕ for a slotted cylinder, $k_o a = 4$ and $\phi_s = 2.5^o$ due to prescriped fields $E_s = E_o cos\pi\phi/\phi_s$ and $E_s = E_o$ on the slot

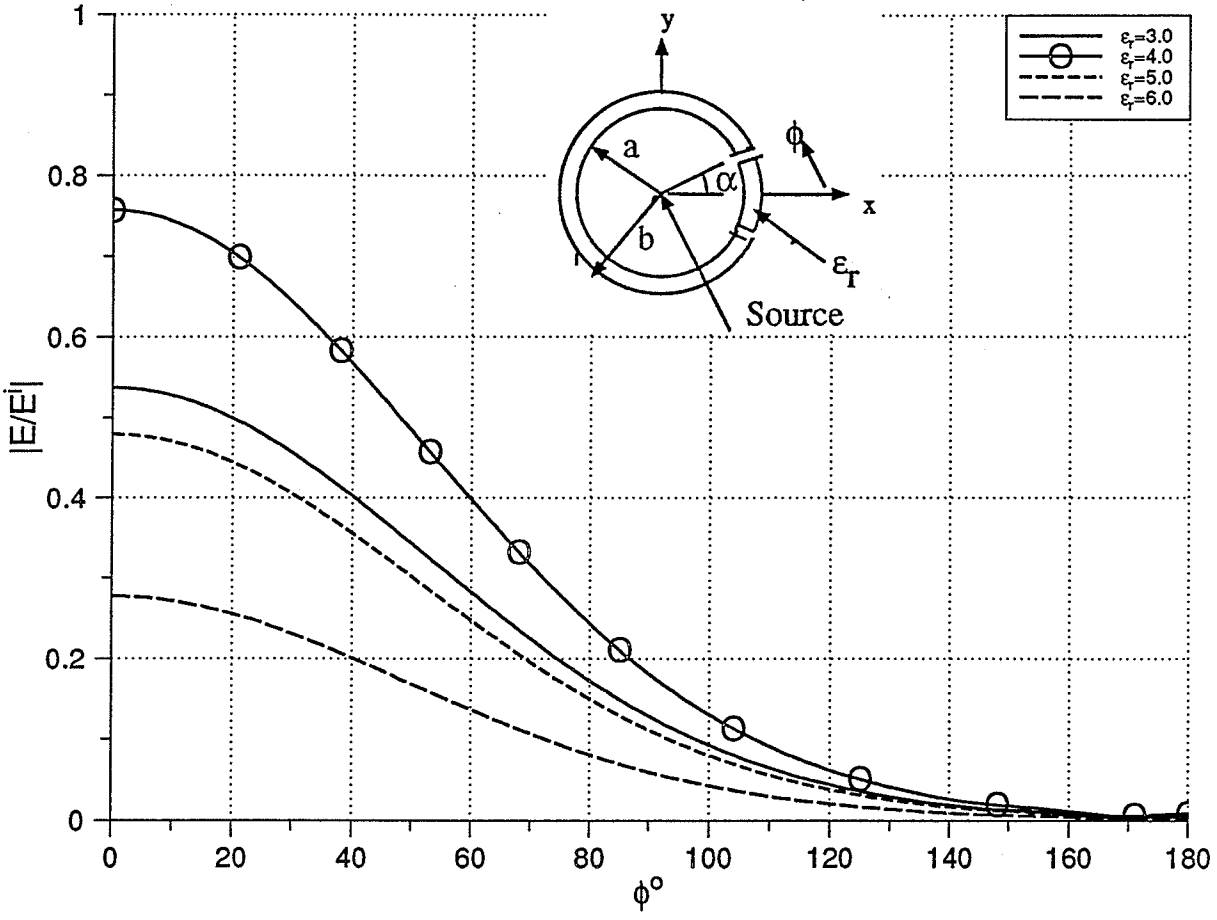

Figure 4.10: Far field amplitude for different dielectric filling a slot in a circular shell

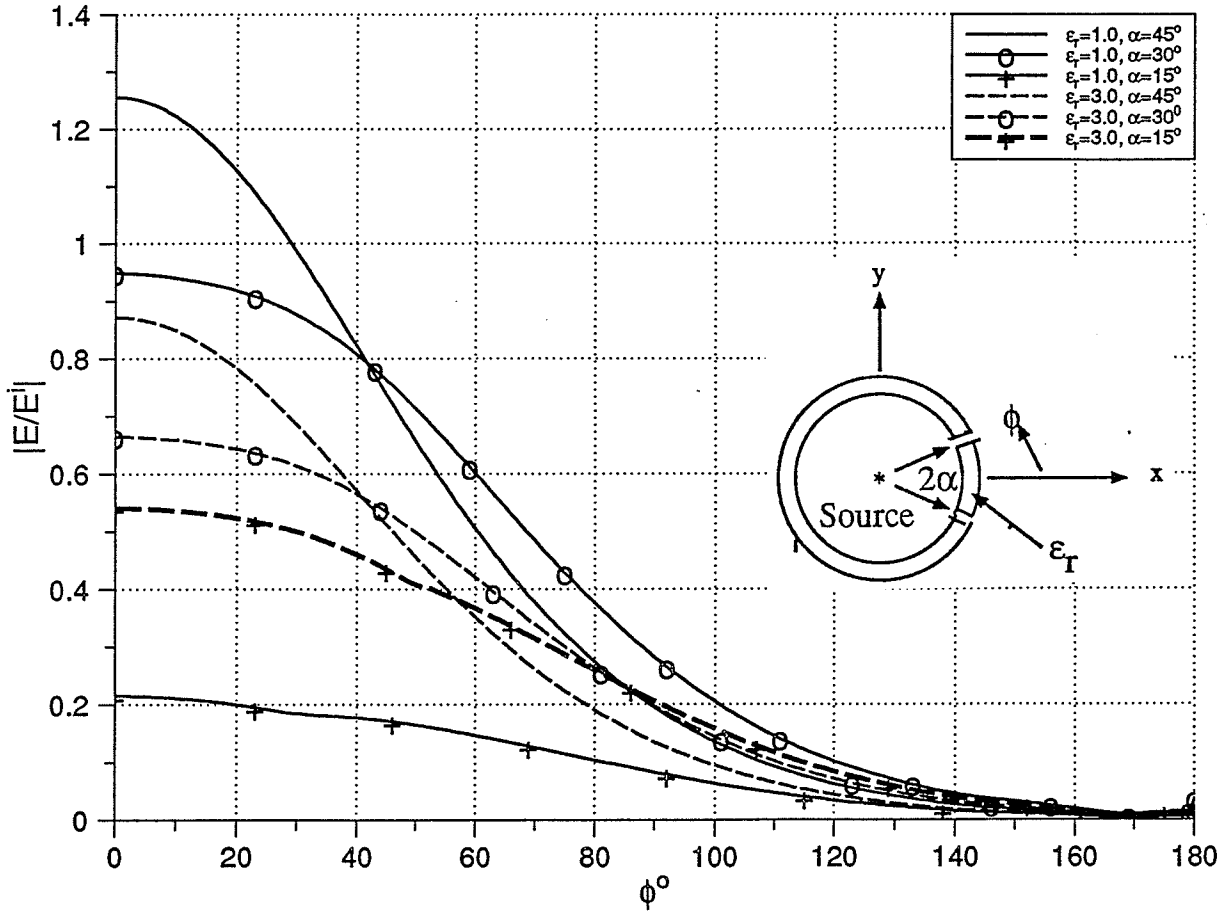

Figure 4.11: The effect of the slot opening on the transmitted far-field amplitude.

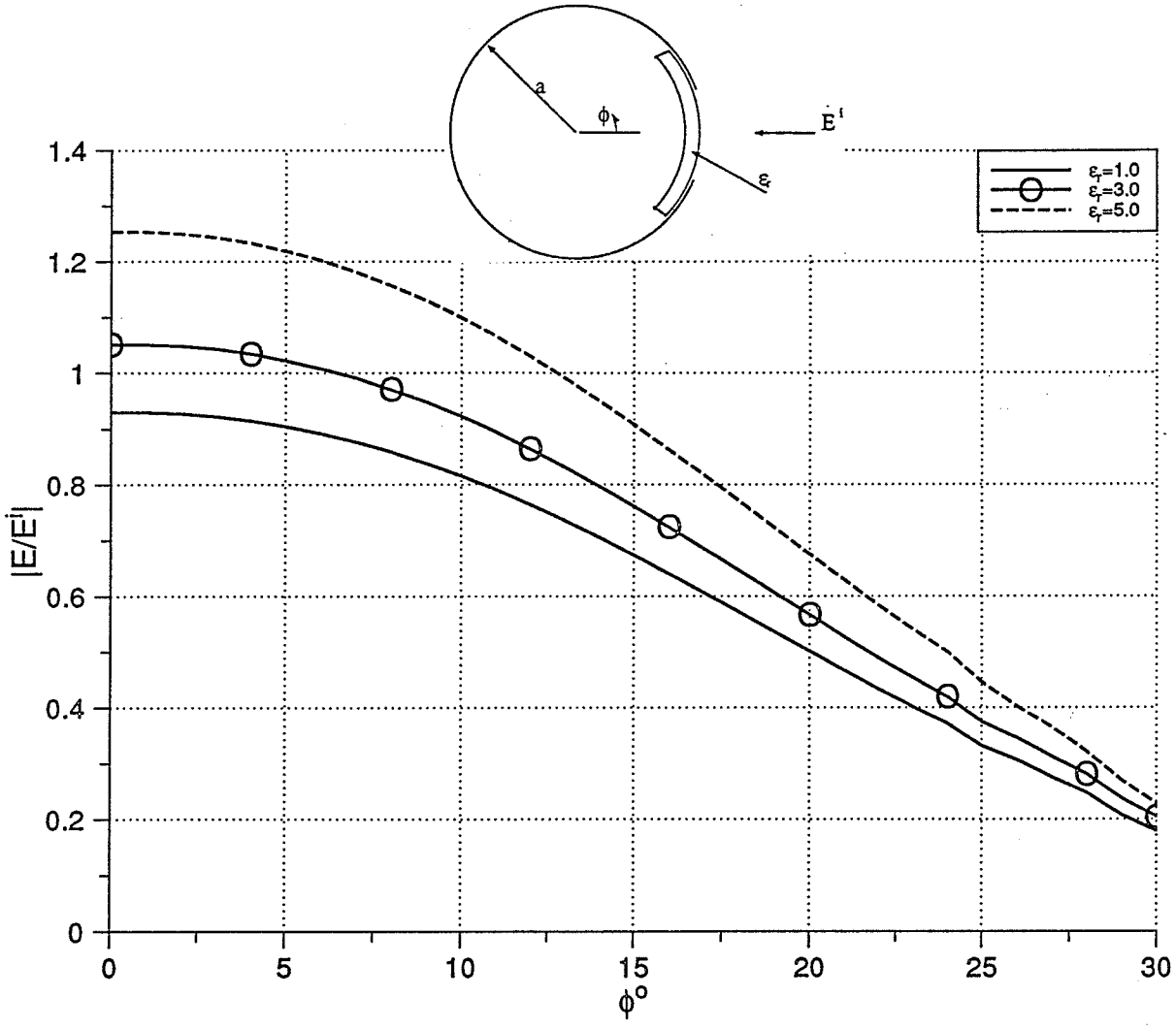

Figure 4.12: Aperture field amplitude versus ϕ

CHAPTER 5

Conclusions

The problems of electromagnetic wave scattering and radiation from homogeneous dielectric and perfectly conducting cylinders of arbitrary cross section have been solved by simple numerical solutions: the multifilament current model and the generalized multiple multipole technique. Both numerical methods are used to solve for a single and multiple scatterers excited by TE and TM polarized electromagnetic waves.

In chapter 2, the multifilament current model and the generalized multiple multipole technique are used to solve for the problem of TE and TM scattering by imperfectly conducting cylinders of arbitrary cross section. Each solution uses a single set of fictitious current sources situated inside the cylinder to simulate its scattered field. The impedance boundary condition is then imposed at selected points on the surface of the cylinder. The result is a system of linear equation for the unknown expansion coefficients which can be solved numerically. The case of perfectly conducting cylinders may be handled as a special case of the imperfectly conducting cylinders by setting the surface impedance to zero. Numerical results, based on these two methods, are examined and found to be in good agreement with the exact analytical solution for circular cylinders and with a MoM solution for elliptic and square cylinders. It is found that the solutions converge faster when the sources are placed on a contour concentric with and similar to the cross section of the cylinder. Furthermore, for the MFCM, it is found that changing r^I any where between $0.05r$ and $0.95r$ has insignificant effect on the convergence of the solution

for circular cylinders. However, in the case of elliptic and square cylinders, the results depend more on the locations of sources. In addition, special consideration should be given to the edges in the rectangular cylinder cases. The MFCM and the GMMP simulations differ in the method by which they treat the singularity of the fields at the edges. In the MFCM simulation, special distribution of the sources is used to simulate the scattered fields; however, sources with higher truncation order are used in the GMMP simulation of the scattered fields.

In chapter 3, the MFCM has been used to solve for the problem of multiple electromagnetic wave scattering from homogeneous dielectric and perfectly conducting cylinders of arbitrary cross section excited by TM or TE polarized electromagnetic waves. In the case of two dielectric cylinders, the solution uses two sets of current filaments for each cylinder. One set is placed inside each cylinder to simulate the fields scattered by the cylinder, the other set is placed outside each cylinder to simulate the fields transmitted inside the cylinder. The boundary conditions are imposed at selected points at the surface of each cylinder. For the problem of perfectly conducting and lossy dielectric cylinders the solution uses a single set of current filaments for each cylinder. The filaments are situated inside each cylinder to simulate its scattered fields. The impedance boundary condition is imposed at selected points at the surface of each cylinder. Numerical results, based on this method, are examined and found to be in good agreement with the MoM solutions. Again, it is found that the solution converges faster when the sources are placed on a contour concentric with and similar to the shape of the cross section. Furthermore, it is found that for a circular cross section a choice of sources location inside each cylinder any where between $0.7a$ and $0.95a$, and for the outer sources any where between $1.3a$ and $1.75a$ has insignificant effects on the convergence of the solution. However, in the case of elliptic cylinders, the location of the sources should be closer

to the boundary. For the square cylinders, the special treatment given to the edges of a single scatterer is applicable to two scatterers.

In chapter 4, the MFCM and the GMMP have been used to solve for the problem of electromagnetic radiation from axially-slotted circular cylinders excited by a prescribed field on the slot or a line source located inside/outside the cylinder. Both solutions use a single set of fictitious current sources situated inside the cylinder to simulate its radiated field. By using a special sources distribution inside the cylinder and using the least-square error, an accurate MFCM solution is obtained and compared with the exact analytical solution. For the GMMP, sources of one and zero truncation order are used to simulate the radiated field. Using the least-square error an accurate solution is obtained and compared with the analytical solution. In addition, the GMMP is used to solve for the radiation from loaded-slotted circular cylinders. The excitation source is asummed to be either an incident TM plane wave or a line source located inside the cylinder. Three sets of sources are used to simulate the fields of the cylinder. The boundary conditions are then imposed at selected points on the boundary surface of the cylinder. The result is a system of linear equation for the unknown expansion coefficients which can be solved numerically.

In general, for the numerical solutions presented in the thesis, there is no general rule of thumb to the choice of the number of sources and matching points because of the large number of parameters involved. However, the convergence can be examined by increasing the number of sources and matching points. In addition, the solution's convergence to a limiting value shouldn't be too sensitive to the change in the location of the sources within reasonable range. In any case, if the results are too sensitive to the change in the sources locations, the number of sources and matching points should be increased. It is understandable that a large cylinder of high permittivity will require more sources and matching points than a smaller one

of lower permittivity in order to achieve the same level of accuracy.

An advantage of using the impedance boundary conditions on both methods over the regular boundary conditions lies in the reduction of the number of sources to one half since only the outer region needs to be simulated. Consequently, only a matrix of (N^I, N^I) elements is needed. The advantage of using the GMMP over the MFCM lies in the simplicity of selecting the sources distributions to simulate complex geometries or objects with sharp edges such as rectangular and slotted cylinders. Furthermore, both methods reduce the computation time significantly in comparison with the MoM solution with the point matching technique. For example, for the elliptic cylinder presented in Fig.2.9, a matrix of order $(23, 23)$ is used in the MFCM with IBCs solution and the CPU time is 0.1 second on a Sun 4 workstation; while, a matrix of $(90, 90)$ is used for the MoM solution and the CPU time is 0.5 second. Also, for obtaining the results shown in Fig. 3.4 a matrix of $(100, 100)$ is used in the MFCM solution and the CPU computation time is $16.49s$ in the Sun 4 workstation while, for the MoM solution, the matrix size is $(200, 200)$ and the CPU computation time is $29.28s$.

Finally, the generalized multiple multipole technique and its special case the multifilament current model can be applied to more complex geometries and they are applicable to three-dimensional problems.

Research based on this thesis has been published in [45], [46], [47], [48] and [49].

REFERENCES

REFERENCES

[1] G. Mie. Elektrische Wellen an zwei parallelen Drahten. *Annalen der Physik*, vol. 2, pp. 201–249, 1900.

[2] I.N. Vekua. *New Methods for Solving Elliptic Equations Amesterdam: North-Holand, 1967. (Translation from Russian: Novye method resheniya ellipticheskikh uravneii .* Gostekhizdat, Moscow, 1948.

[3] C. Hafner. *The Generalized Multipole Technique for computational Electromagnetics.* Artech House, Norwood, MA., 1990.

[4] C.R. Mullin, R. Sandburg, and C.O. Velline. A Numerical Technique for the Determination of Scattering Cross section of Infinite Cylinders of arbitrary cross sections. *IEEE Trans. on Antennas Propgat.*, vol. AP-12, pp. 141–149, January 1965.

[5] H.Y. Yee and N.F. Audeh. Uniform Wave guides with Arbitrary Cross Section Considered by the Point-Matching Method. *IEEE Trans. on MTT*, vol. MTT-13, pp. 847–851, November 1965.

[6] J.E. Goell. A Circular-Harmonic Computer Analysis of Rectangular Dielectric Waveguides. *Bell System Technical Journal*, vol. , pp. 2133–2160, September 1969.

[7] J.R. James and I.N.L. Gallett. Point Matching Solution for Propagating Modes on Arbitrary Shaped Dielectric Rods. *The Radio and Electronic Engineer*, vol. 42, pp. 103–113, March 1972.

[8] L. Lewin. On the Inadequacy of Discrete Mode-Matching Techniques in Some Waveguide Discontinuity Problems. *IEEE Trans. on MTT*, vol. MTT-18, pp. 364–372, July 1970.

[9] R.H.T. Bates. Analytic Constraints on Electromagnetic Field Computations. *IEEE Trans. on MTT*, vol. MTT-23, pp. 605–623, July 1975.

[10] A. Ludwig. A New Technique for Numerical Electromagnetics. *IEEE AP-S Newsletter*, vol. 31, pp. 40–41, February 1989.

[11] R.F. Harrington. *Field Computation by Moment Methods.* Macmillan, New York, 1968.

[12] G. Klaus. *3D Streufeldberechnungen mit Hilfe der MMP-Methode.* Dissertation-7792, ETH Zurich, 1985.

[13] M.F. Iskander, A. Lakhtakia, and C.H. Durney. A New Iterative Procedure to Solve for Scattering and Absorption by Dielectric Objects. *Proc. IEEE*, vol. 70 No. 11, November 1982.

[14] A.C. Ludwig. A Comparison of Spherical Wave Boundary Value Matching Versus Integral Equation Scattering Solution for a Perfectly Conducting body. *IEEE Trans.*, vol. AP-34, No 7, July 1986.

[15] Y. Leviatan, P.G. Adams, and J. Perini. Single-Post Inductive Obstacle in Rectangular Waveguide. *IEEE Trans.*, vol. MTT-31, pp. 806–812, October 1983.

[16] M. Nishimura, S. Takamatsu, and H. Shigesawa. A Numerical Analysis of Elctromagnetic Scattering of a Perfect Conducting Cylinder by Means of Discrete Singularity Method Improved by Optimization Process. *Inst. Elec. Comm. Japan*, vol. 67-B No. 5, May 1984.

[17] A.C. Ludwig. The Generalized Multipole Technique. *IEEE 1989 Antennas Propagat. Inter. Syn. Proc.*, vol. 1, pp. 160–163, June 1989.

[18] J. H. Richmond. Scattering by a dielectric cylinder of arbitrary cross section shape. *IEEE trans. Antennas Propagat.*, vol. AP-13, pp. 334–341, May 1965.

[19] J. H. Richmond. TE-wave Scattering by a dielectric cylinder of arbitrary cross section shape. *IEEE trans. Antennas Propagat.*, vol. AP-14, pp. 460–464, July 1966.

[20] A. Taflove K. Umashankar and S. Rao. Electromagnetic scattering by arbitrary shaped three-dimensional homogeneous lossy dielectric objects. *IEEE trans. Antennas Propagat.*, vol. AP-34, pp. 758–766, 1986.

[21] Y. Leviatan and Amir Boag. Analysis of electromagnetic scattering from dielectric cylinder using a multifilament current model. *IEEE trans. Antennas Propagat.*, vol. AP-36, pp. 1119–1127, October 1987.

[22] Y. Leviatan, Amir Boag, and Alona Boag. Analysis of TE scattering from dielectric cylinder using a multifilament current model. *IEEE trans. Antennas Propagat.*, vol. AP-35, pp. 1026–1030, July 1988.

[23] M. G. Andreasen. Scattering from cylinders with arbitrary surface impedance. *IEEE. Proceeding*, vol. , pp. 812–818, August 1965.

[24] K. M. Mitzner. An integral equation approach to scattering from a body of finite conductivity. *Radio Sci.*, vol. 2, pp. 1459–1470, December 1967.

[25] D. S. Jones. *'Methods in electromagnetic wave propagation.* Clarendon Press, 1979.

[26] V.H. Weston. Theory of Absorbers in Scattering. *IEEE Trans. Antennas Propagat.*, vol. AP-11, pp. 578–584, 1963.

[27] A. Sebak and L. Shafai. Performance of various integral equation formulations for numerical solution of scattering by impedance objects. *Cand. J. Phys.*, vol. , pp. 317–376, 1984.

[28] A. Sebak and L. Shafai. Scattering from arbitrarily-shaped objects with impedance boundary conditions. *IEE. Proc. part H*, vol. 62, pp. 606–615, 1989.

[29] M.G. Andreasen. Scattering from parallel metallic cylinders with arbitrary cross section. *IEEE trans. Antennas Propagat.*, vol. AP-12, pp. 746–754, November 1964.

[30] B.A. Howarth and T.J. Pavlasek. Multiple Induction: a Novel Formulation of Multiple Scattering of Scalar Waves . *J. App. Phys.*, vol. 44, pp. 1162–1167, 1973.

[31] B.A. Howarth. Multiple Scattering Resonances between Parallel Conducting Cylinders. *Can. J. Phys*, vol. 51, pp. 2415–2427, 1973.

[32] G. O. Olaofe. Scattering by two cylinders. *Radio Sci*, vol. 5 No 11, pp. 1351–1360, November 1970.

[33] H. Ragheb and M. Hamid. Scattering by N parallel conducting circular cylinders. *Int'l. J. of electronics*, vol. 59, pp. 407–421, 1985.

[34] A. Z. Elsherbeni and M. Hamid. Scattering by parallel conducting circular cylinders. *IEEE Trans. Antennas Propagat.*, vol. AP-35, 1987.

[35] S. N. Karp and N. Zitron. Higher-order approximation in multiple scattering, 1, Two-dimensional scalar case. *J. Math. Phys.*, vol. 2 No 3, pp. 394–402, 1961.

[36] R.A. Hurd. Radiation Patterns of a Dielectric-Coated Axially-Slotted Cylinder. *Can. J. Phys.*, vol. 34, pp. 638–642, march 1956.

[37] A. Olte. Radiation of an Elementary Cylinder Antenna Through a Slotted Enclousure. *IEEE Trans. Antennas Propagat.*, vol. AP-13, No 5, pp. 691–703, Sept 1965.

[38] J. Richmond and M. Gilreath. Fluch-Mounted Dielectric-Loaded Axial Slot on Circular Cylinder. *IEEE Trans. Antennas Propagat.*, vol. AP-23, No. 3, pp. 348–351, May 1975.

[39] Y. Leviatan and M. Haller. Analysis of Electromagnetic Scattering from a Slot-Perforated Conducting Cylindrical Shell Using a Multifilament Current Model. *J. Electromag. Wave and Apllic.*, vol. 5 N0. 1, pp. 59–74, 1991.

[40] T. B. A. Senior. Impedance boundary conditions for imperfectly conducting surfaces. *Appl. Sci. Res.*, vol. 8, pp. 418–436, 1960.

[41] Roger F. Harrington. *Time-Harmonic Electromagnetic Fields.* McGraw Hill, New York, 1961.

[42] S. Eisler and Y. Leviatan. Analysis of electromagnetic scattering from metallic and penetrable cylinder with edges using a multifilament current model. *IEE. Proc., Pt.H*, vol. 136, pp. 431–438, December 1989.

[43] A. Z. Elsherbeni and A. Kishk. Modeling of Cylindrical Objects by Circular Dielectric and Conducting Cylinders. *IEEE. Trans. Antennas Propagat.*, vol. AP-40, No. 1, pp. 96–99, Jan. 1992.

[44] E. Arvas and T.K. Sarkar. TM transmission Through Dielectric-Filled Slots in a Conducting Cylindrical Shell of Arbitrary Cross Section. *IEEE Trans. Electromagn. Compat.*, vol. EMC-29, No. 2, pp. 150–156, May 1987.

[45] M. Ouda and A. Sebak. Scattering from Lossy Dielectric Cylinders Using a Multifilament Current Model With Impedance Boundary Conditions. *IEE part H*, vol. In Press, 1993.

[46] M. Ouda, M. Hussein, A. Sebak, and Y. Antar. Multiple Scattering by Dielectric Cylinders Using a Multifilament Current Model. *J. Electromag. Wave and Apllic.*, vol. In Press, 1993.

[47] M. Ouda, A. Sebak, and Y. Antar. Scattering from Lossy Dielectric Cylinders Using a Generalized Multiple Multipole Technique With Impedance Boundary Conditions. In *Proce. IEEE Antennas and Propagation Society International Symposium.*, pp. 2001–2004, Hyatt Regency Chicago, Chicago, Ill., USA, July 1992.

[48] M. Ouda and A. Sebak. Radiation and Scattering Analysis of Two-Dimensional Conducting and Dielectric Objects Using the Generalized Multiple Multipole Technique. In *Proce. Symposium on Antenna Technology and Applied Electomagnetics, Workshop: Review of Electromagnetic Simulation Technigue*, pp. 291–296, Delta Winnipeg, Winnipeg, Manitoba, August 1992.

[49] M. Ouda, A. Sebak, and Y. Antar. Analysis of Electromagnetic Interference in Two Dimensional Problems Using the Generalized Multipole Technique. In *Proce. Symposium on Antenna Technology and Applied Electomagnetics*, pp. 345–350, Delta Winnipeg, Winnipeg, Manitoba, August 1992.